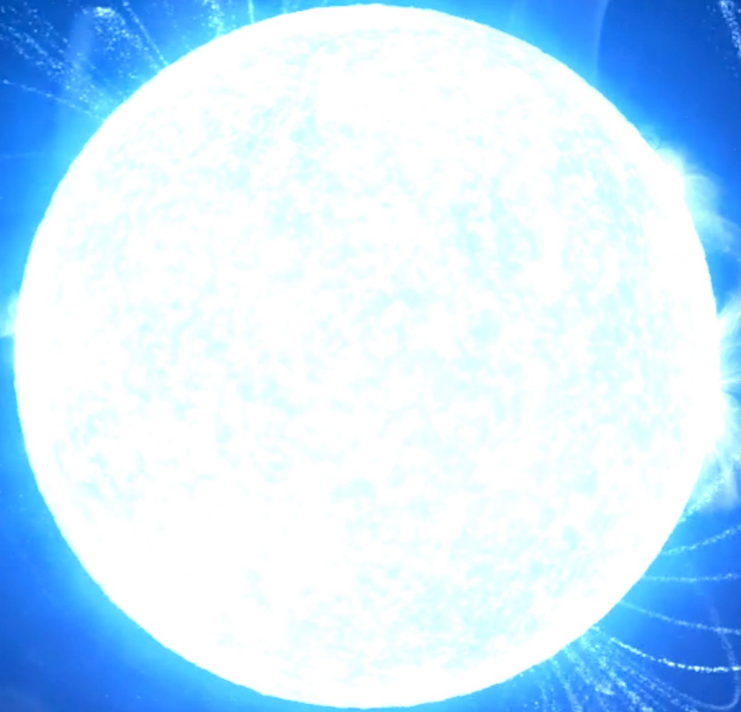


Stellar Magnetism and Extrasolar Space Weather

Julián David Alvarado-Gómez

Leibniz Institute for Astrophysics Potsdam (AIP)

 @AstroRaikoh

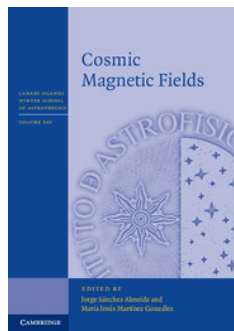


Leibniz-Institut für
Astrophysik Potsdam

Image credit: Goddard Scientific Visualization Studio

7th Institute of Space Sciences Summer School: Multiwavelength Approach to Exoplanets | 10.07.2024

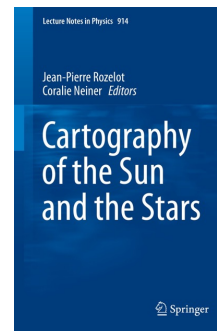
Detecting and Mapping Stellar Magnetic Fields



Cosmic Magnetic Fields

Lecture notes of the XXV Canary Islands Winter School of Astrophysics.

Ch. 3 by O. Kochukhov (Uppsala U.)



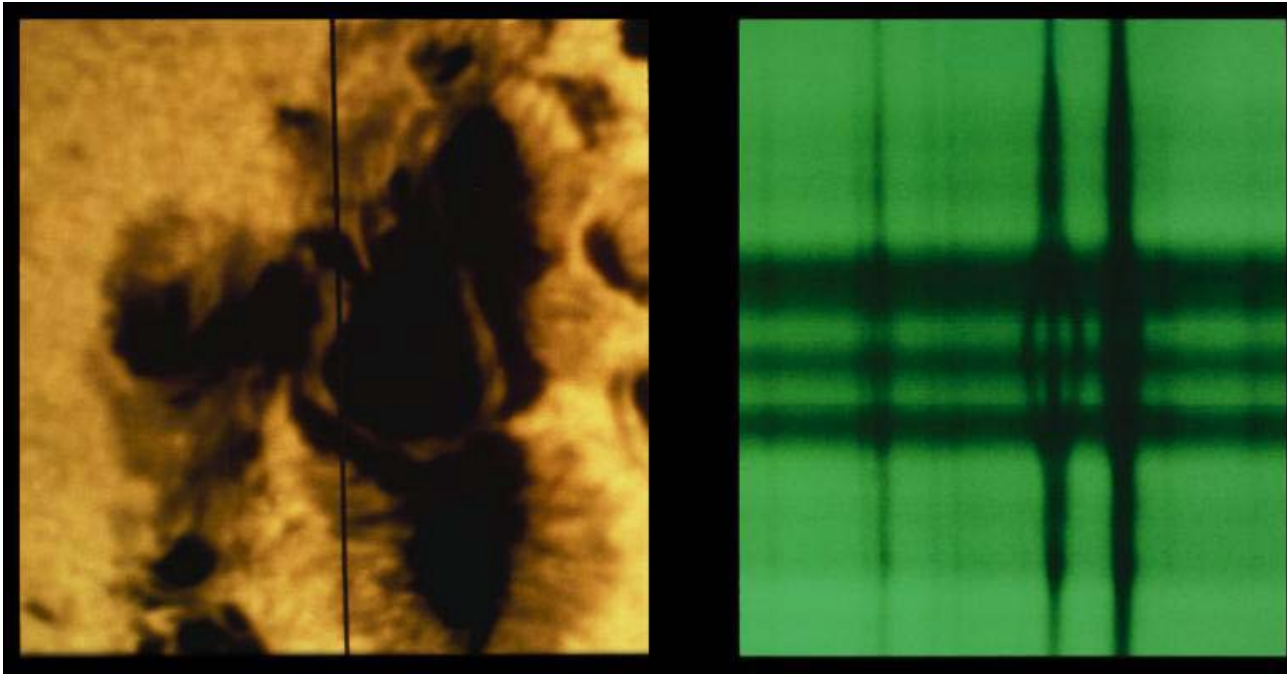
Cartography of the Sun and the Stars

Lecture notes in Physics (LNP) 914.

Ch. 9 by O. Kochukhov (Uppsala U.)

Magnetic fields and Astrophysics: Zeeman Effect and Spectropolarimetry

1908: First measurement of a magnetic field in an Astrophysical object (Sunspot) by G. E. Hale through the Zeeman Effect.



Line Splitting:

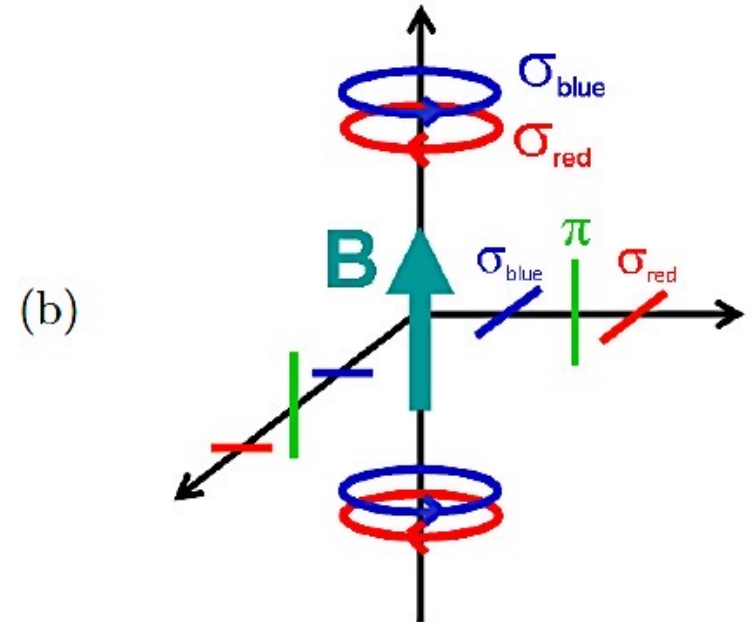
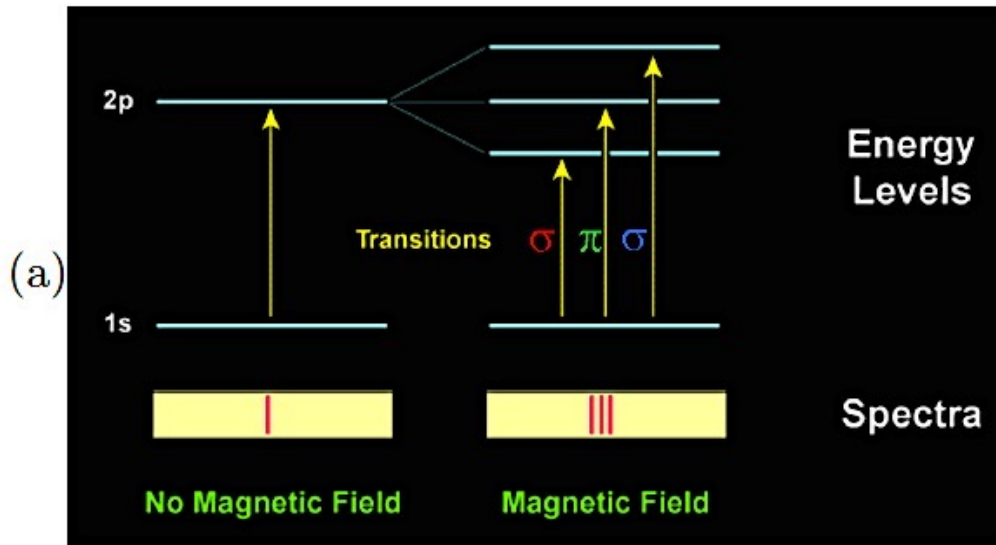
$$\Delta\lambda = 4.67 \times 10^{-13} g_{\text{EFF}} B \lambda^2$$

Effective Landé Factor:

$$g_{\text{EFF}} = \frac{1}{2} (g_L + g_U) + \frac{1}{4} (g_L + g_U)[J_L(J_L + 1) - J_U(J_U + 1)]$$

The **Zeeman Effect** also induces a signal in the **polarization state** of the splitting components, depending on the magnetic field geometry and the position of the observer.

(a) Schematic view of Zeeman splitting

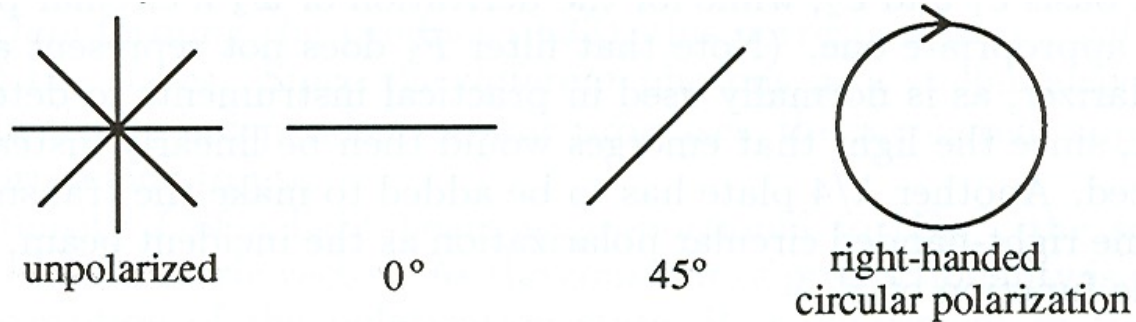


(b) Different polarization states of the Zeeman components

Splitting and Polarization: \longrightarrow

Recover the vector properties of B .

The **polarization state of the light** usually is described in the formalism of the Stokes parameters I , Q , U and V .



I : Total Intensity.

$$I = I_{\text{LIN}}(0^\circ) + I_{\text{LIN}}(90^\circ) = I_{\text{LIN}}(45^\circ) + I_{\text{LIN}}(135^\circ) = I_{\text{CIRC}}(\text{right}) + I_{\text{CIRC}}(\text{left})$$

$$Q = I_{\text{LIN}}(0^\circ) - I_{\text{LIN}}(90^\circ)$$

$$U = I_{\text{LIN}}(45^\circ) - I_{\text{LIN}}(135^\circ)$$

$$V = I_{\text{CIRC}}(\text{right}) - I_{\text{CIRC}}(\text{left})$$

Stokes parameters correspond to + and - of intensities, therefore they can be **measured**.

Spectroscopy: Stokes I

Spectropolarimetry: Stokes I , Q , U and V

Stokes I : Radiative Transfer

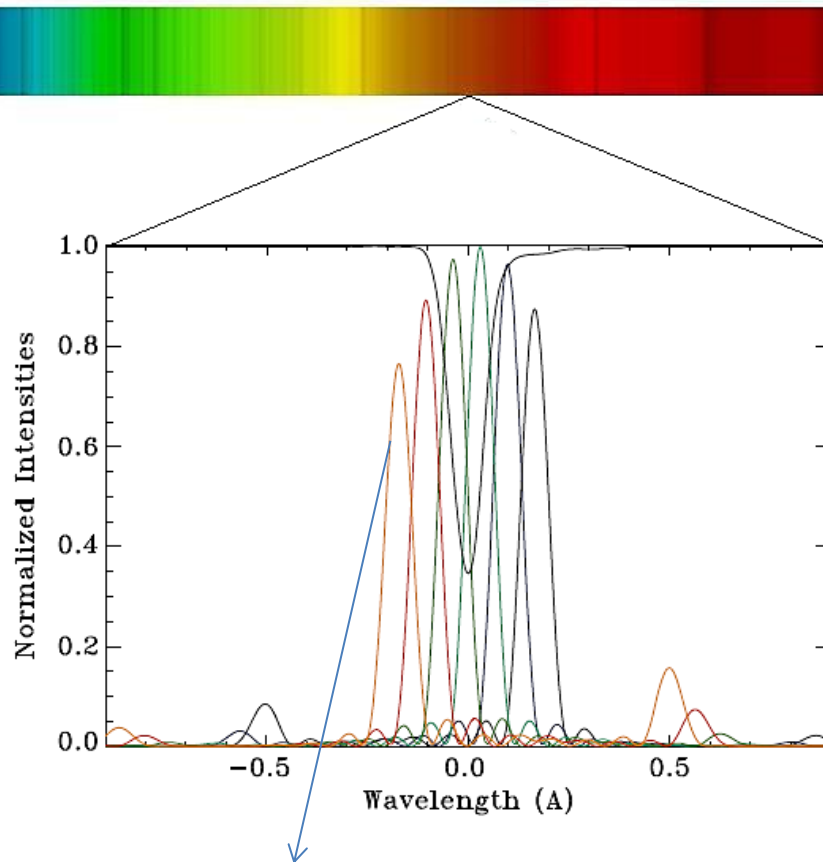


Stokes I , Q , U , V : Polarized Radiative Transfer

Magnetic Field Measurements

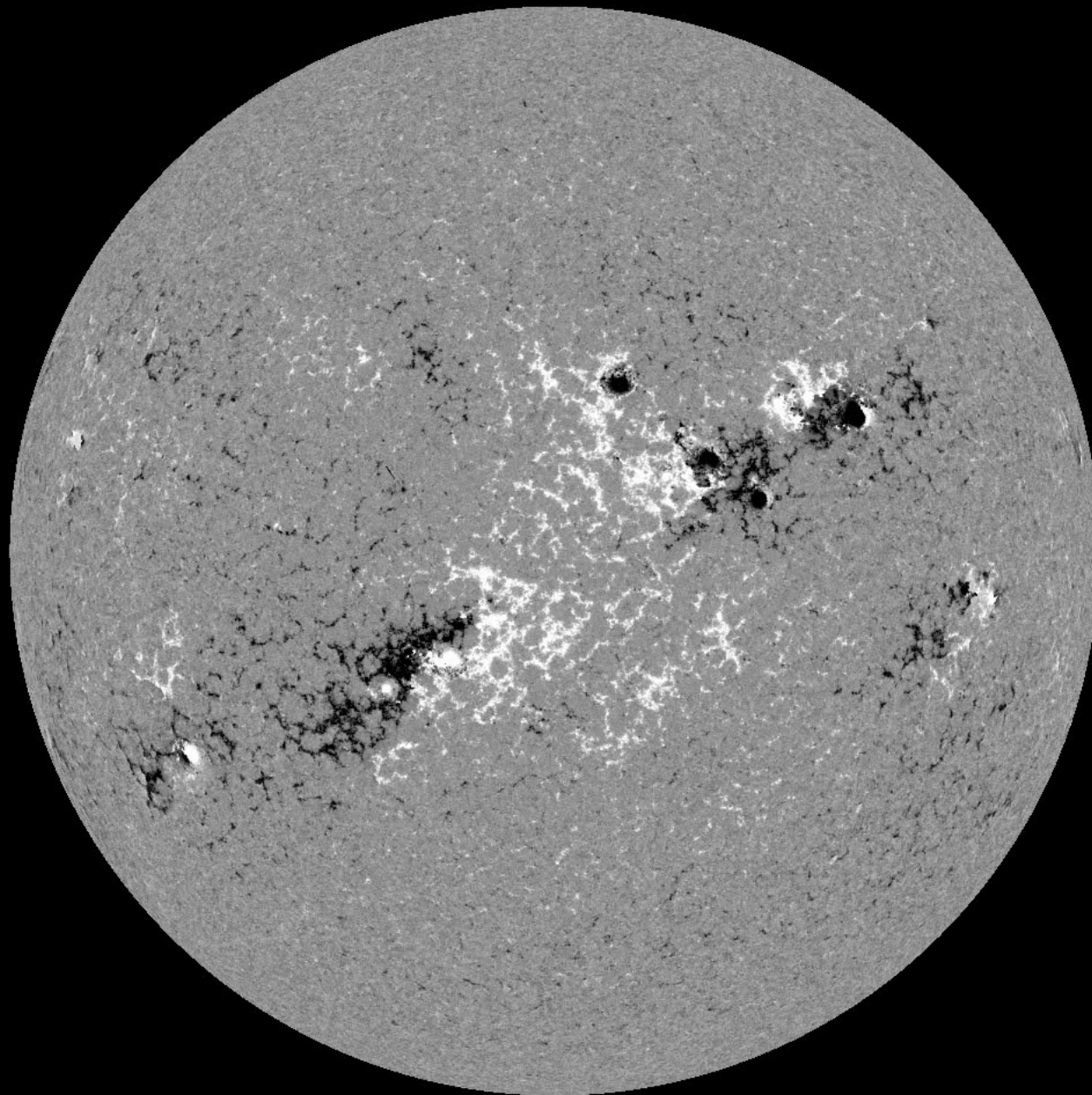
The Sun

Helioseismic and Magnetic Imager (HMI): $6173.3 \pm 0.1 \text{ \AA}$ (Fe I line | $g_{\text{EFF}} = 2.499$)



Tuning Filters + Polarization selectors

- Images are generated in each of the 6 tuning filters.
- Polarization selectors are used to calculate Stokes Q, U and V.
- A spectral inversion code is used to recover the vector magnetic field (Milne-Eddington atmosphere).
- Maps of the surface magnetic field (Magnetograms).



SDO/HMI Quick-Look Magnetogram: 20140513_140000

Disk-Integrated Stokes Parameters:

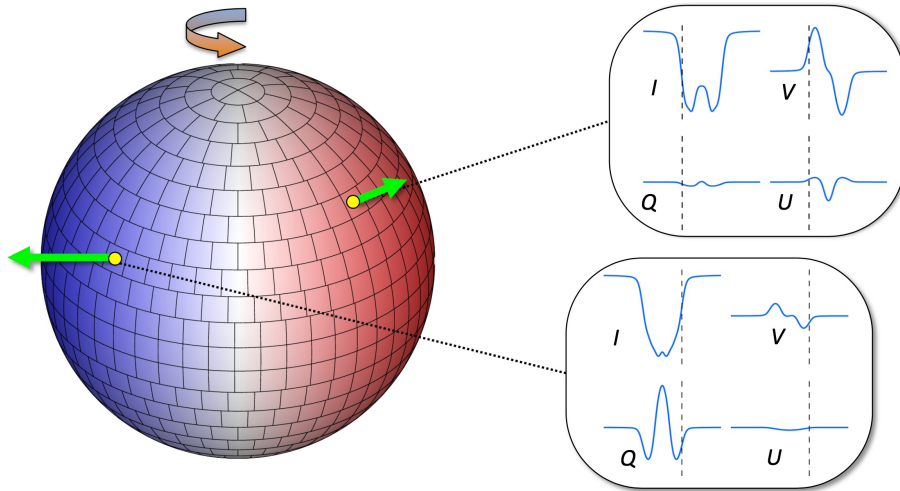


Image Credit: O. Kochukhov (XXV IAC Winter School)

Weak field approximation:
[Zeeman splitting smaller than the line width]

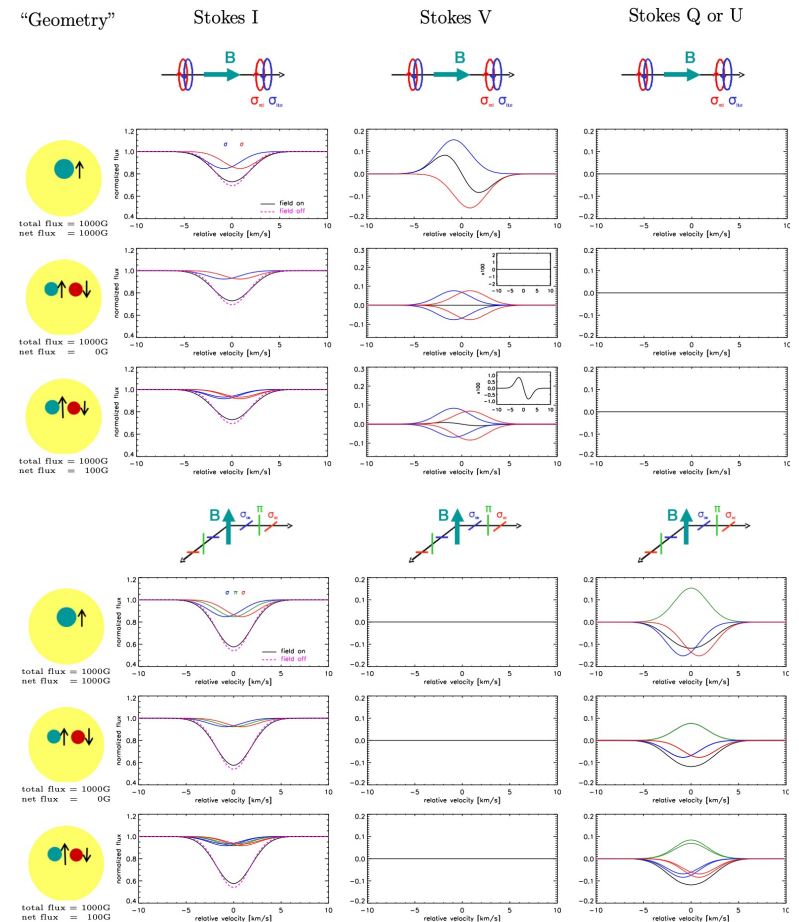
$$\bar{g}\Delta\lambda_B \ll \Delta\lambda_D, \quad \bar{g}B \ll 2500 \text{ G}$$

$$I \approx I_0$$

$$V(\lambda) \approx -\Delta\lambda_B \bar{g} \cos\theta \frac{\partial I}{\partial \lambda} = -4.67 \times 10^{-13} \bar{g} \lambda_0^2 B_{\parallel} \frac{\partial I}{\partial \lambda}$$

A common assumption made in stellar magnetic field studies.

- Summing surface contributions with varying B , μ , V_D , T , $[\text{Fe}/\text{H}]$...
- Complex Stokes signatures depending on B and P_{ROT} (cancellation effects).



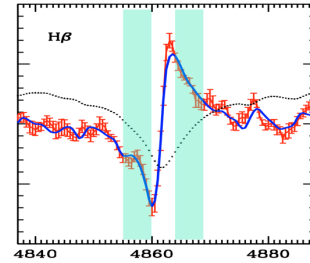
Reiners (2012)

Observational techniques used in stellar magnetic field studies:

- Photopolarimetry
 - Narrow-band (Stokes V) \longrightarrow
 - Broad-band (Stokes Q-U) [Limited applicability]

Zeeman effect in the wings of broad lines (e.g. H β)

$$(V_r - V_b)/2 = 4.67 \times 10^{-13} \bar{g} \lambda^2 \langle B_z \rangle dI/d\lambda$$



Landstreet (1982)

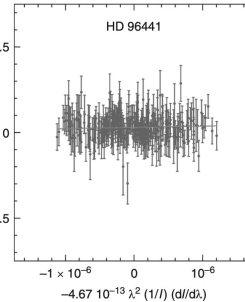
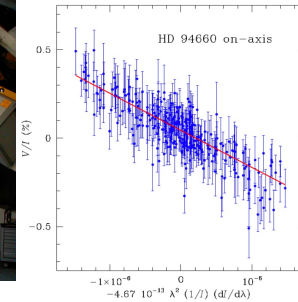
Typically applied to broad-line early type stars
(typical error: ~50 G).

- Spectropolarimetry
 - Low resolution ($\lambda/\Delta\lambda \sim 1000 - 5000$) \longrightarrow
 - Medium resolution ($\lambda/\Delta\lambda \sim 5000 - 20000$) [No instruments currently available]
 - High resolution ($\lambda/\Delta\lambda \sim 30000 - 120000$)

Zeeman effect in H lines and in unresolved blends



FORS1/2@VLT



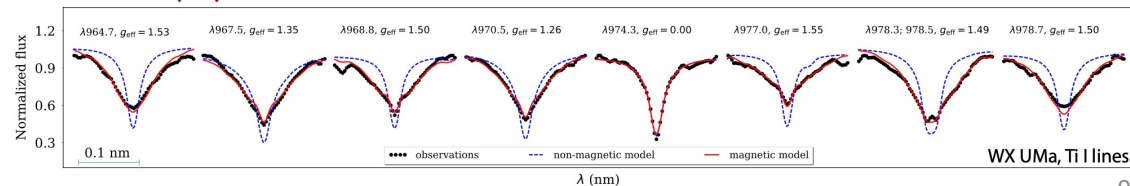
Bagnulo+ (2002)

$$\frac{V}{I} = -4.67 \times 10^{-13} \bar{g} \lambda^2 \langle B_z \rangle \frac{1}{I} \frac{dI}{d\lambda}$$

Precision for bright targets ~20 – 30 G.

- Spectroscopy
 - Zeeman broadening (ZB) / intensification (ZI) of magnetic sensitive lines \longrightarrow

Requires: $|B| \geq 0.5 - 1$ kG, (slow rotators), S/N > 200



WX UMa, Ti II lines

Shulyak+ (2017)

High resolution (night-time) spectropolarimetry

NARVAL@TBL

ESPaDOnS@CFHT

HARPSpol@ESO-3.6m



D: 2 m
R ~ 65000
370 – 1050 nm

D: 3.6 m
R ~ 70000
370 – 1050 nm

D: 3.6 m
R ~ 110000
378 – 691 nm

$$\Delta\lambda = 4.67 \times 10^{-13} g_{\text{EFF}} B \lambda^2$$



$$\Delta\nu = 1.4 \lambda_0 g_{\text{EFF}} B$$

$$V(\lambda) \approx -\Delta\lambda_B \bar{g} \cos\theta \frac{\partial I}{\partial \lambda} = -4.67 \times 10^{-13} \bar{g} \lambda_0^2 B_{\parallel} \frac{\partial I}{\partial \lambda}$$

For the typical values of the involved quantities, the Zeeman signature is **below the sensitivity** of current instrumentation.

Solution: Multi – Line Technique

Least Squares Deconvolution (LSD)

(Donati et al. 1997; Kochukhov et al. 2010)

“Add” the polarization signal throughout the entire spectral range.

$$I(v) = 1 - \sum_i w_I^i Z_I(v - v^i), \quad w_I^i = d_i$$

Sum over all spectral lines (i)

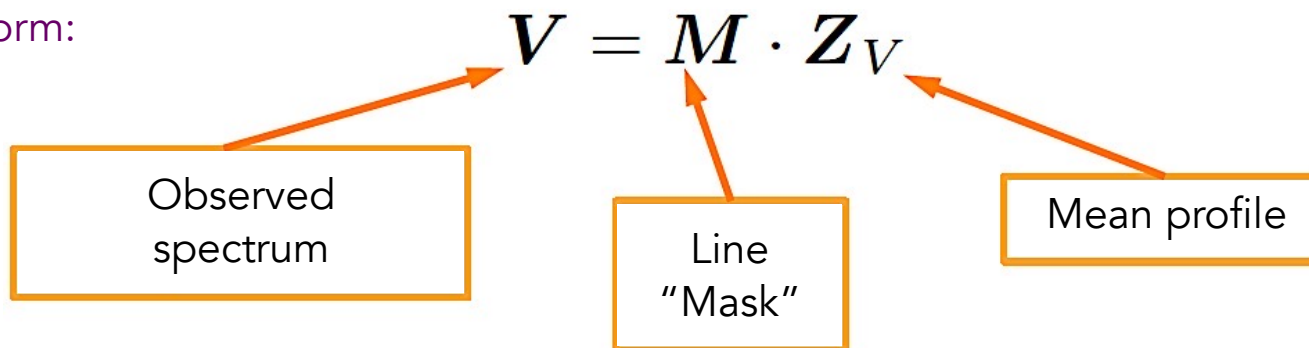
$$V(v) = \sum_i w_V^i Z_V(v - v^i, \mathbf{B}), \quad w_V^i = \bar{g} \lambda_i d_i$$

• Self-Similarity

$$Q(v) = \sum_i w_Q^i Z_Q(v - v^i, \mathbf{B}), \quad w_Q^i = \bar{G} \lambda_i^2 d_i$$

• Scaled by depth and the Landé factors

Matrix form:



Mean profile for a given line mask and observed spectra:

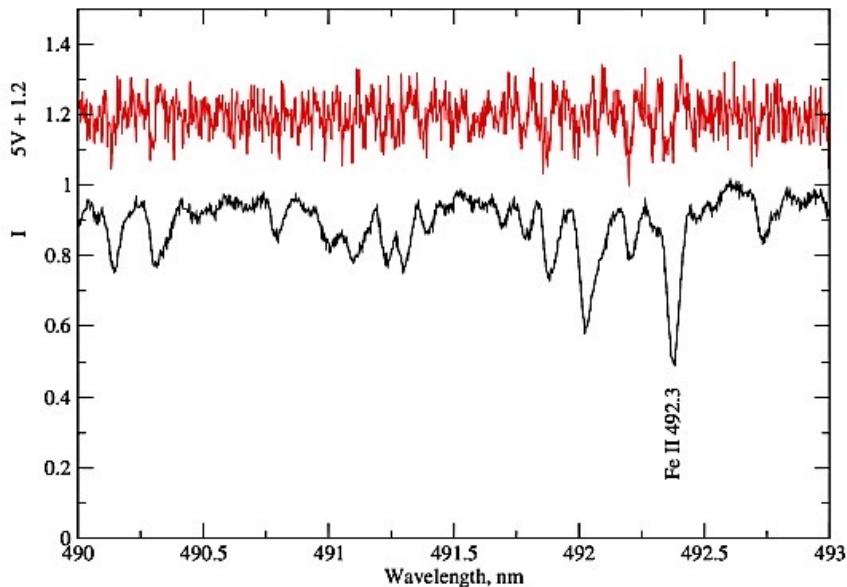
$$\mathbf{Z}_V = \underbrace{(\mathbf{M}^T \cdot \mathbf{S}^2 \cdot \mathbf{M})^{-1}}_{\text{Inverse Auto-Correlation Matrix}} \cdot \underbrace{\mathbf{M}^T \cdot \mathbf{S}^2 \cdot \mathbf{V}}_{\text{Weighted Cross Correlation}}$$

S: Inverse Variance
(errors)

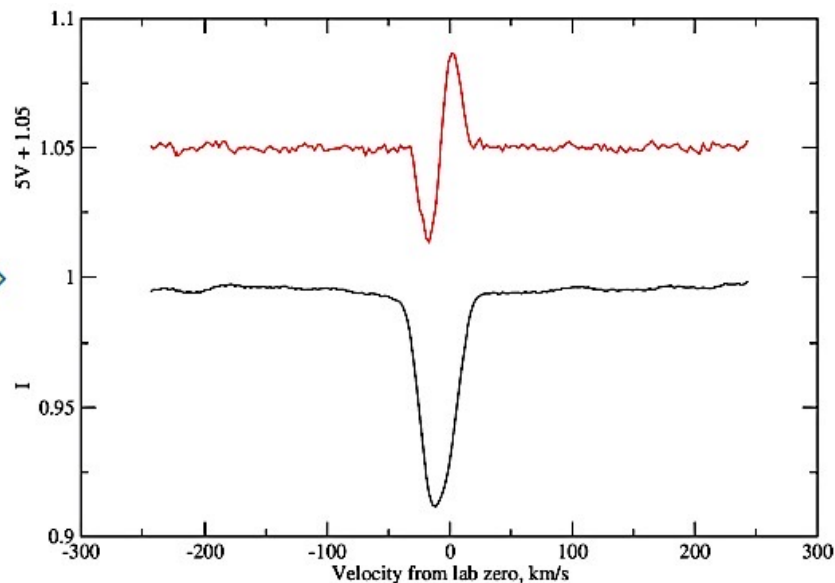
Inverse Auto-Correlation Matrix

Weighted Cross
Correlation

(Kochukhov+ 2010)



Observed Stokes I and V spectra



LSD Stokes I and V profiles

SNR Gain $\sim \sqrt{N}$

N: Number of spectral lines included

Polarimetric Sensitivity: 10^{-5}

Zeeman-Doppler Imaging (ZDI):

Tomographic inversion technique based on time-series of polarized radiation modulated by rotation.

Usually: Only Stokes V

Requires: Good Phase Coverage

Requires: Stellar Parameters

Assumes: Static Magnetic Field

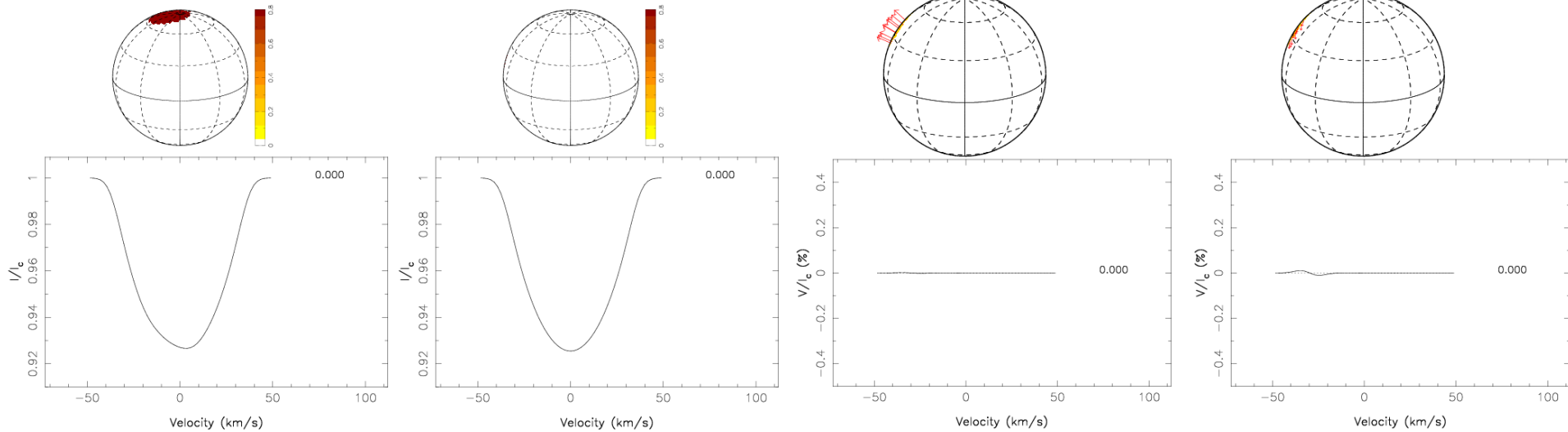
Ideally: Combined with DI

Includes: Regularization function

Recovers: The large-scale magnetic field distribution on the stellar surface (ZDI maps)

Brightness mapping (DI)

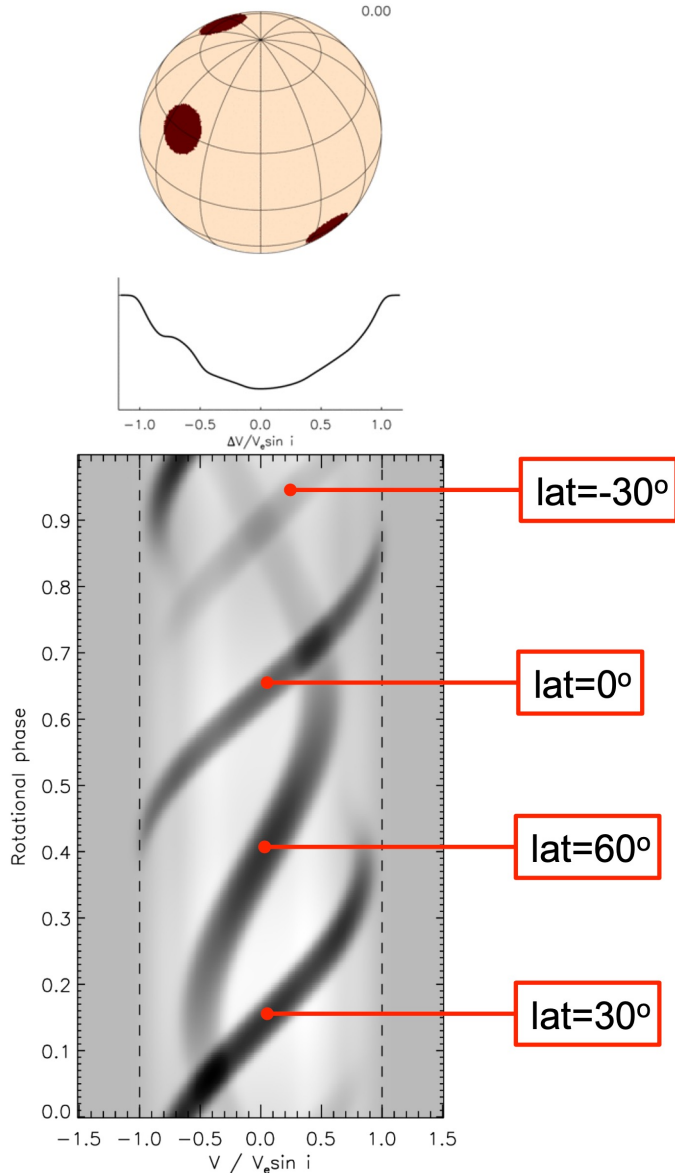
Magnetic field mapping (ZDI)



Credit: J.-F. Donati

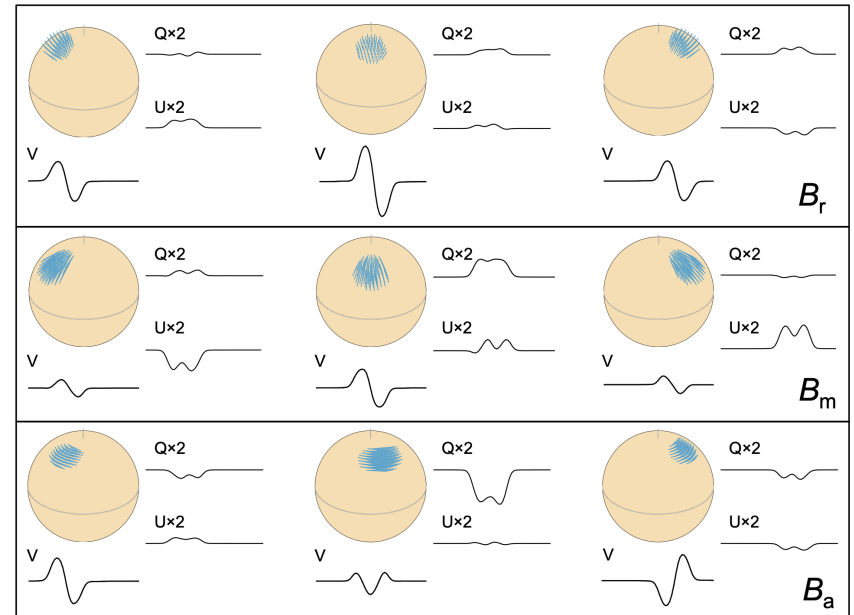
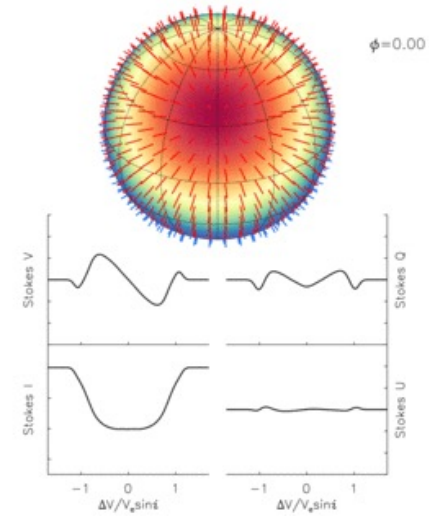
Doppler Imaging (DI):

Distortions travel across the line as the star rotates profile.
 [feature latitude – stellar inclination]



Zeeman-Doppler Imaging (ZDI):

Same principles as DI + Zeeman effect information.
 [Stokes profiles variation over P_{ROT} time-scales]



Credit: O. Kochukhov and L. Rosén

Spatial resolution of DI/ZDI reconstructions

The spatial resolution is controlled by multiple factors each one affecting the final map in a separate manner:

- **Latitude**: from the velocity position of the distortion
- **Longitude**: from the time-series behavior / phase coverage
- **Map spatial resolution**:

- A single exposure: **[at the stellar equator]**

$$\delta l = 90^\circ \frac{\Delta \lambda}{\lambda} \frac{v_c}{v_e \sin i}$$

- Spectropolarimetric time-series: $\delta l \sim 360^\circ \cdot \Delta \phi$

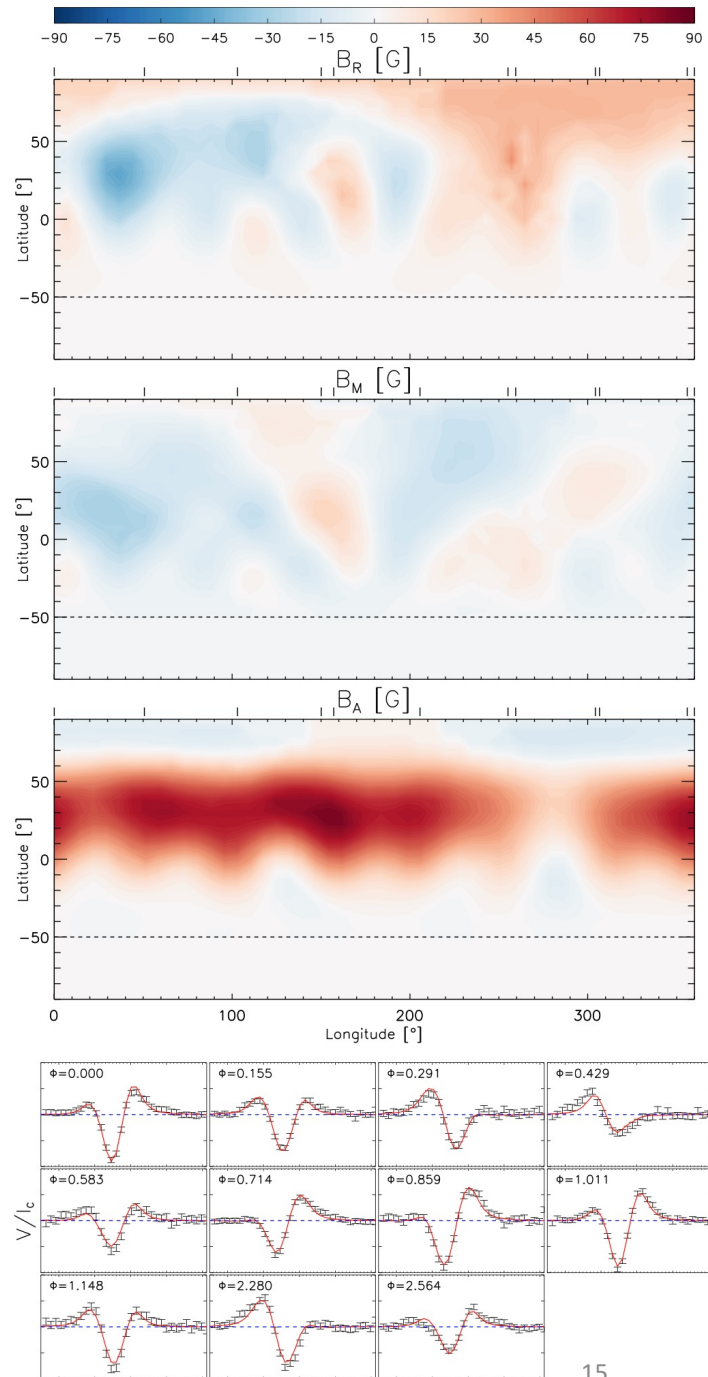
↓
Observing phase coverage difference [Average]

- Visible surface fraction: **Stellar inclination**

Example: ZDI reconstruction of HD 1237 using HARPSpol [R = 120000]:

- Single exposure: $\delta l = 42.45^\circ$
- Time-series: $\delta l \approx 34.20^\circ$

HD 1237 (G8V)
 M = 1.0 M_⊙
 P_{ROT} = 7.7 days
 T_{EFF} ≈ 5572 K
 vsin(i) = 5.3 km/s

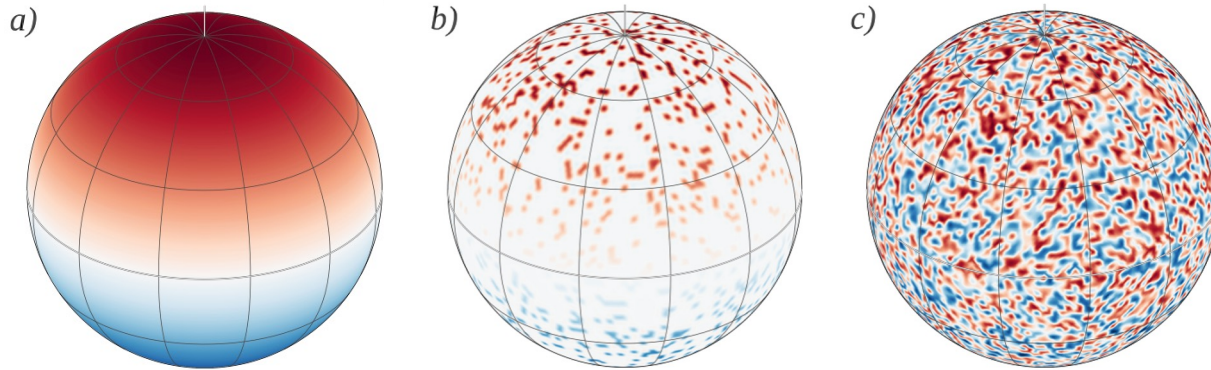


(Alvarado-Gómez+ 2015)

Regularization in DI/ZDI inversions

The 1D time-series to 2D image reconstruction attempted by DI/ZDI is an **ill-posed inverse problem** (Goncharskij+ 1977).

There are infinite possible surface magnetic field distributions that could give rise to the observed spectropolarimetric time-series.



(Kochukhov 2021)

Regularization procedure:

Find the simplest solution that reproduces the observations [Occam's razor]

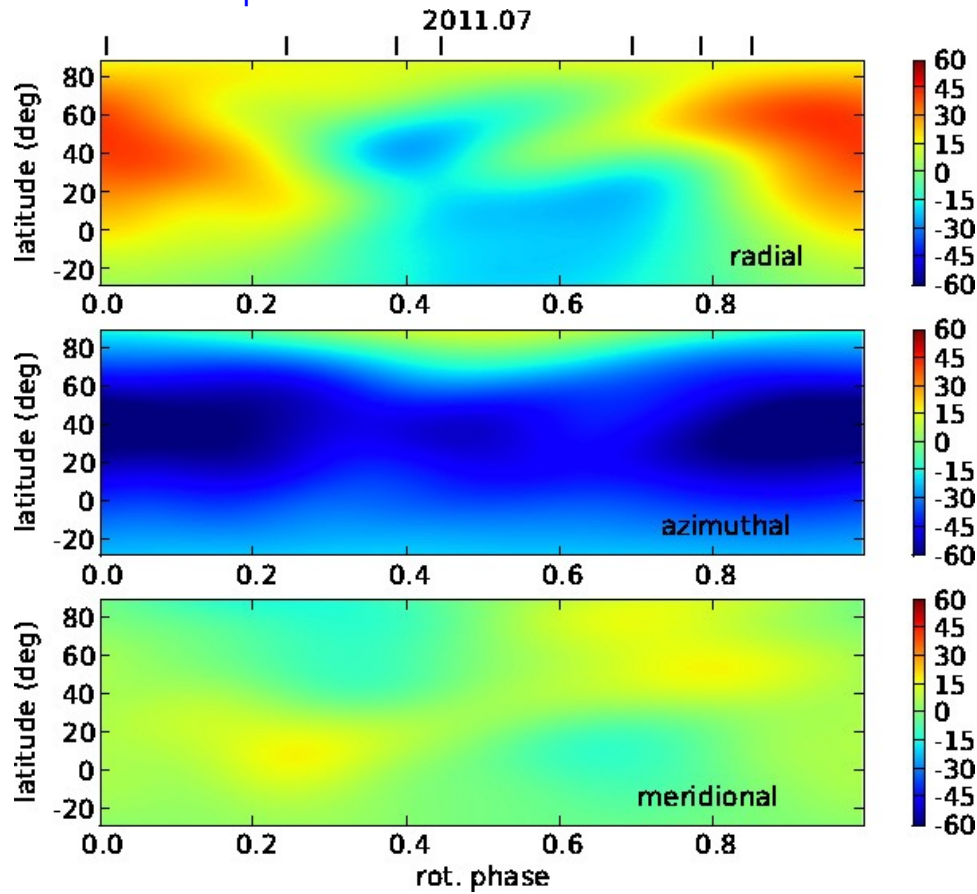
- **Tikhonov regularization**: Small local gradients (Tikhonov & Arsenin 1977)
- **Maximum entropy**: Minimum information content (Skilling & Brian 1984)

[Both procedures give similar results]

Regularization achieves:

- Uniqueness and stability of the reconstruction
- **Avoid over-fitting (noise)**
- Convergence to a global minimum [$\chi^2 + R(x) \rightarrow \min$]
- Grid-independent solutions

Some examples:



Morgenthaler et al. (2012)

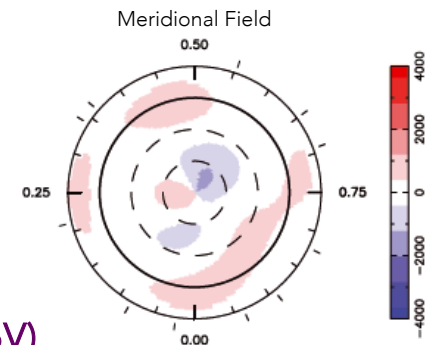
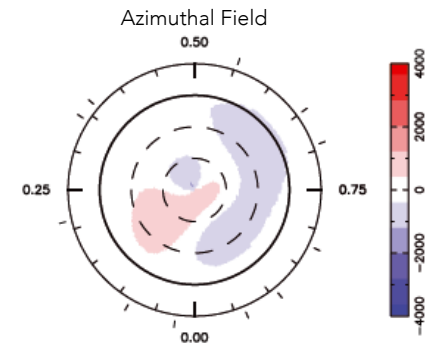
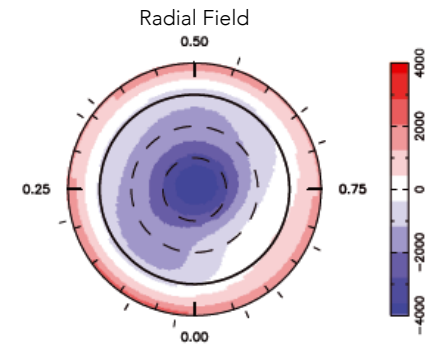
ξ Boo A (G8V)

$M = 0.85 M_{\odot}$

$P_{\text{ROT}} = 6.43$ days

$T_{\text{EFF}} = 5600$ K

$v \sin(i) = 3.0$ km/s



Morin et al. (2010)

WX UMa (M6V)

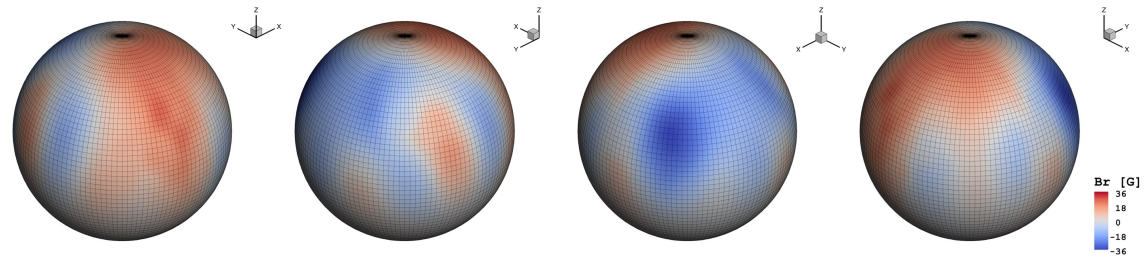
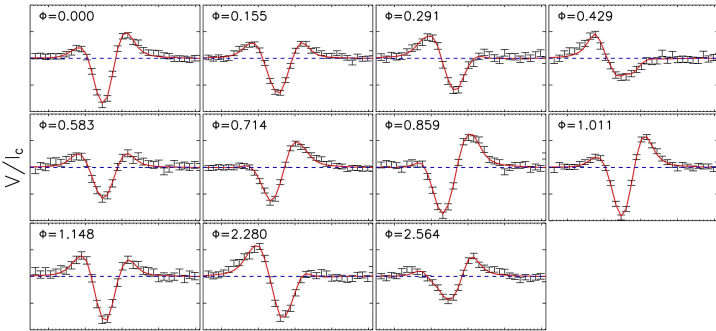
$M = 0.1 M_{\odot}$

$P_{\text{ROT}} = 0.78$ days

$T_{\text{EFF}} \approx 2800$ K

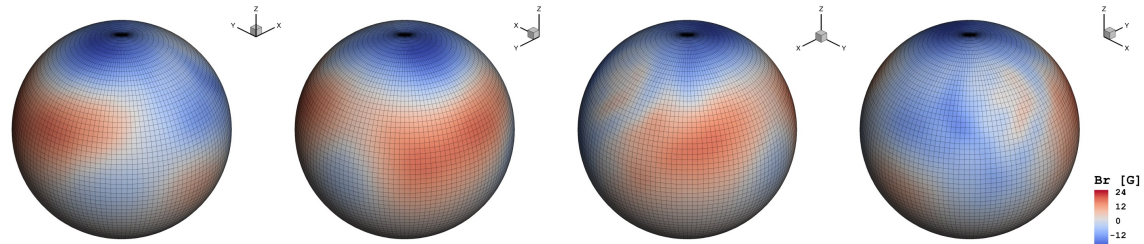
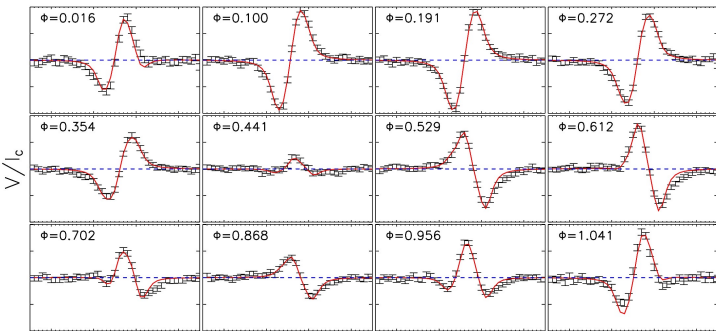
$v \sin(i) = 5.0$ km/s

HD 1237 (G8V, ~880 Myr)



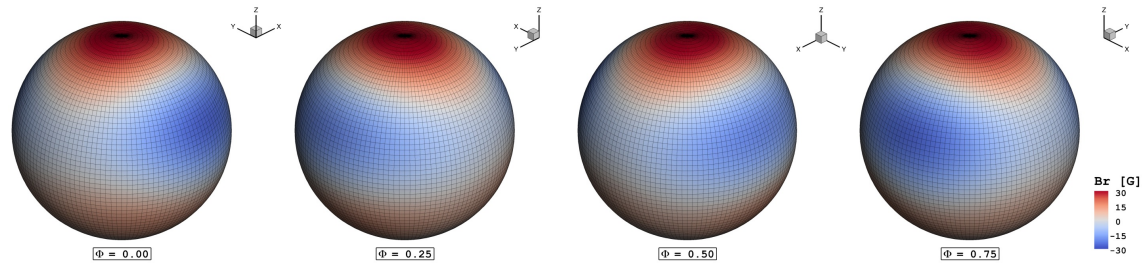
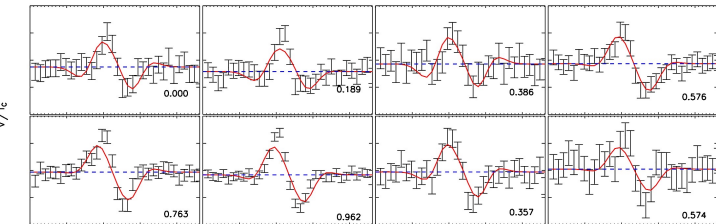
Alvarado-Gómez et al. (2015)

ϵ Eridani (K2V, ~440 Myr)



Piskunov et al. (2011); Jeffers et al. (2014); Alvarado-Gómez et al. (2016a)

HD 147513 (G5V, ~450 Myr)

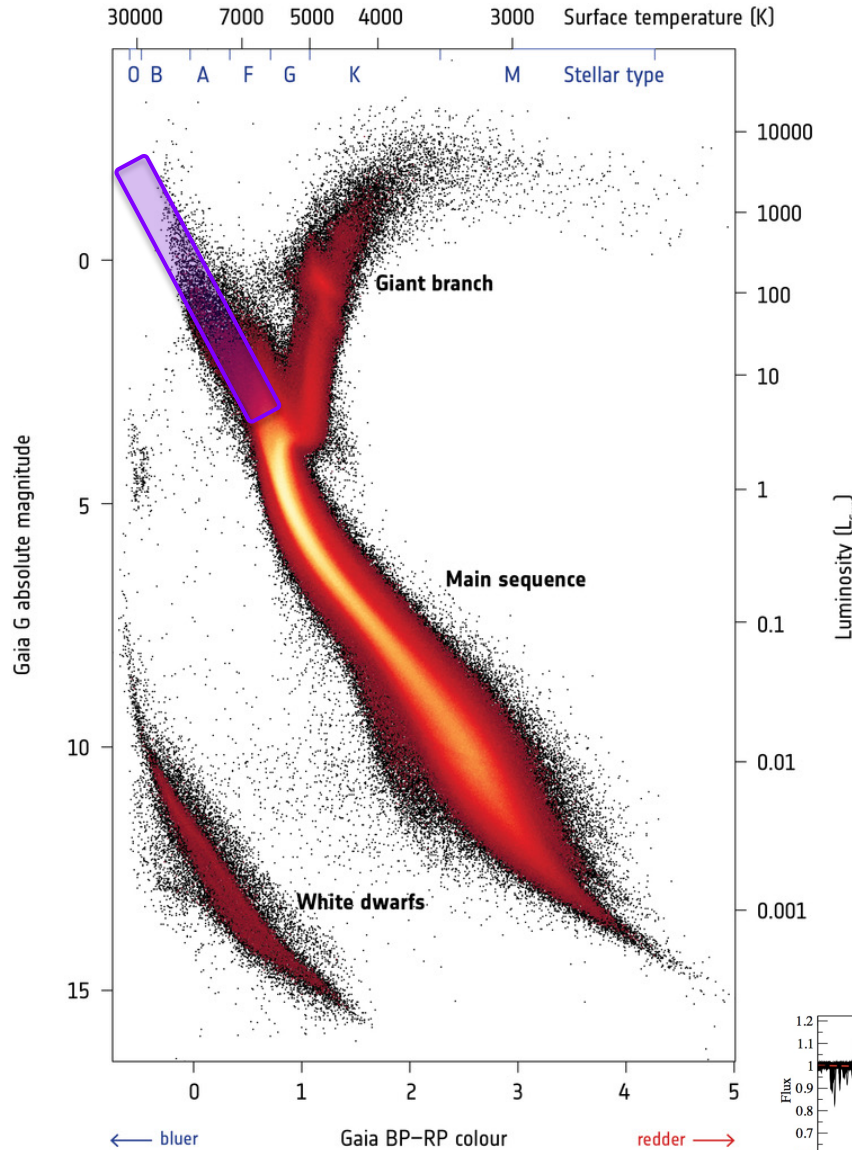


Hussain, Alvarado-Gómez et al. (2016)

Magnetism across the H-R diagram

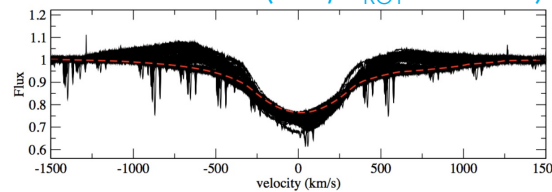
Intermediate mass and massive stars (Main Sequence)

$$[1.5 M_{\odot} \leq M_{\star} < 8 M_{\odot} \mid M_{\star} \geq 8 M_{\odot}]$$

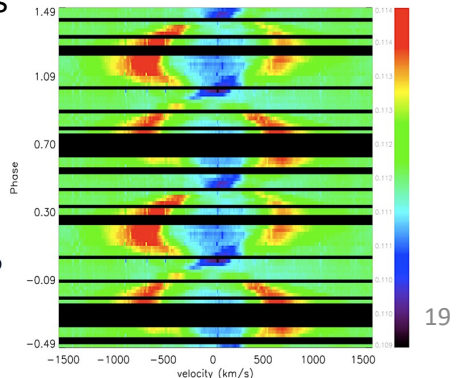


- Around 10% of O to early-F type stars have strong global fields
- Observed field strengths: from ~ 0.1 kG to 34 kG
- Slow rotation (P_{ROT} up to 100 yr). Fossil origin for the magnetic fields
- Magnetism correlates with *chemical peculiarity* (Bp/Ap stars)
- Extremely periodic rotational modulation:
 - Magnetic fields
 - Photometric variability
 - Line profiles
 - SED
- Evidence for rigid magnetospheres around rapidly-rotating massive stars

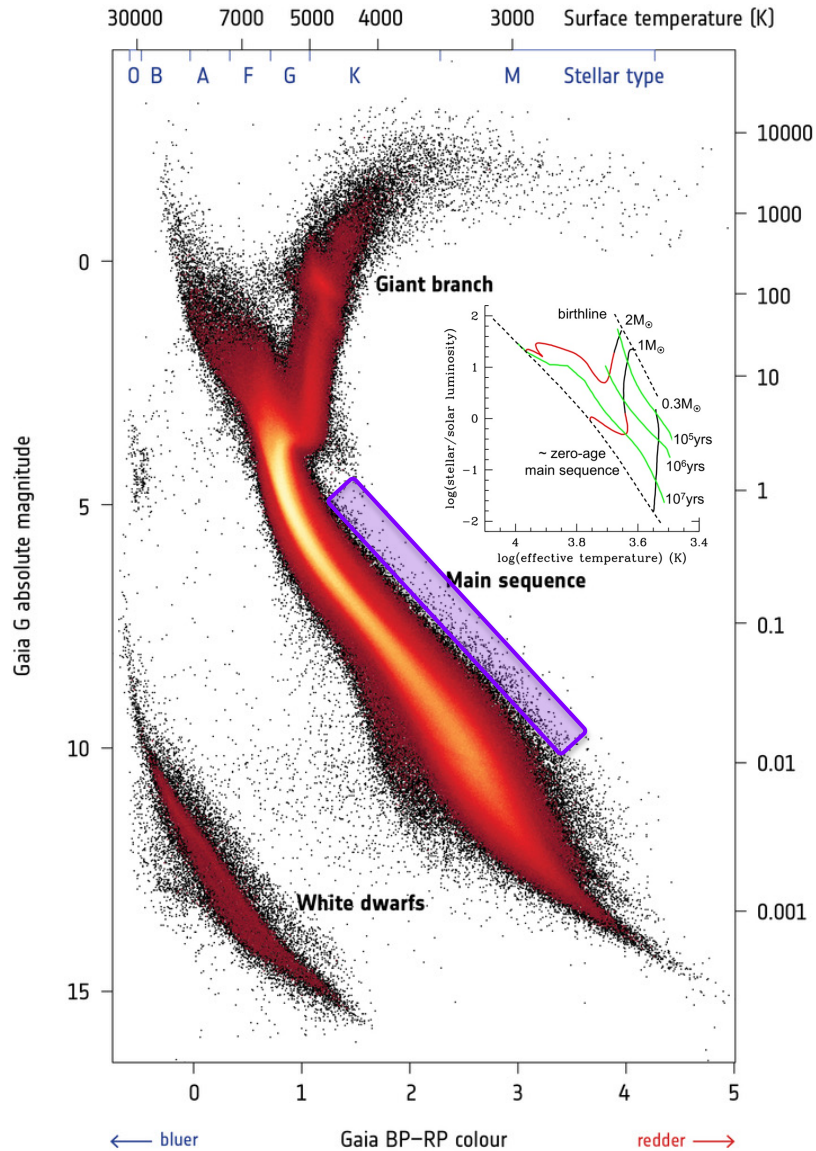
HR 7355 (B2V, $P_{\text{ROT}} = 0.52$ d)



(Grunhut+ 2008)

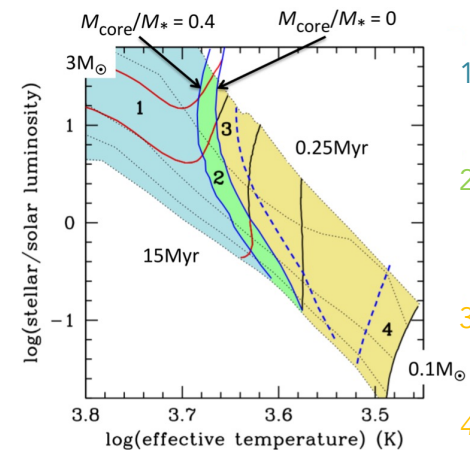


Magnetism across the H-R diagram



Young stars (Pre-main Sequence) [$0.3 M_{\odot} \leq M_{\star} < 2 M_{\odot}$]

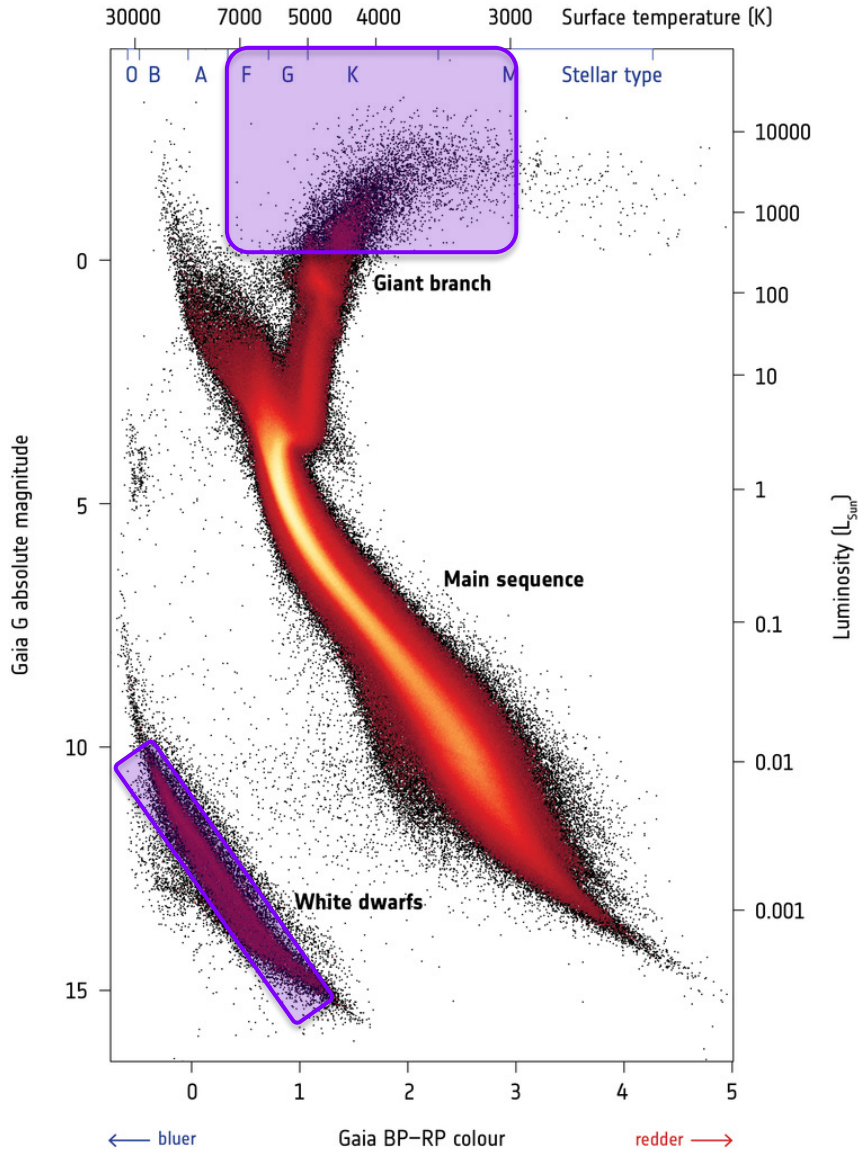
- Complex spectra (highly variable). Obscured/veiled in optical wavelengths.
- All stars appear to be magnetic with detections reported using both, ZB and ZDI.
- ZB Measurements:
 - $|B| \sim 2 - 3$ kG (with multiple components)
 - Observed field strengths do not correlate with stellar properties or accretion rates
- ZDI Measurements:
 - $B_V \sim 0.1 - 2$ kG
 - Large variety of field geometries that appear correlated with stellar mass



1. Complex, non-axisymmetric, weak dipolar components [~ 0.1 kG]
2. Largely axisymmetric. Higher order multipoles dominate (octupole) [~ 0.5 kG]
3. Axisymmetric, often strong dipolar fields (\sim kG). Close to the fully-convective limit
4. Possible additional topologies.

(Gregory+ 2012, 2013)

Magnetism across the H-R diagram

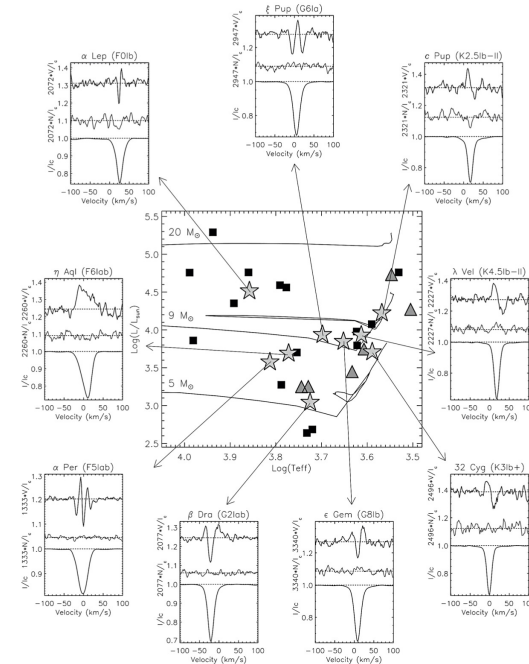


Giant I Super-Giant stars (Post-main Sequence)

$$[3 M_{\odot} \leq M_{\star} < 20 M_{\odot}]$$

(Grunhut+ 2010)

- Signatures of complex and relatively weak (< 1G) magnetic fields
- No ZDI maps available (prohibitively long P_{ROT})
- Incidence of magnetic fields could be as high as 67% (F to M) [Low-number statistics]
- Dynamo action (B-flux conservation)



White dwarfs (Post-main Sequence)

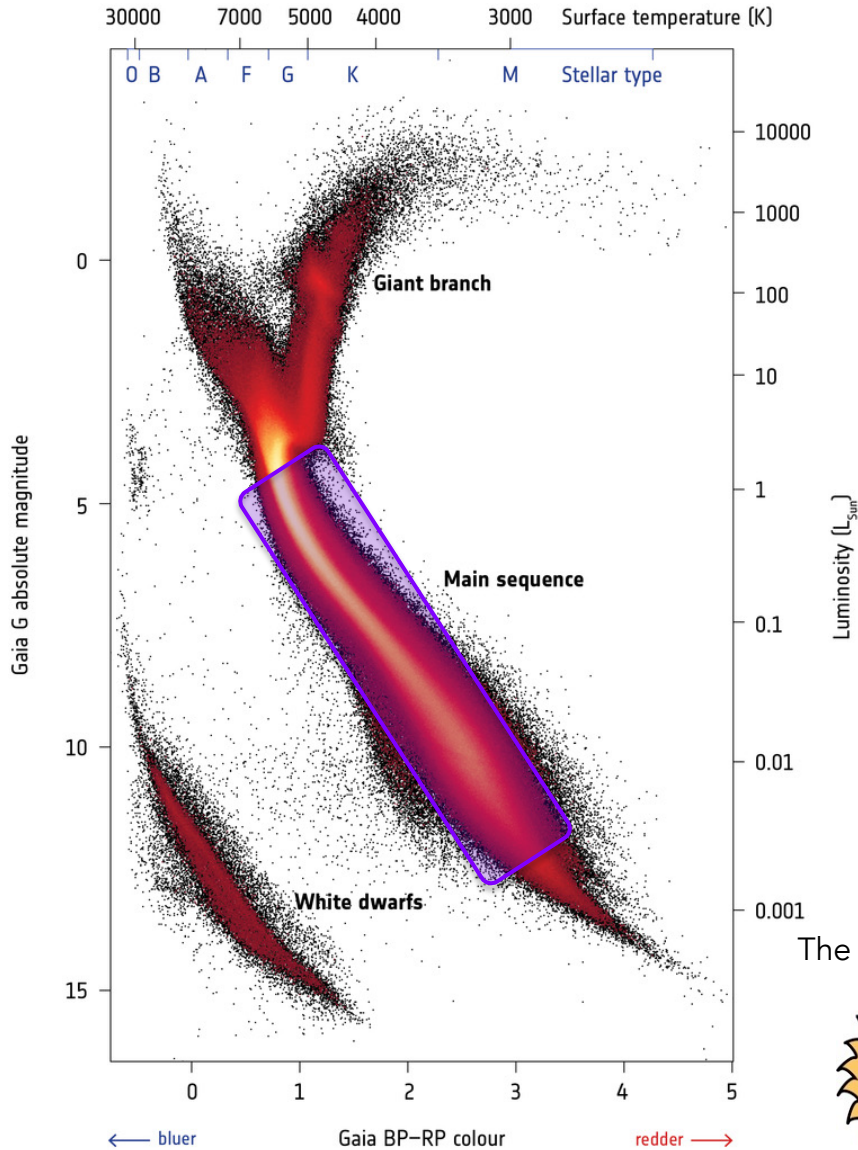
$$[0.17 M_{\odot} \leq M_{\star} < 1.33 M_{\odot}]$$

- About 10% of WDs are magnetic with field strengths between $10^5 - 10^9$ G (B-flux conservation)
- Relatively stable periodic variations in the field indicating simple geometries (confirmed by ZDI)
- Magnetic WDs tend to be more massive than average (mergers?)
- Very strong B: more sophisticated Zeeman treatment

Magnetism across the H-R diagram

Cool Stars (Main Sequence)

$$[0.08 M_{\odot} \leq M_{\star} < 1.5 M_{\odot}]$$



- All stars have magnetic fields.
- Observed field strengths:
 - Sun-like stars: 1 G up to ~1 kG
 - M-dwarf stars: 1 – 2 kG (ZDI) | 1 – 8 kG (ZB)
- Observed field topologies:
 - Sun-like stars: Complex, evolving fields
 - M-dwarf stars: Mixed behaviour
- Sun-like stars: Magnetic field properties correlated with rotation (age) and activity indicators (Ca HK, X-rays). Cyclic behavior observed (ZDI)
- M-dwarf stars: Apparent bi-modality (ZDI) with respect to rotation and activity proxies (X-rays, H α). Field strength correlated with Rossby number (Ro)
- ~150 cool main sequence stars have ZDI maps

The BCool Project



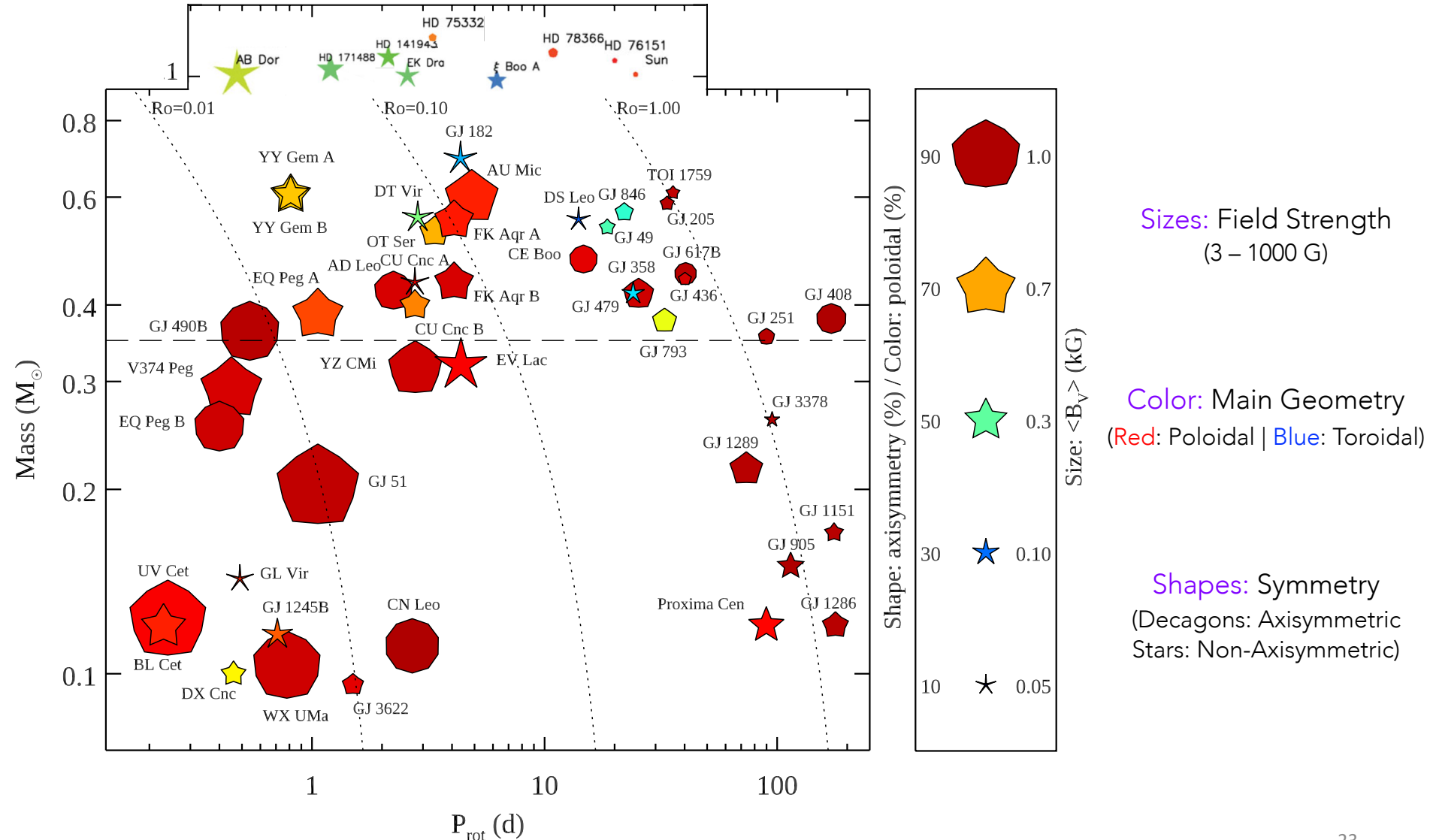
UPPSALA
UNIVERSITET



<https://bcool.irap.omp.eu>

The "Confusogram"

Donati & Landstreet (2009); Donati (2011); Kochukhov (2021)



Instrumentation in High-Resolution Spectropolarimetry



D = 2 m | R ~ 65000
 $\lambda \sim 370 - 1050$ nm



D = 3.6 m | R ~ 70000
 $\lambda \sim 370 - 1050$ nm



D = 3.6 m | R ~ 120000
 $\lambda \sim 378 - 691$ nm

New instruments/upgrades:



RV precision < 3 m/s
Now observing!



R ~ 75000 | $\lambda \sim 0.98 - 2.35$ μ m
RV precision ~ 1 m/s
Now observing!



R ~ 50k / 100k | $\lambda \sim 1.0 - 2.7$ μ m
RV precision ~ 1–2 m/s
[8m-class telescope]
Now observing!

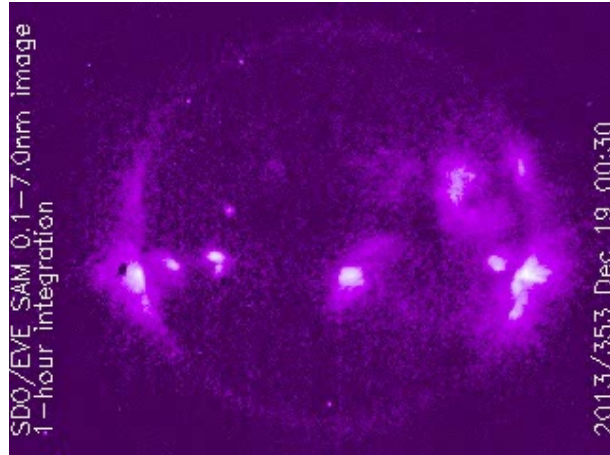


R ~ 120k | $\lambda \sim 384 - 913$ nm
RV precision ~ 1–2 m/s
[8m-class telescope]
Now observing!

Studying the Space Weather in Cool Main-Sequence Stars (Part I: Quiescence)

What constitutes the "Space Weather" of a given system?

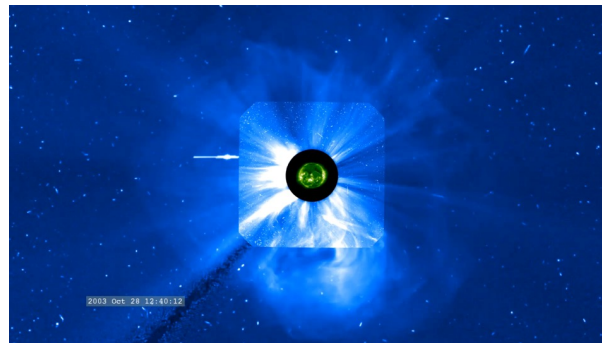
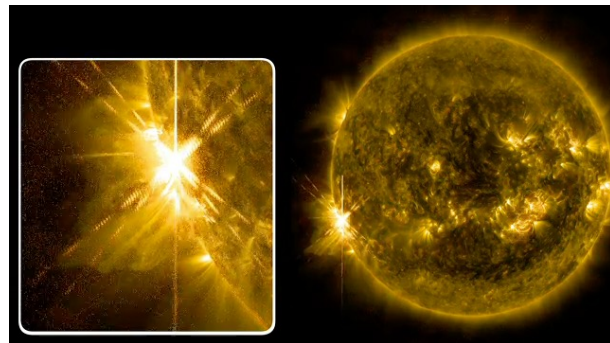
High-Energy Emission



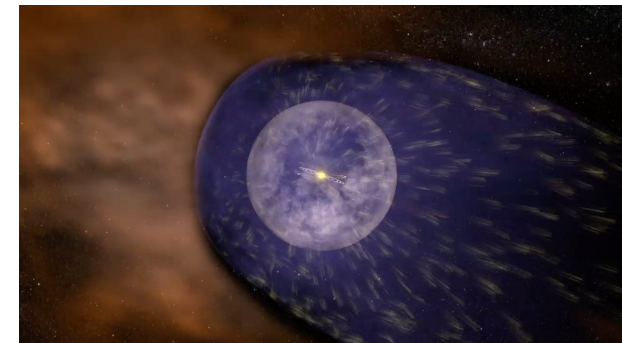
Corona/Stellar Wind Structure + Planetary Conditions



Transient Phenomena (Flares/CMEs/EPs)



Astrospheres



NASA Goddard (SVS)

Advanced Observational Techniques



Detailed Numerical Simulations

The solar corona

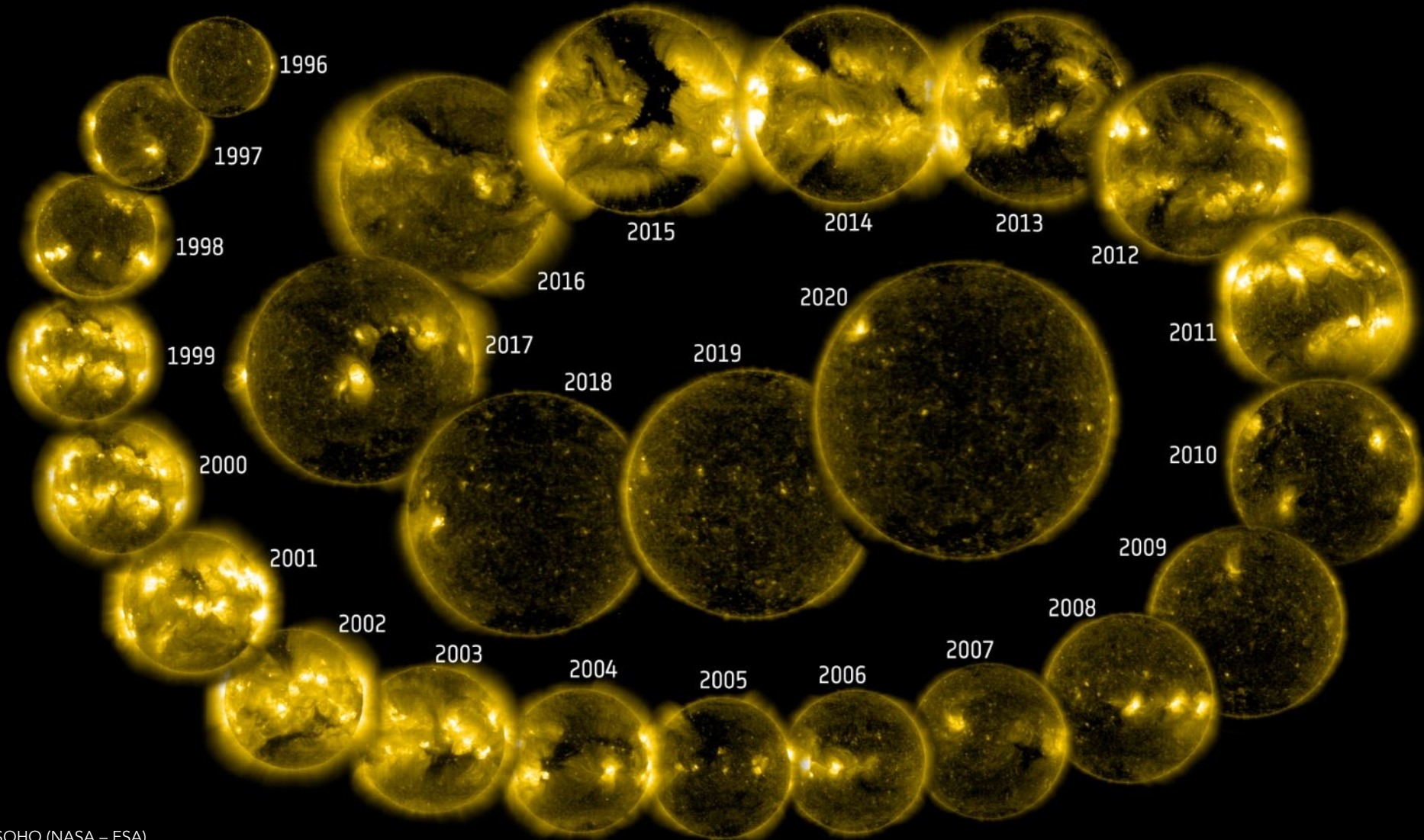
Outermost part of the solar atmosphere.

Consists of a rarefied ($\sim 10^8 - 10^9 \text{ cm}^{-3}$) and hot ($\sim 10^6 \text{ K}$) plasma.



Emission centered around the Extreme Ultraviolet (EUV) and X-ray wavelengths.
Constitutes the base of the solar wind.

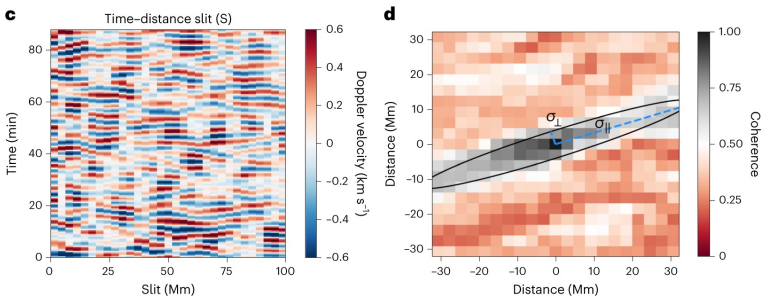
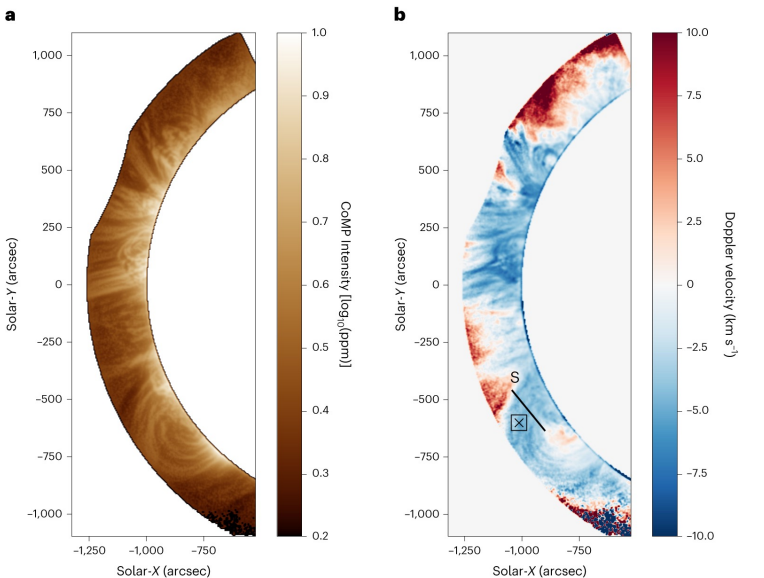
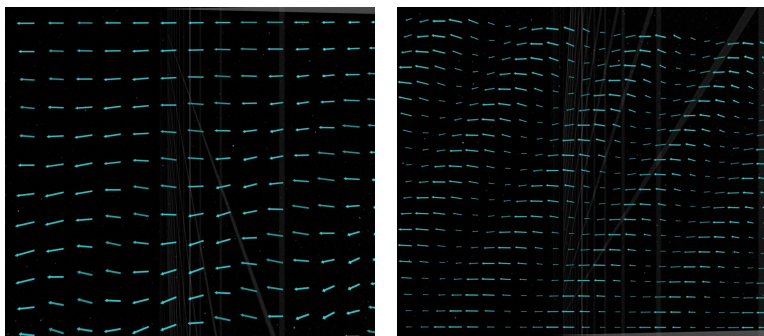
Coronal heating problem: unsolved but with consensus on a **magnetic origin**.



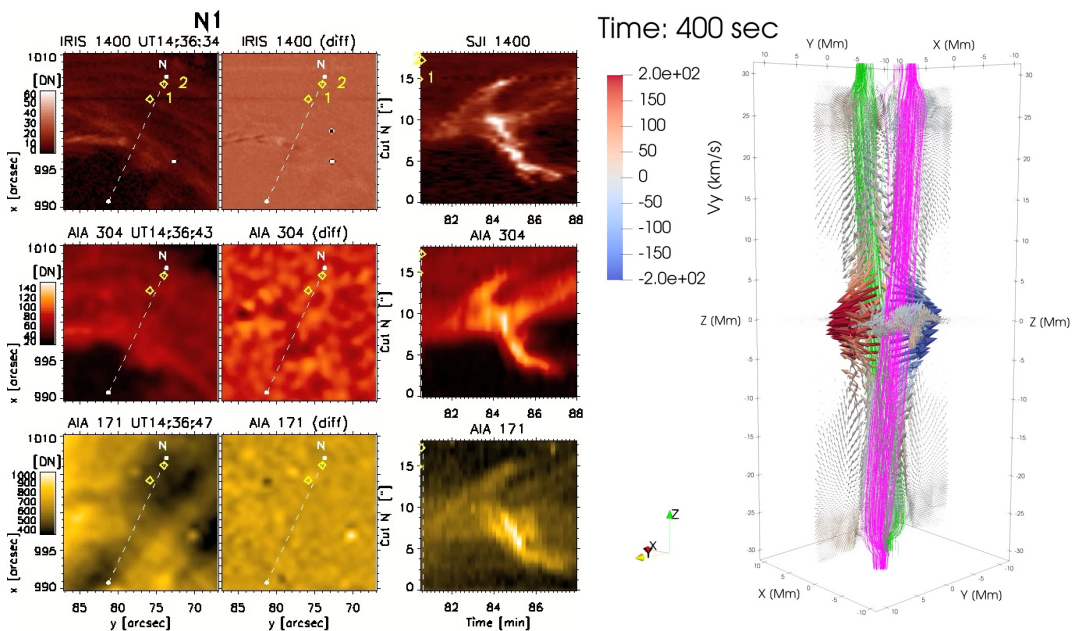
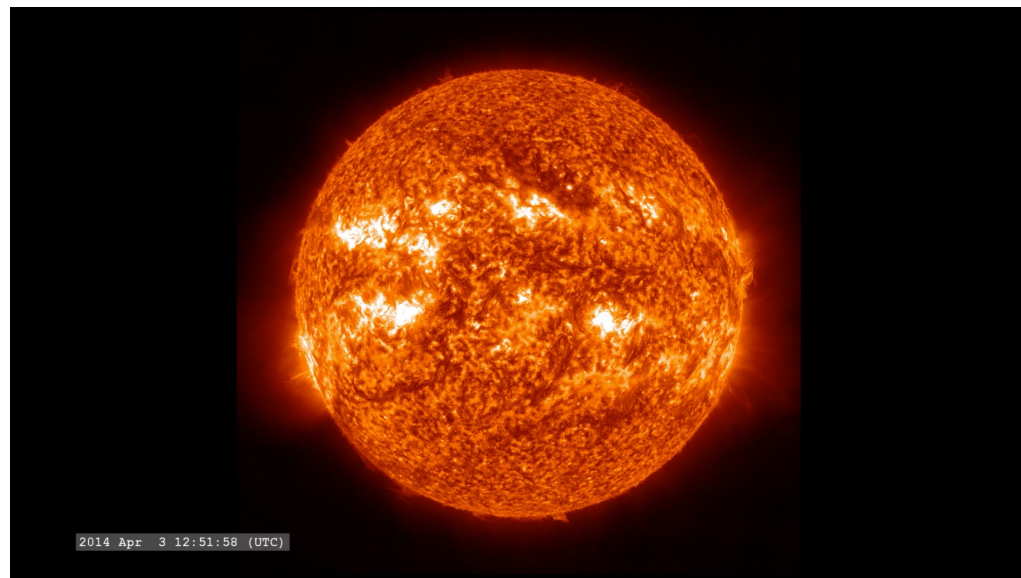
SOHO (NASA – ESA)

EUV images of the Solar Coronal Cycle
(Fe XV filter at 284 Å | $T \sim 2.0 \times 10^6$ K).

Alfvén waves & Nanoflares (steady & impulsive heating)



Sharma & Morton (2023)

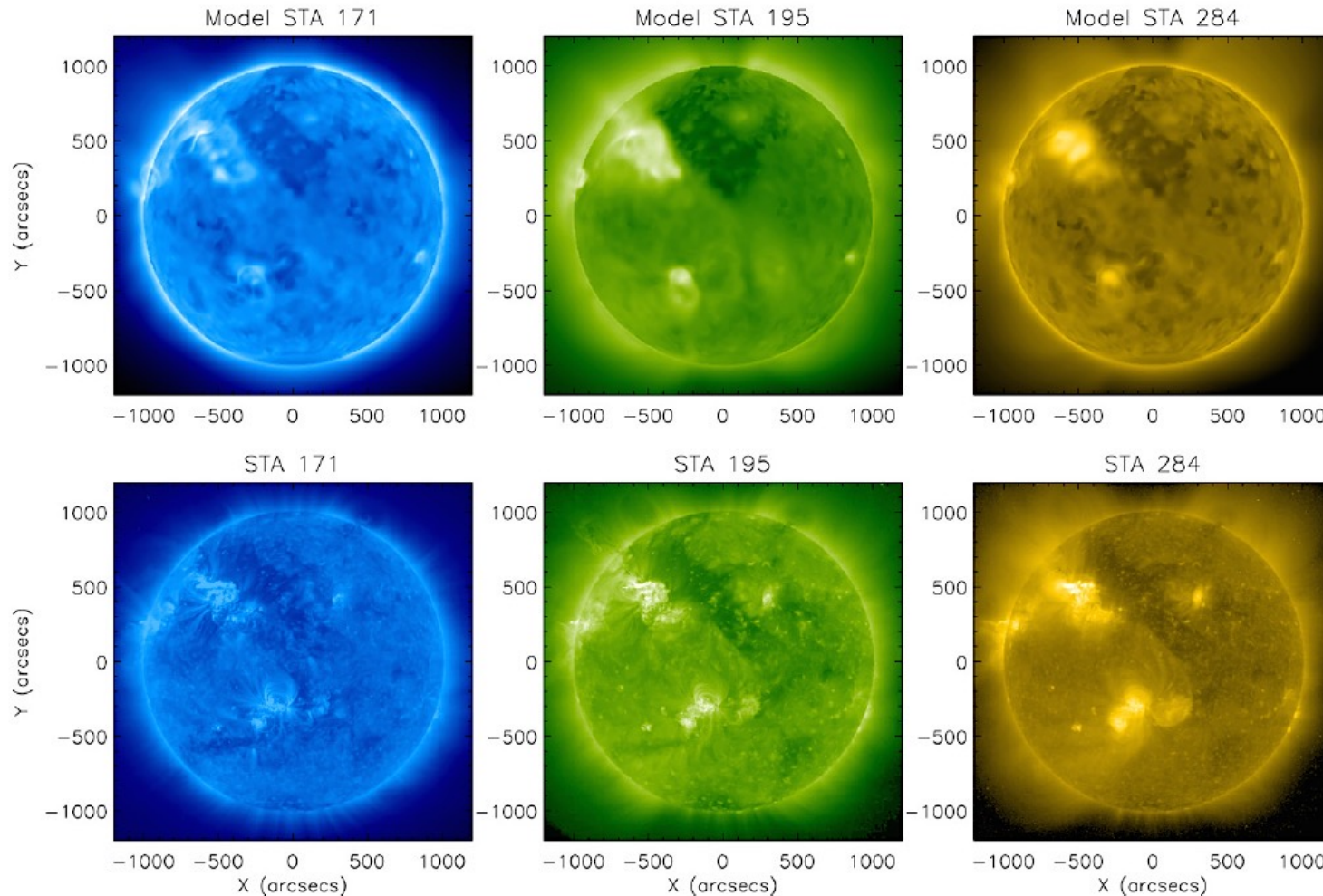


Antolin+ (2021)

The Alfvén Wave Solar Model (AWSoM)

State-of-the-art 3D MHD code incorporating Alfvén wave turbulence dissipation + radiative cooling + electron heat conduction... Driven by the surface magnetic field.

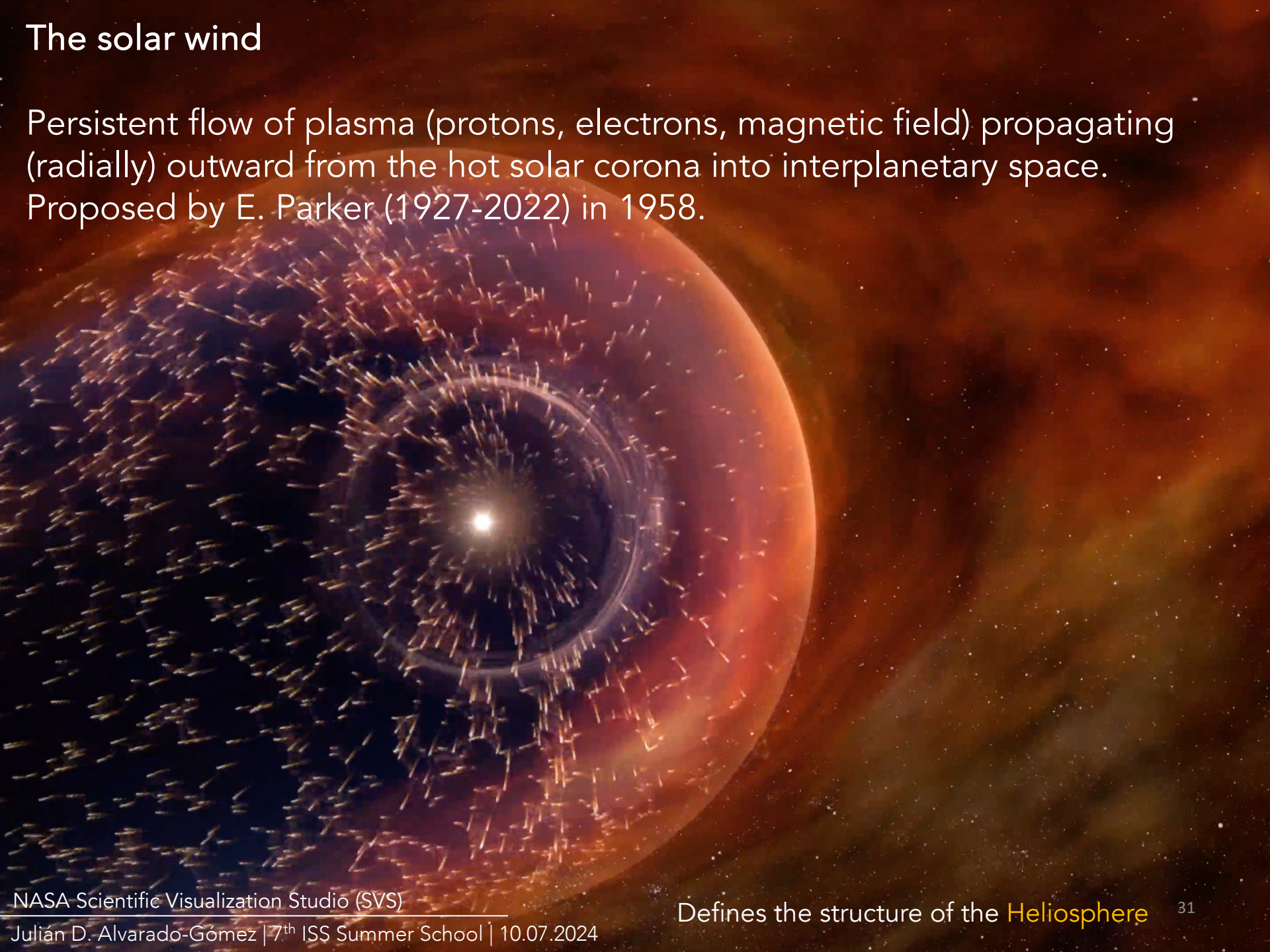
Part of the Space Weather Modelling Framework – SWMF (Gombosi+ 2018)



van der Holst et al. (2014)

The solar wind

Persistent flow of plasma (protons, electrons, magnetic field) propagating (radially) outward from the hot solar corona into interplanetary space. Proposed by E. Parker (1927-2022) in 1958.



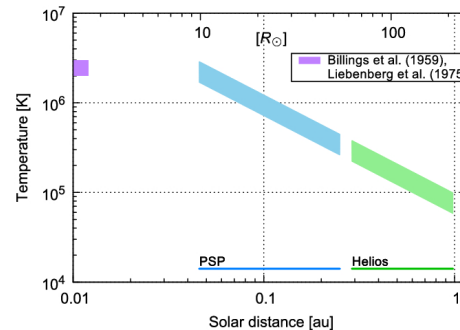
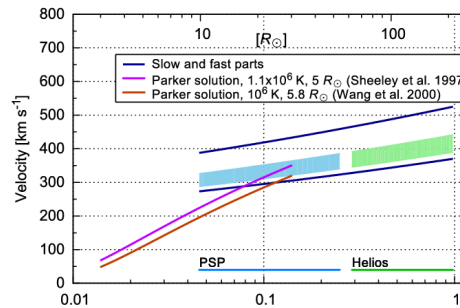
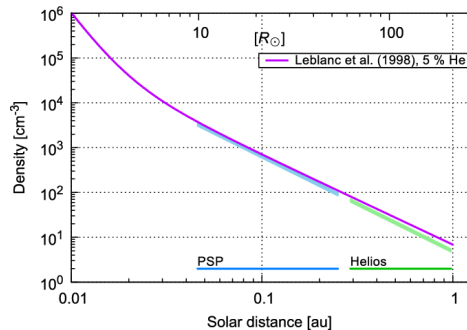
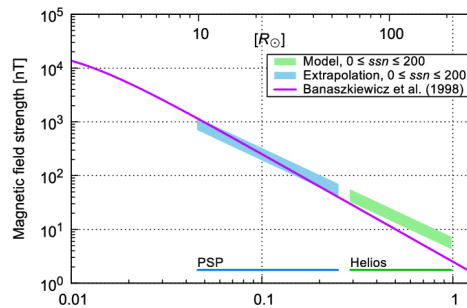
Classically divided in two components:

Fast (~400 – 800 km/s) | Slow (~250 – 400 km/s) [at 1 au]

Differences extend well beyond their speeds:

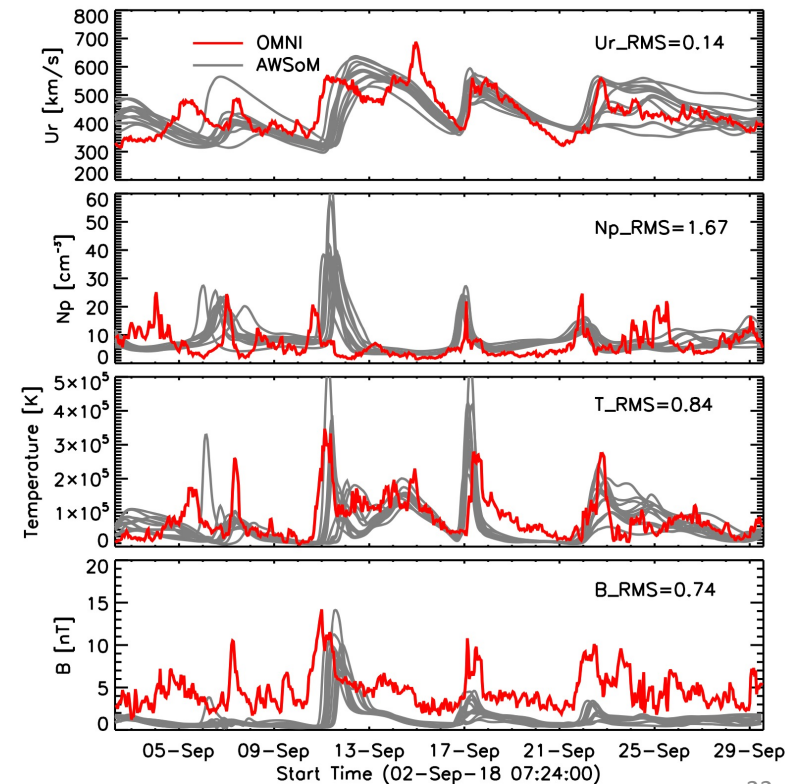
- Origin **Fast: Coronal holes** | **Slow: Streamers near the current sheet** [?]
- Densities **Fast: low** [a few cm^{-3} at 1 au] | **Slow: high** [tens of cm^{-3} at 1 au]
- Composition: **Fast: (nearly) Photospheric** | **Slow: \uparrow low-FIP elements** [x3-4]
- Kinetic properties

Radial profiles



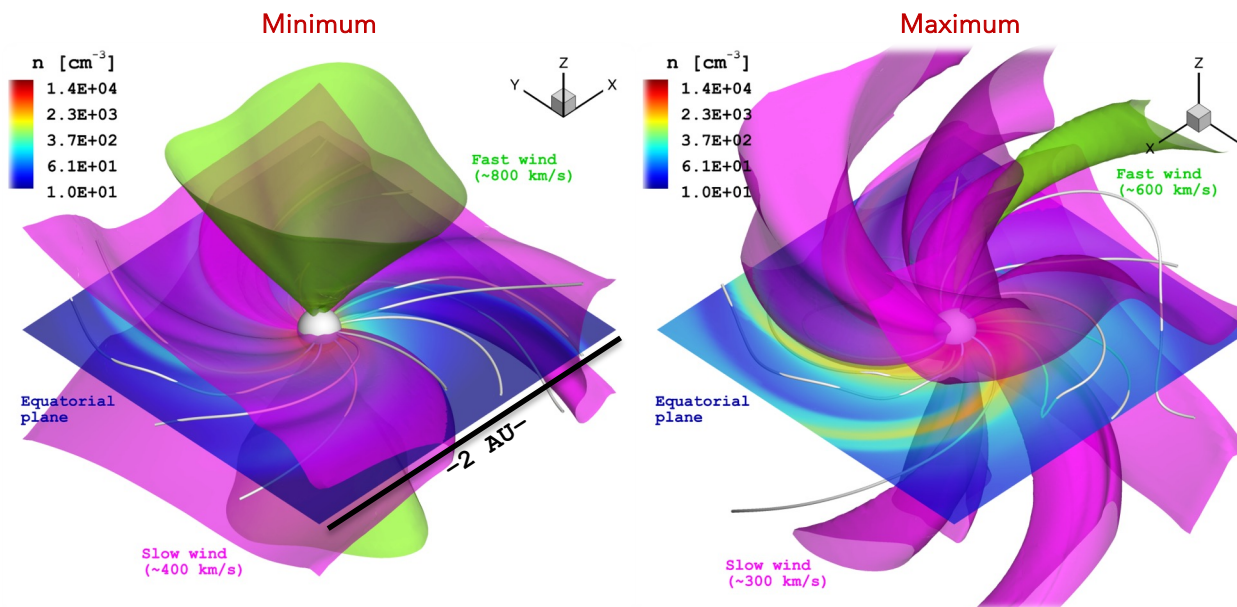
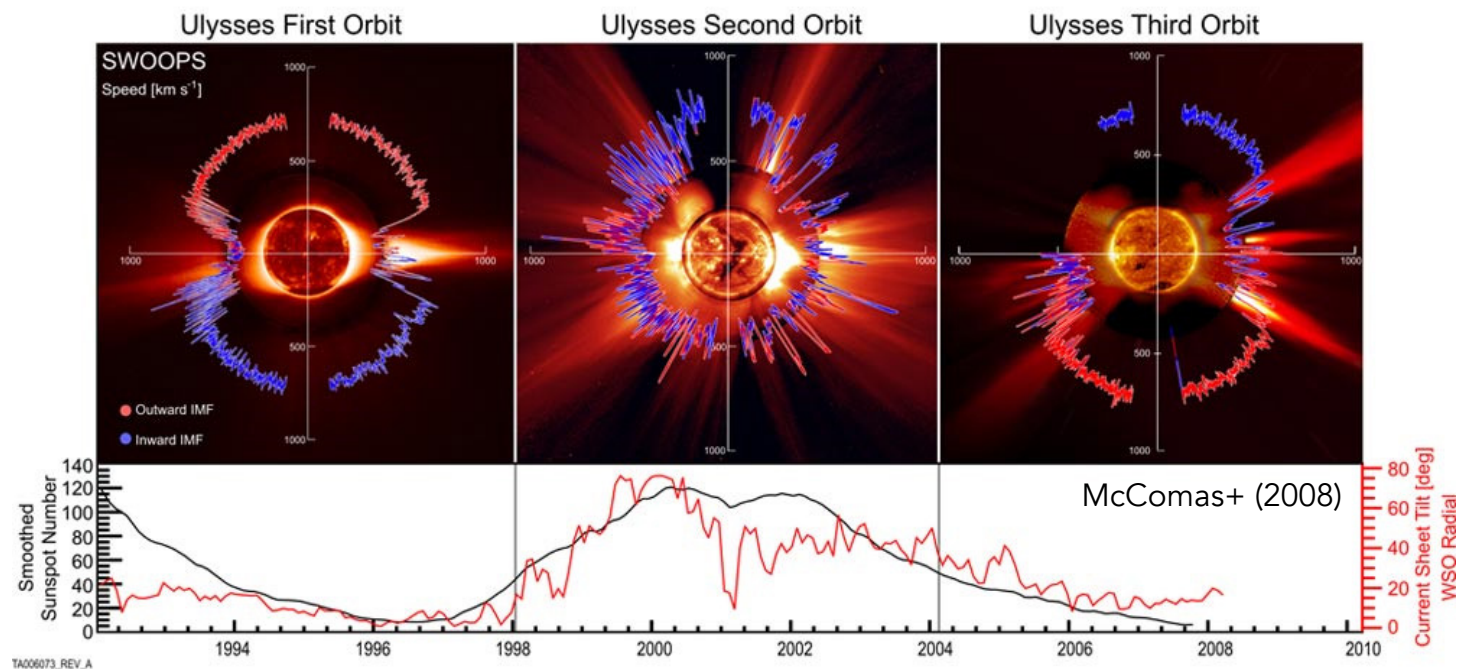
Temmer (2021)

AWSoM Validation [1 au]



Sachdeva+ (2019)

The structure of the solar wind is dictated by the solar (large-scale) magnetic field.



Detecting winds from cool stars

SPRINGER LINK

Find a journal Publish with us Track your research Search

Home > [Living Reviews in Solar Physics](#) > Article

The evolution of the solar wind

Review Article | [Open access](#) | Published: 26 April 2021

Volume 18, article number 3, (2021) [Cite this article](#)



[Living Reviews in Solar Physics](#)

[Aims and scope](#) →

Download PDF ↓

✓ You have full access to this [open access](#) article

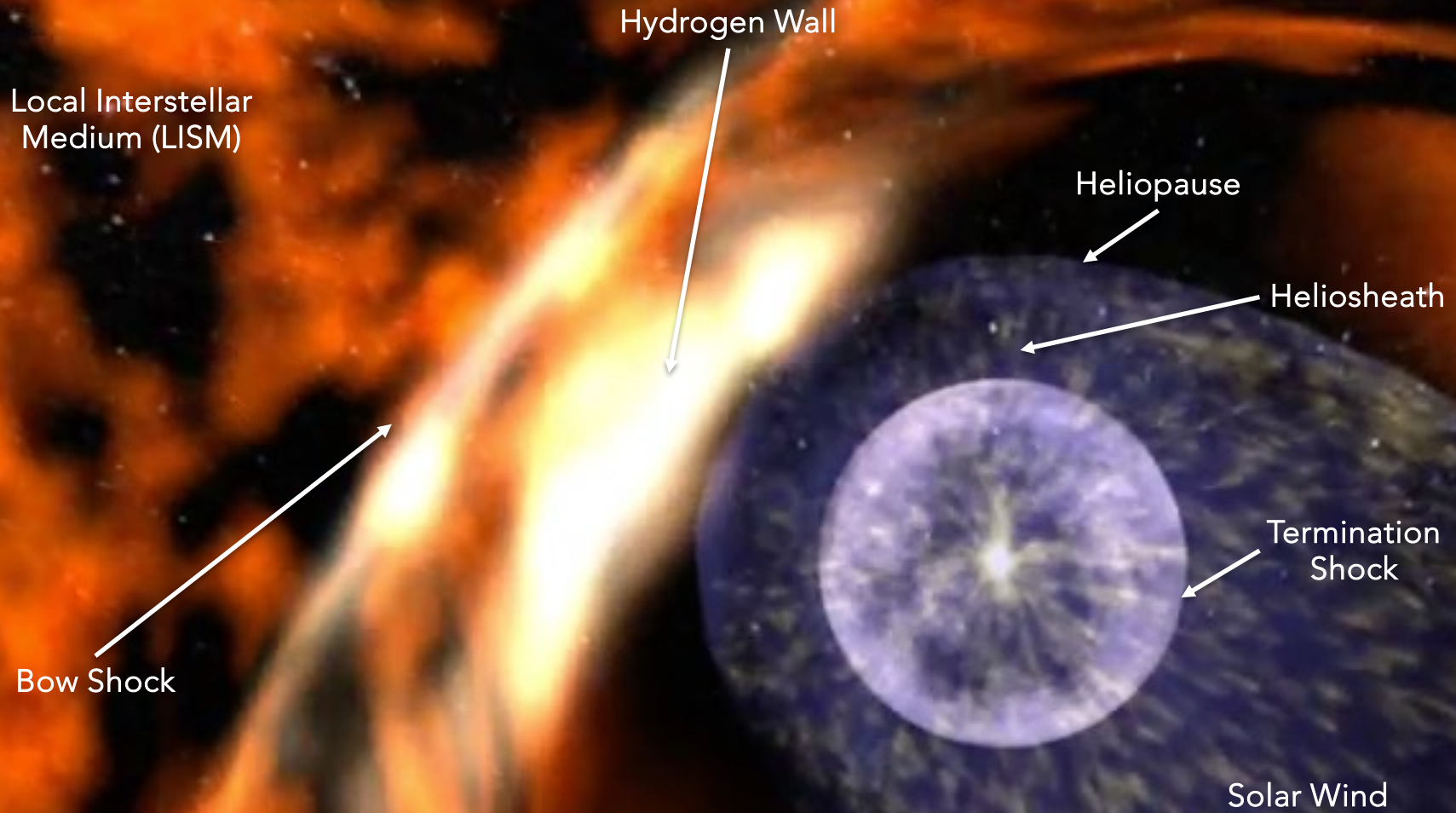
Vidotto (2021)

Table 1 Some proposed methods to detect winds of Sun-like stars

From: [The evolution of the solar wind](#)

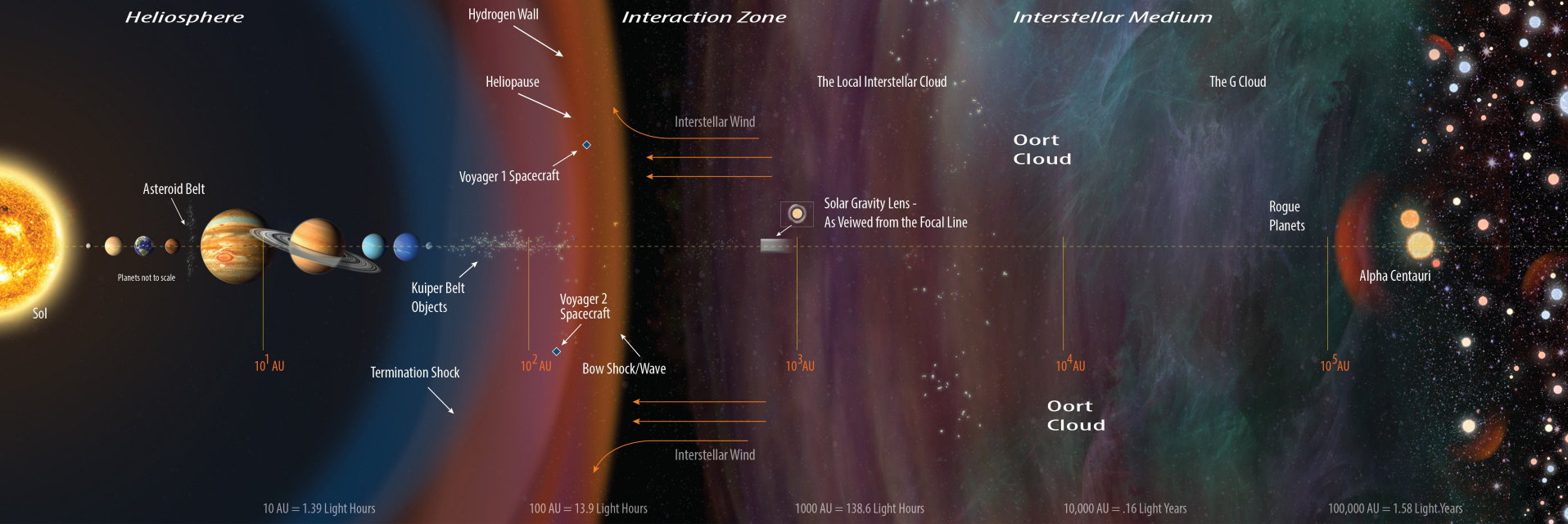
Section number, method	Requirement for detection	Key references
2.1 Astrospheric Ly- α	Partially neutral ISM, $\lesssim 10$ pc	Wood (2004)
2.2 Radio free-free emission	Denser winds and/or radio flares	Lim and White (1996) and Güdel (1992)
2.3 Exoplanets as probes	Evaporating planet	Vidotto and Bourrier (2017)
2.4 Prominences in H- α	Fast rotation	Jardine and Collier Cameron (2019)
2.5 Detection of CME-dominated winds	Fast CME associated with a flare	Crosley and Osten (2018)
2.6 Propagation of radio emission	Point source (planet?) within wind	Vidotto and Donati (2017)
2.7 X-ray emission from the stellar wind	Hot coronal winds	Lim and White (1996) and Llama et al. (2013)
2.8 Charge-exchange induced X-rays	Partially neutral ISM	Wargelin and Drake (2001) and Wargelin and Drake (2002)
2.9 Accretion onto white dwarfs	Close binary with cool dwarf secondary	Debes (2006)

Winds from cool stars: Astrospheres



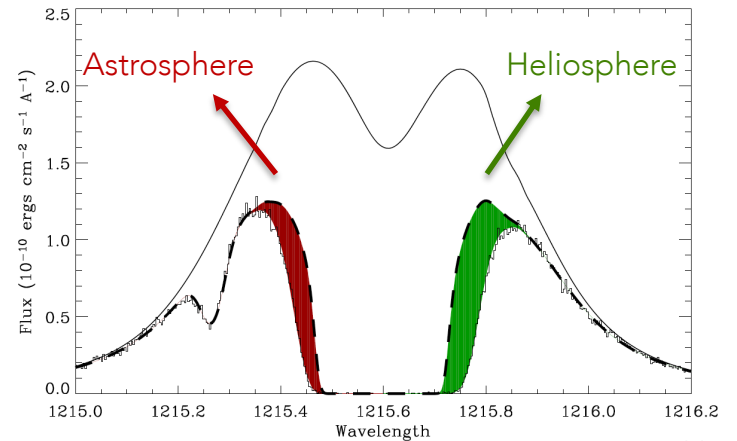
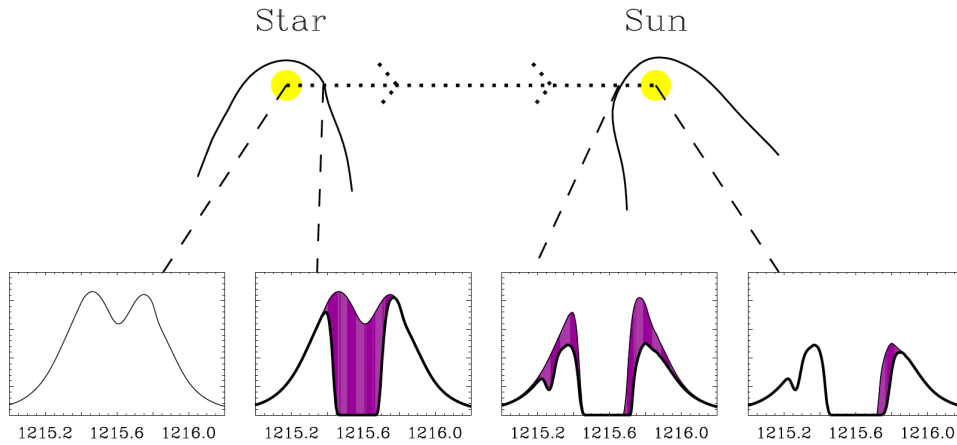
NASA Goddard (SVS)

The Interstellar Medium



Ly- α astrospheric method

Keck Institute for Space Studies



Current constrains on winds from cool stars are model dependent

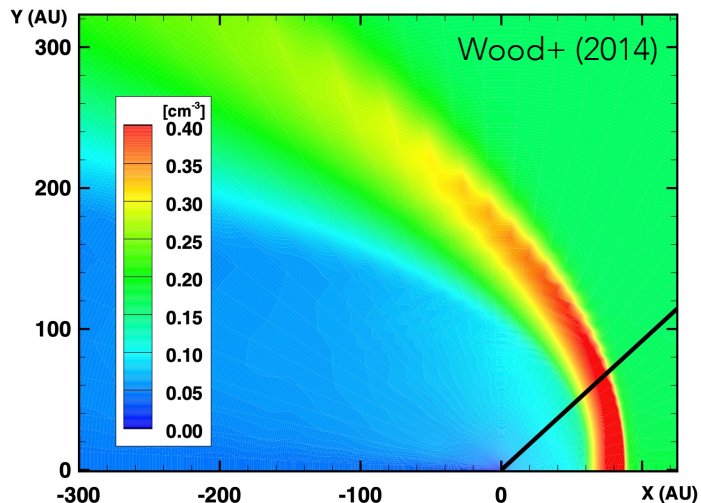


Figure 2. H I density distribution of a hydrodynamic model of the π^1 UMa astrosphere, assuming $\dot{M} = 0.5 M_{\odot}$, which leads to the best fit to the data in Figure 3. The black line indicates our line of sight to the star.

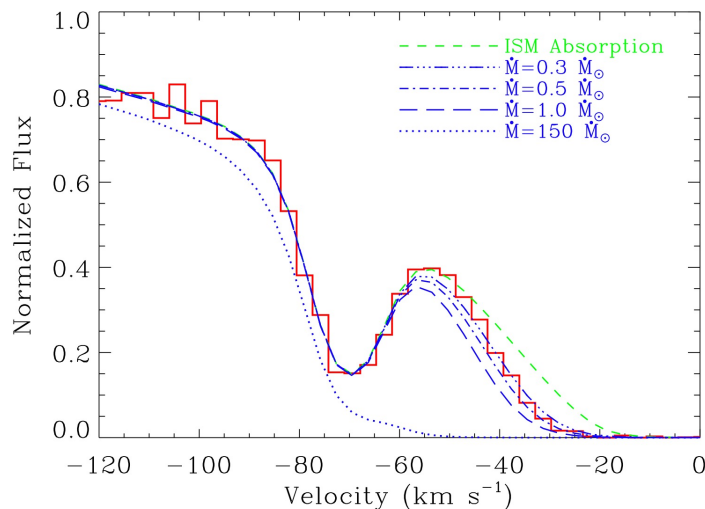
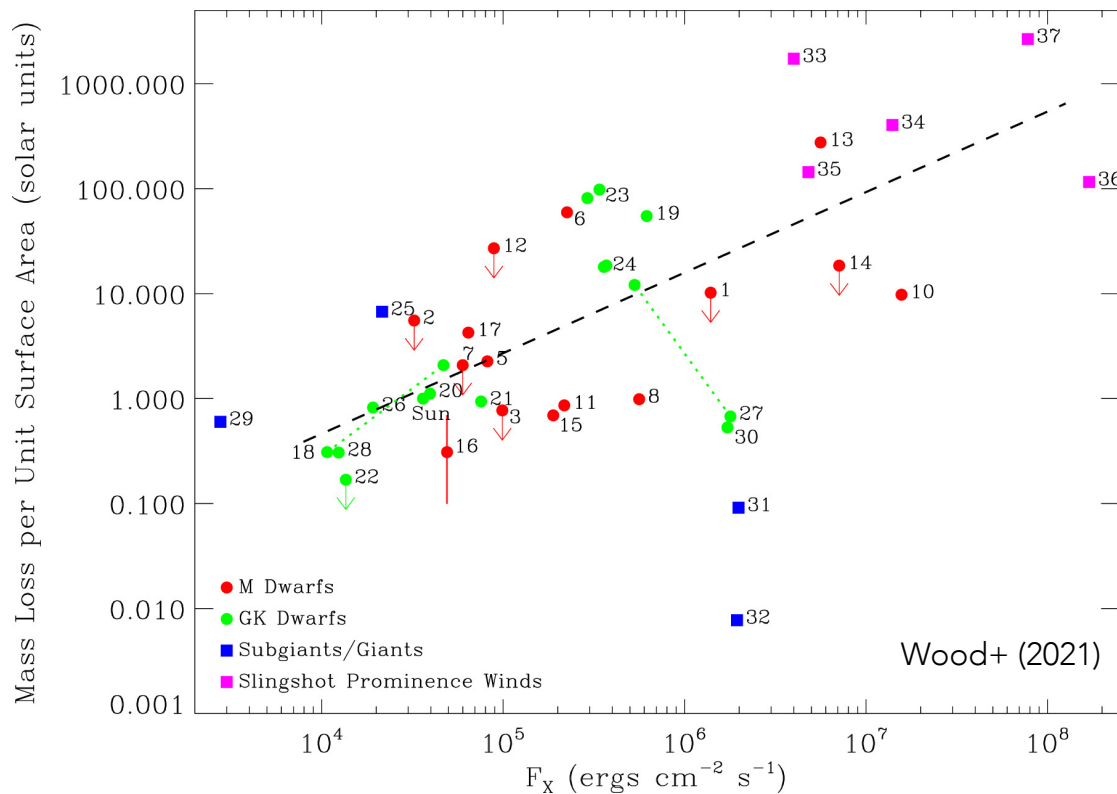


Figure 3. Zooming in on the blue side of the Ly α profile from Figure 1(c), the astrospheric absorption signature is compared with absorption predictions from four hydrodynamic models of the astrosphere, assuming four different mass-loss rates for π^1 UMa (after the astrospheric absorption is added to that of the ISM).

Stellar wind mass loss – coronal activity plane



Large scatter. Weak correlation for GKM stars: $\dot{M}_{\star} \propto F_X^{0.77 \pm 0.04}$ (excluding Subgiants/giants)

Sun-like stars: Weak wind for the young Sun

M-dwarfs: Varied behavior but generally weak (steady) winds. (dynamo bi-stability?)

The stellar wind of Proxima Centauri

Proxima Centauri (M5.5V)

$$M_{\star} \approx 0.122 M_{\odot}$$

$$R_{\star} \approx 0.154 R_{\odot}$$

$$P_{\text{ROT}} \approx 83 \text{ days}$$

Earth-like planet in the HZ

$$(P_{\text{ORB}} \approx 11.2 \text{ d})$$

(Anglada-Escudé+ 2016, Suárez-Masareño+ 2020)

Super-Earth orbiting around 1.44 AU

$$(P_{\text{ORB}} \approx 5.3 \text{ yr})$$

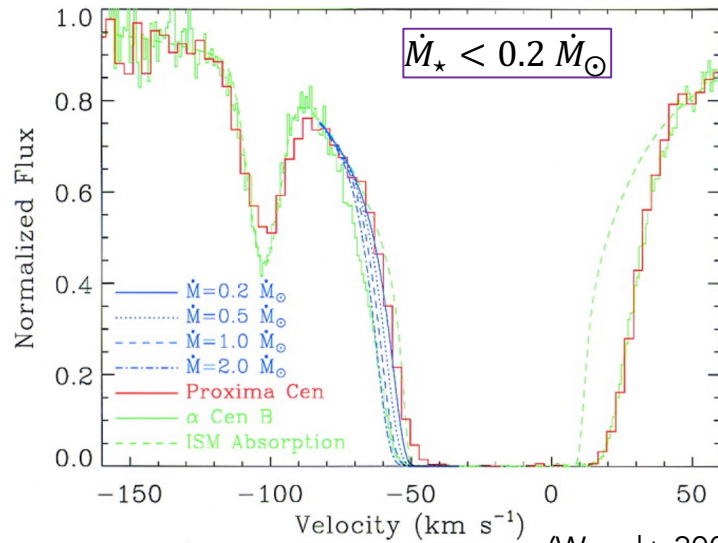
(Damasso+ 2020, Benedict & McArthur 2020)

Candidate short-period Sub-Earth planet

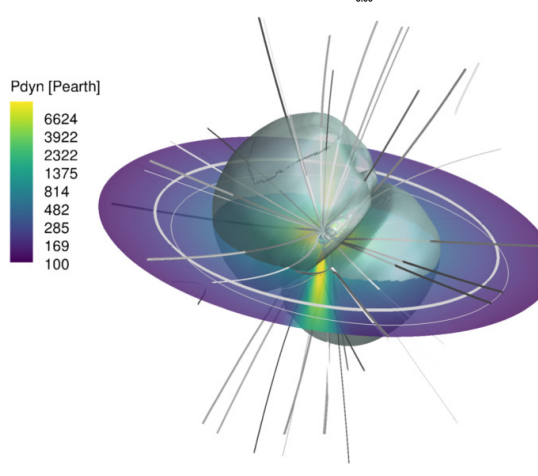
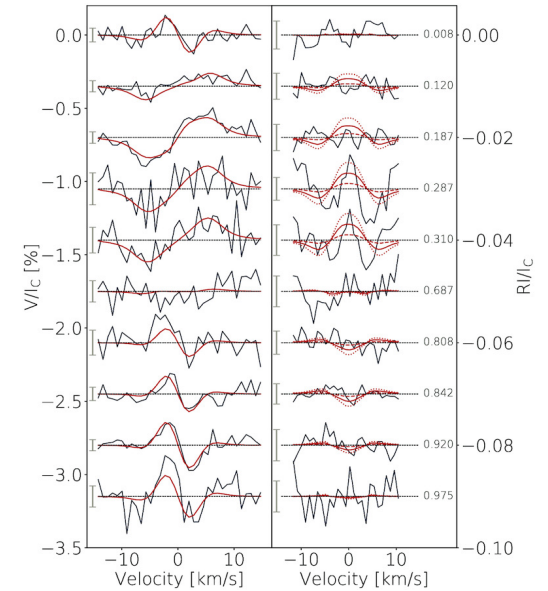
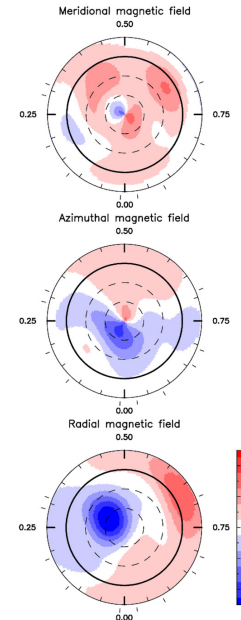
$$(P_{\text{ORB}} \approx 5.12 \text{ d})$$

(Suárez-Masareño+ 2020, Faria+ 2022)

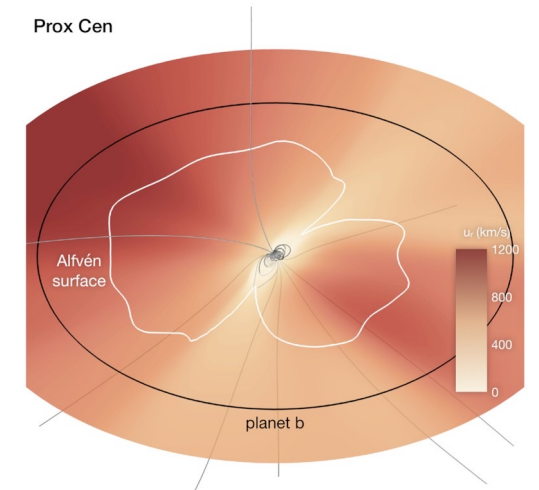
Lyman- α Astrosphere (STIS/HST)



Large-Scale Magnetic Field Reconstruction (HARPSpol + ZDI | Klein+ 2021)



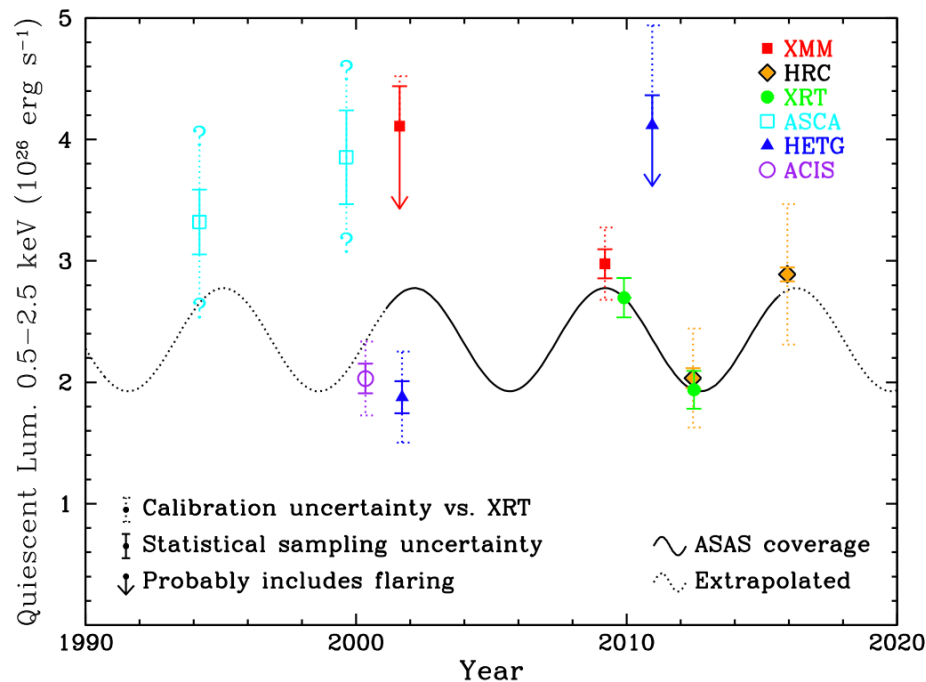
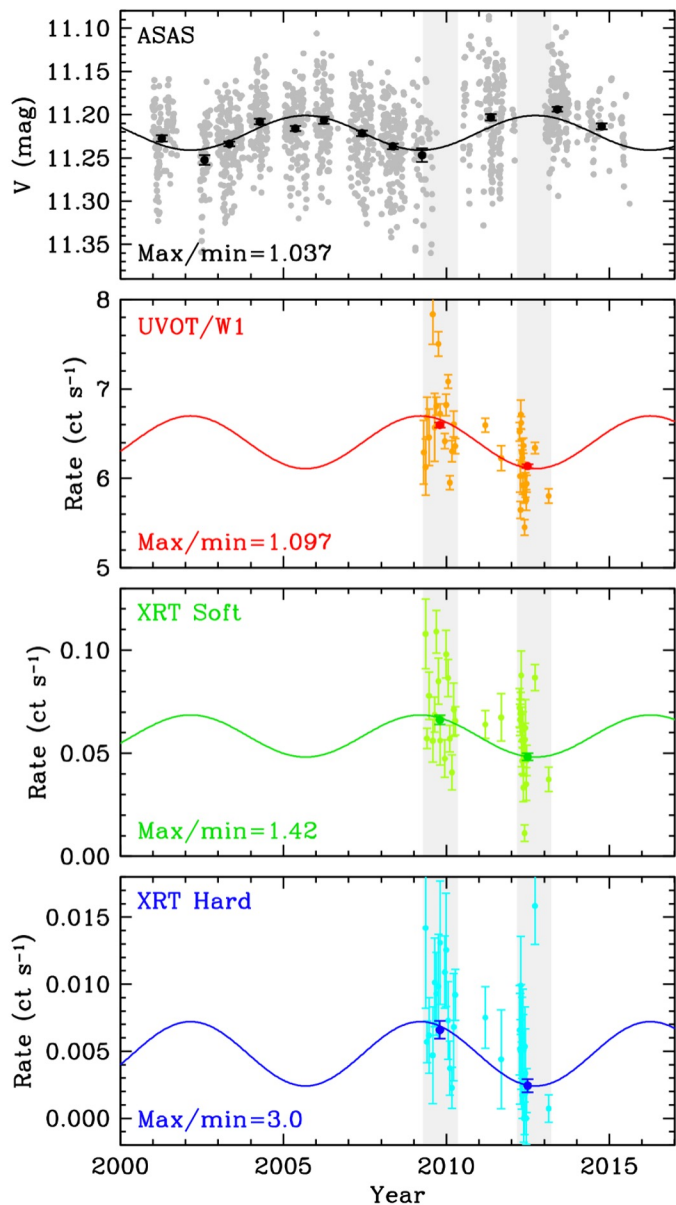
(Garraffo+ 2016, 2022)



(Kavanagh+ 2021)

Stellar Wind Models (AWSoM/SWMF | 3D MHD)

The Activity Cycle of Proxima Centauri



The X-ray Stellar Cycle of Proxima Cen

Show affiliations

Wargelin, Bradford ; Saar, Steven ; Do Nascimento, José-Dias

Stellar cycles in fully convective M stars were generally thought to be impossible until a few years ago, when ~8 examples were discovered from analysis of ASAS photometric monitoring data. Proxima Cen (dM5.5) was one of those stars, and also had (limited) supporting evidence for a cycle from Swift observations in the X-ray and UV, where emission is more directly tied to magnetic activity cycles (in contrast to spot/plage countereffects in photometry) and displays much larger cycle amplitudes. With several additional years of data, now spanning 8 epochs over more than 12 years, we find that an **~8-year** cycle is clearly apparent in both X-rays and the UVOT/W1 band, and provide an update on the previously suggested association of X-ray cycle amplitude with Rossby number.

Publication:

AAS High Energy Astrophysics Division meeting #20, id. 116.64. Bulletin of the American Astronomical Society, Vol. 55, No. 4 e-id 2023n4i116p64

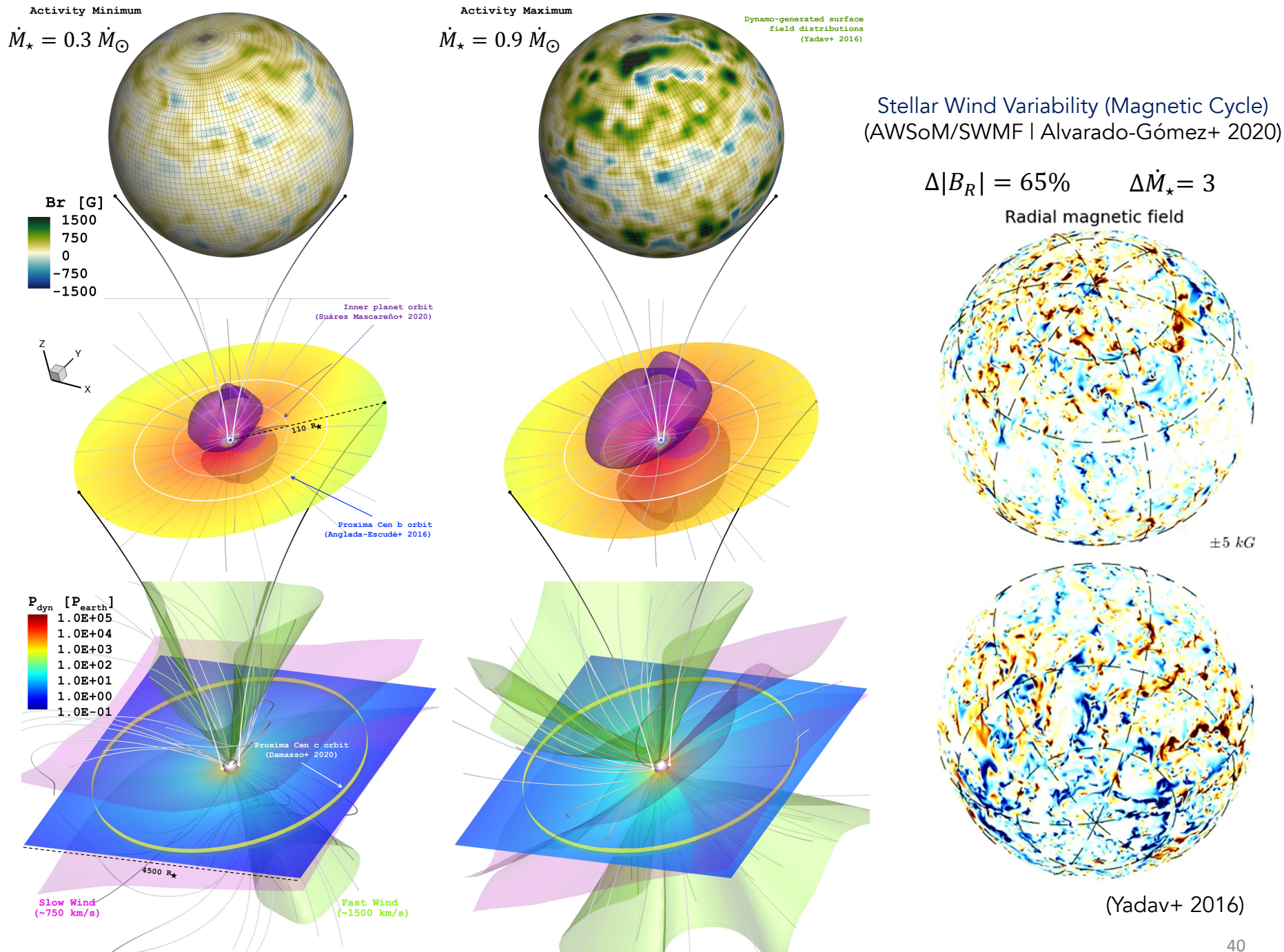
Pub Date:

September 2023

Bibcode:

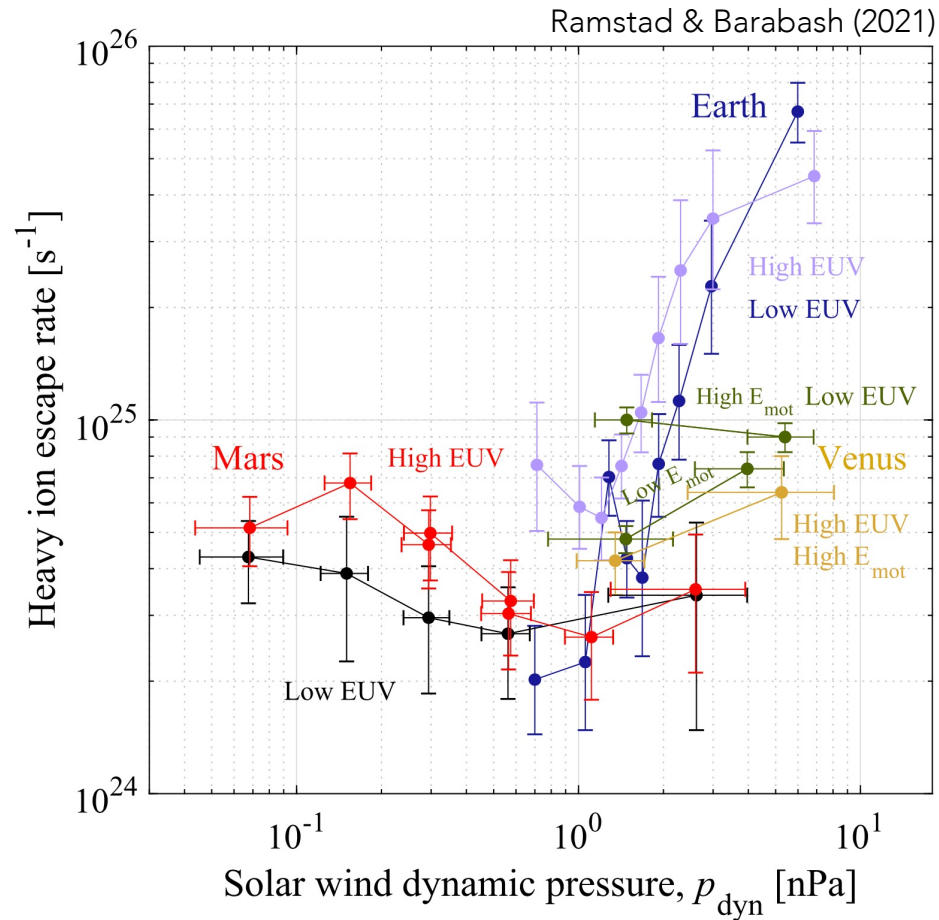
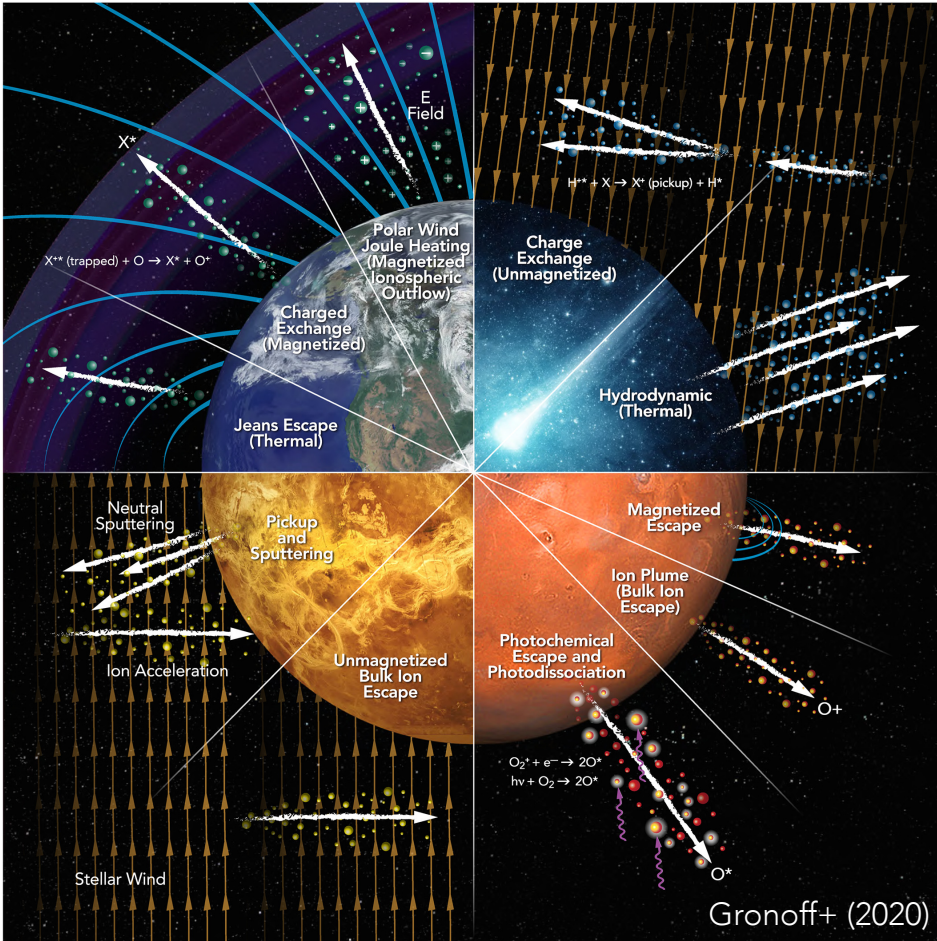
2023HEAD...2011664W ?

Wargelin+ (2017)



Stellar winds and Exoplanets

Stellar winds are fundamental to understand atmospheric retention/escape of exoplanets.



Several process taking place for magnetized/unmagnetized planets

Solar system: Guide for exoplanets
Exoplanetary systems: Increased diversity (stars, planets)

Do intrinsic magnetic fields protect planetary atmospheres from stellar winds?

Space Weather of the TRAPPIST-1 System

(Garraffo et al. 2017)

TRAPPIST-1 (M8V)

$M_{\star} \approx 0.08 M_{\odot}$

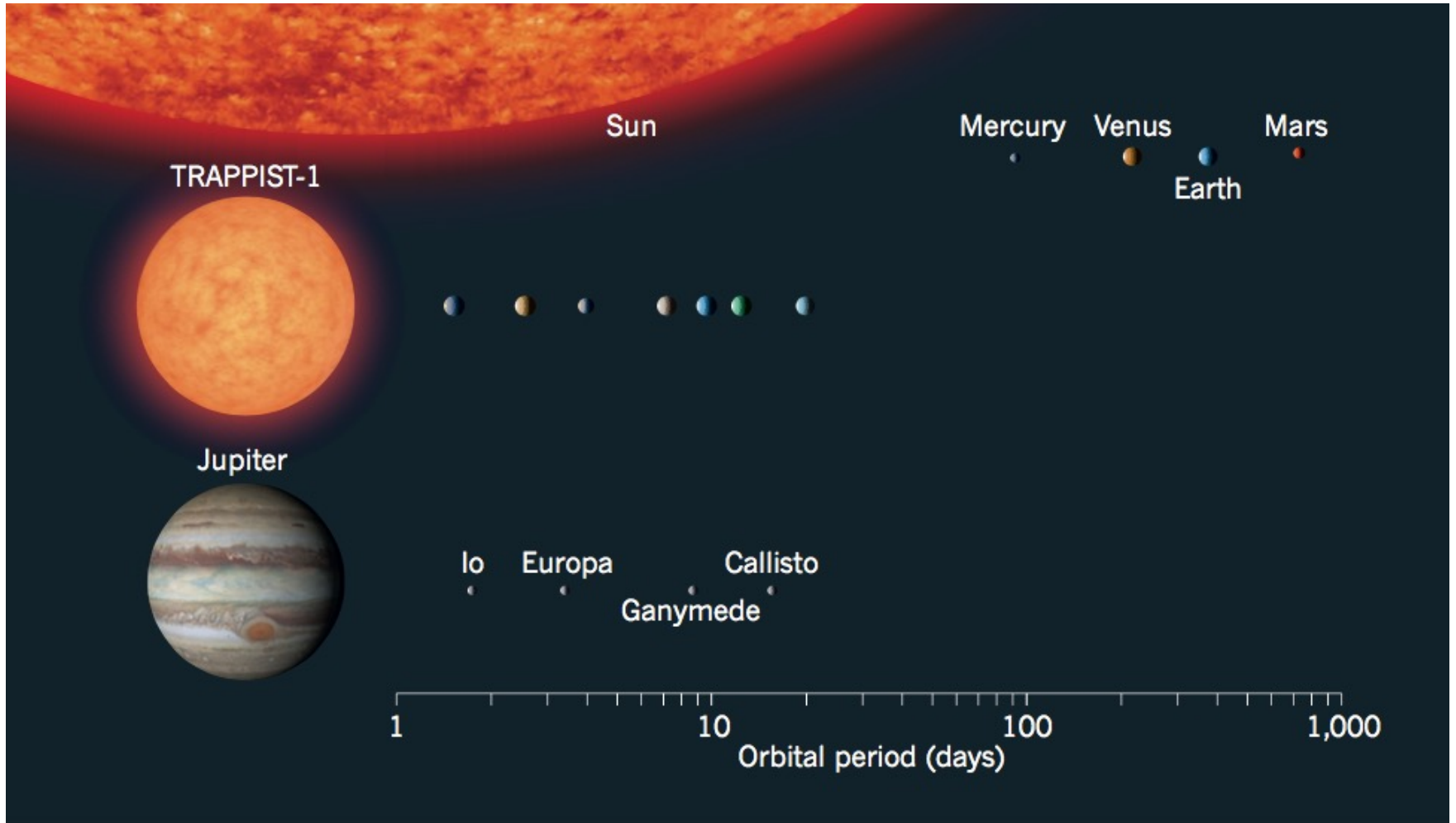
$R_{\star} \approx 0.114 R_{\odot}$

$P_{\text{ROT}} \approx 1.4$ days

7 planets within 0.01 – 0.063 AU

($P_{\text{ORB}} \approx 1.5 – 20$ days)

(Guillon et al. 2017, 2016; Luger et al. 2017)



Space Weather of the TRAPPIST-1 System

(Garraffo et al. 2017)

TRAPPIST-1 (M8V)

$M_{\star} \approx 0.08 M_{\odot}$

$R_{\star} \approx 0.114 R_{\odot}$

$P_{\text{ROT}} \approx 1.4$ days

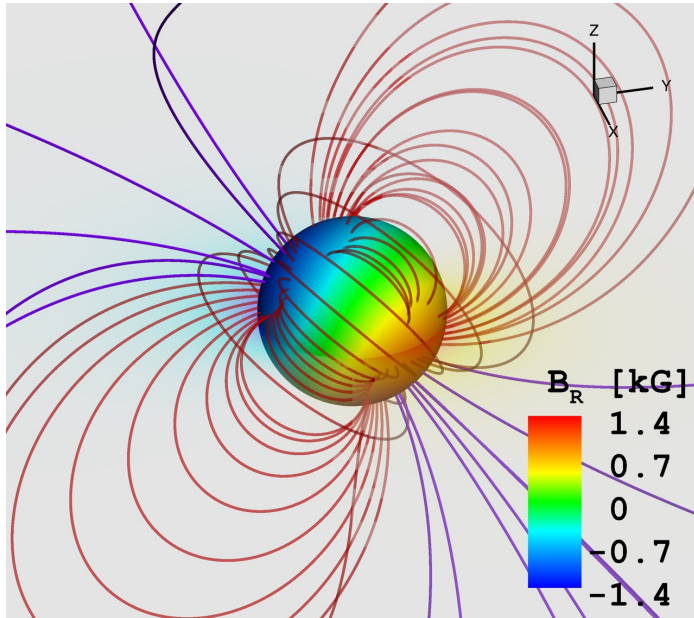
7 planets within 0.01 – 0.063 AU

($P_{\text{ORB}} \approx 1.5 - 20$ days)

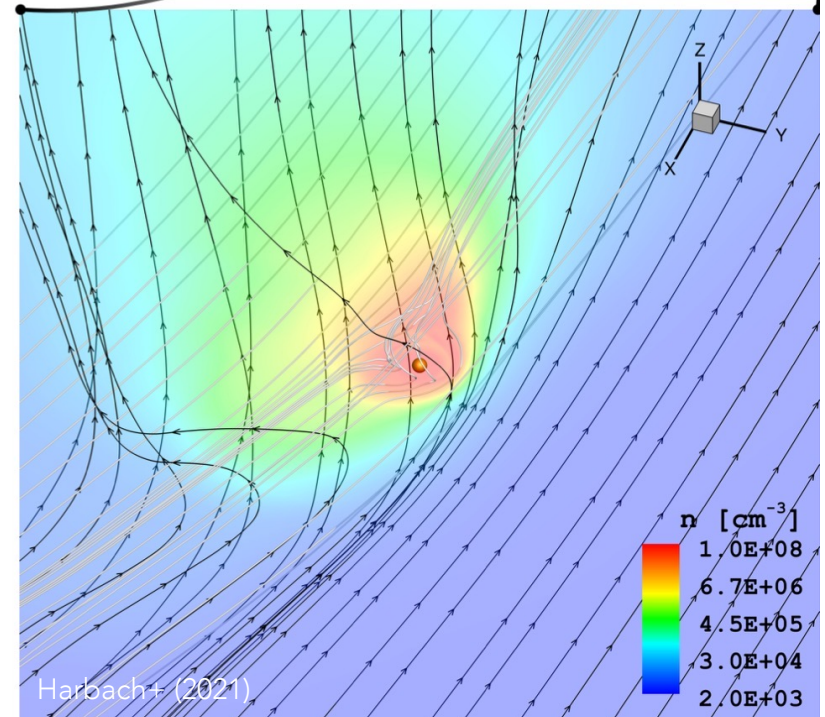
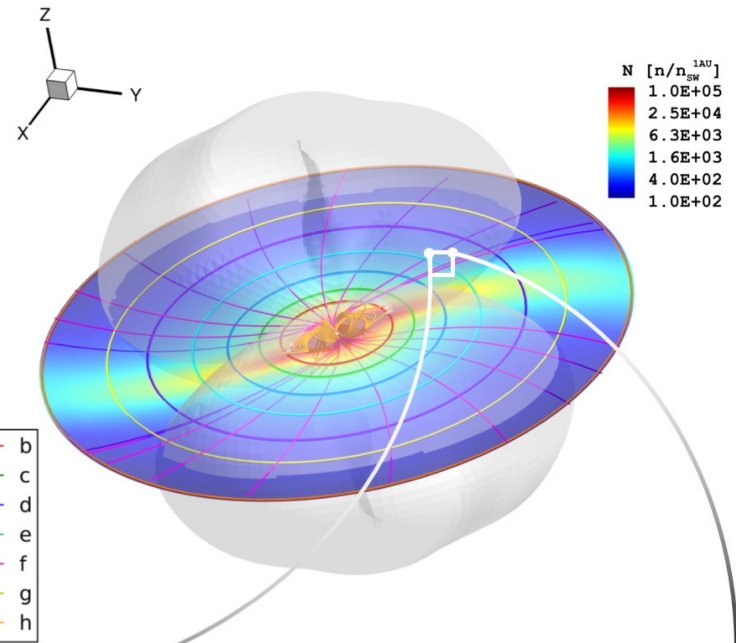
(Guillon et al. 2017, 2016; Luger et al. 2017)

No ZDI map available → Proxy: GJ3220

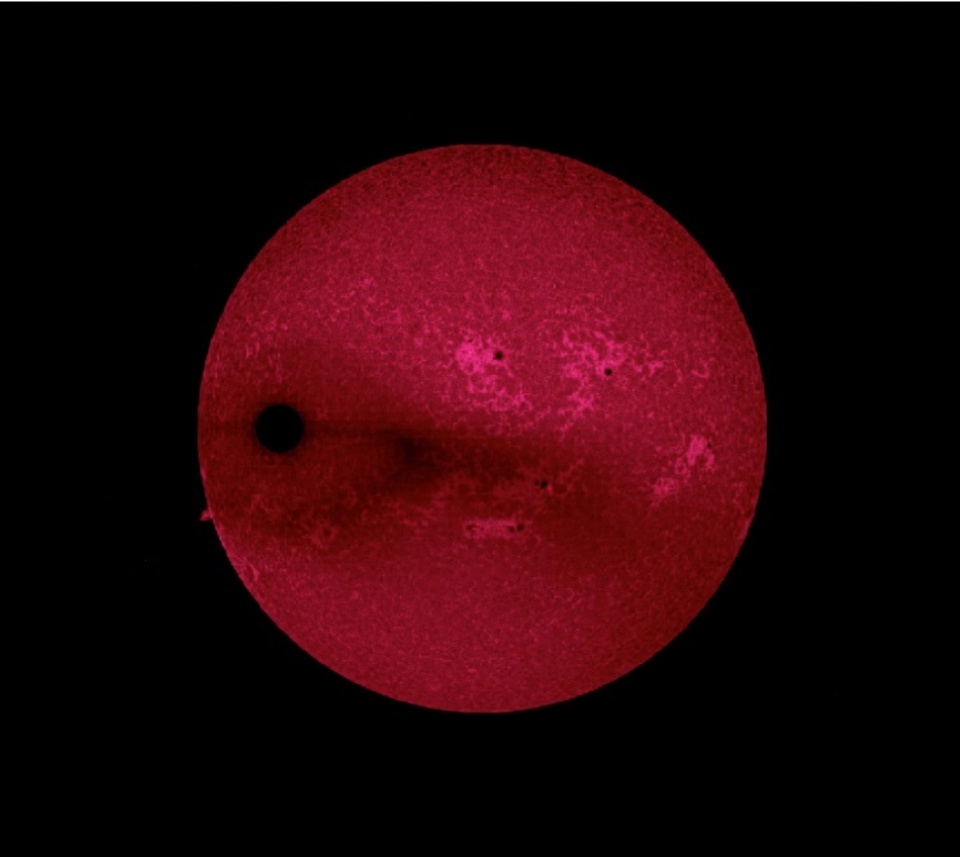
(M6.5V, $P_{\text{ROT}} \approx 1.5$ days; Morin et al. 2010)



- Extreme environment for all planets: \underline{n} and Ur
- Depending on B_{\star} : 4/6 planets would be located inside the Alfvén Surface (e.g. Cohen et al. 2014).

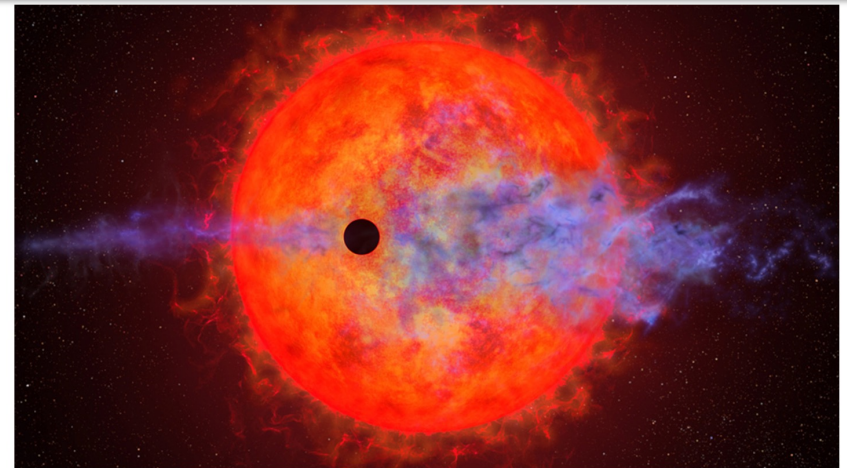
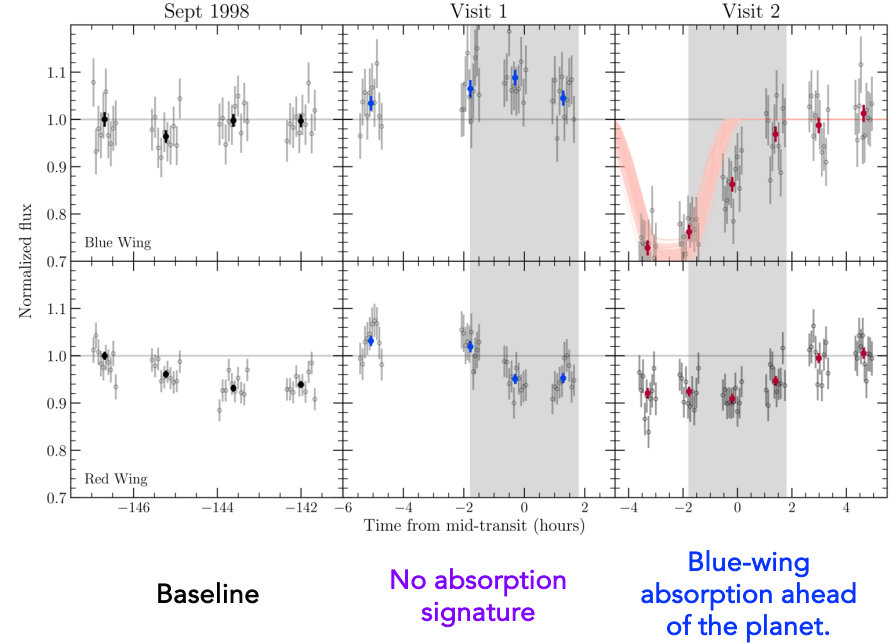


Stellar Wind – Planetary Outflow Interaction (sub-Alfvénic regime)



Harbach+ (2021)

The planetary 'tail' (escaping atmosphere)
gets pushed in front of the planet



This artist's illustration shows a planet (dark silhouette) passing in front of the red dwarf star AU Microscopi. The planet is so close to the eruptive star a ferocious blast of stellar wind and blistering ultraviolet radiation is heating the planet's hydrogen atmosphere, causing it to escape into space. Four times Earth's diameter, the planet is slowly evaporating its atmosphere, which stretches out linearly along its orbital path. This process may eventually leave behind a rocky core. The illustration is based on measurements made by the Hubble Space Telescope. NASA, ESA, and Joseph Olmsted (STScI)

But during one orbit observed with NASA's Hubble Space Telescope, the planet looked like it wasn't losing any material at all, while an orbit observed with Hubble a year and a half later showed clear signs of atmospheric loss.

Stellar Wind Environment of Barnard's Star b

Barnard's Star (M4V) Super-Earth orbiting around 0.4 AU

$M_{\star} \approx 0.144 M_{\odot}$

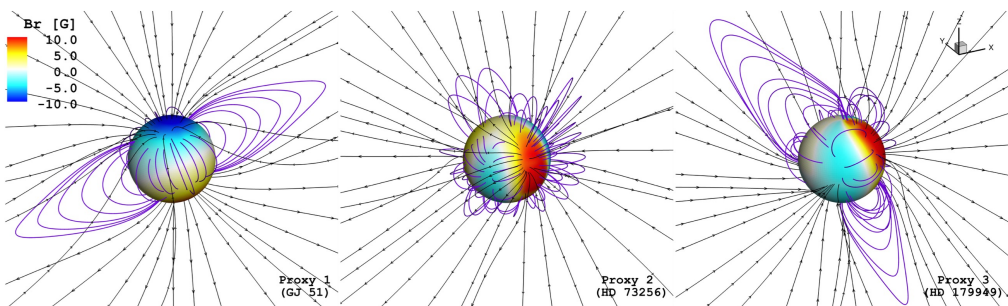
($P_{\text{ORB}} \approx 232.8$ days)

$R_{\star} \approx 0.196 R_{\odot}$

(Ribas et al. 2018)

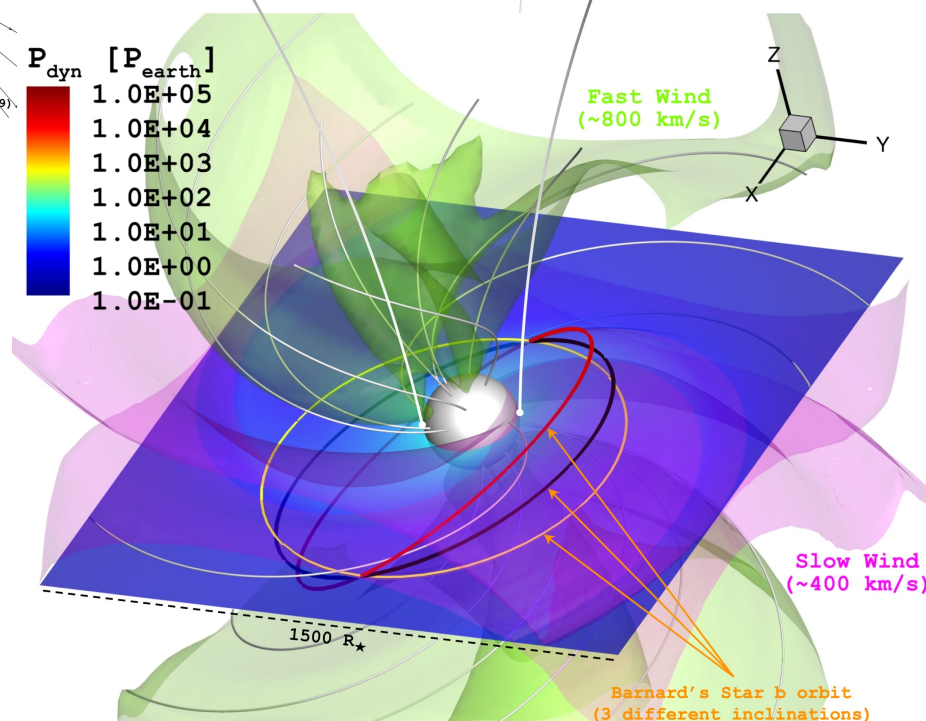
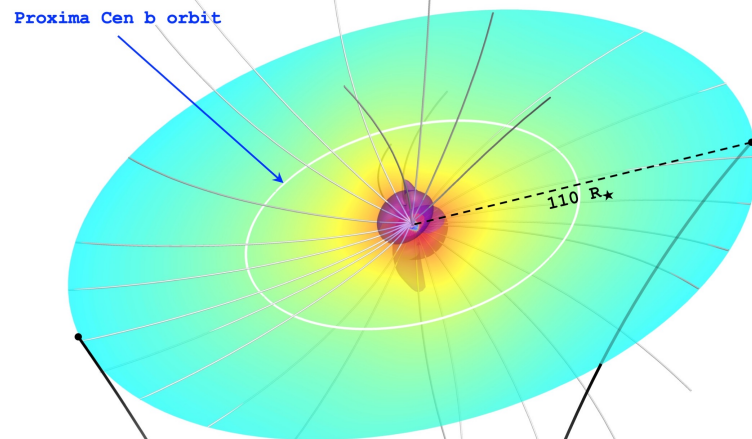
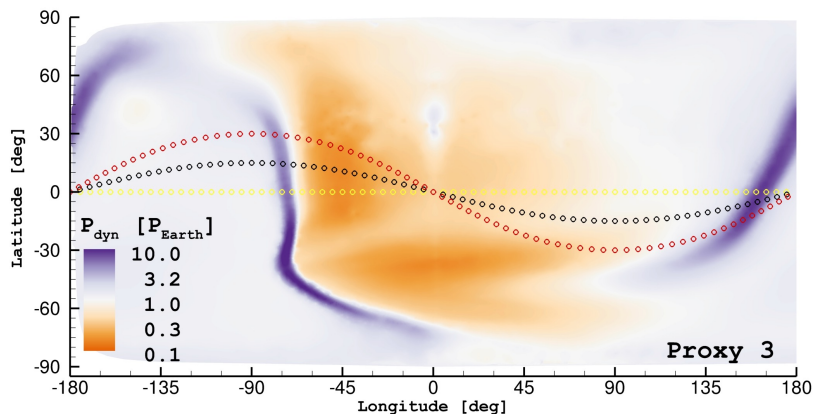
$P_{\text{ROT}} \approx 130$ days

No ZDI map available \rightarrow 3 Different proxies
Based on Rossby Number (Spectral Type + Rotation)



Wind dynamic pressure: Comparable to present-day Earth values.

Similar results for all proxies.



Alvarado-Gómez et al. (2019)

Breezing through the Space Environment of Barnard's Star b

04.12.19 Science Update

Home > News > Breezing through the Space Environment of Barnard's Star b

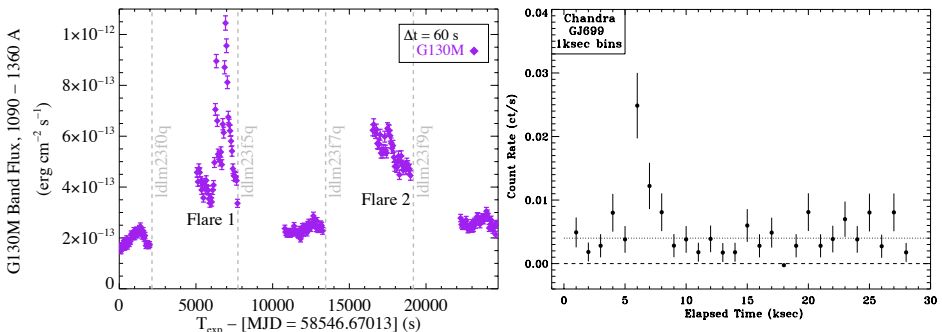
THE ASTRONOMICAL JOURNAL, 160:237 (14pp), 2020 November
© 2020. The American Astronomical Society. All rights reserved.

<https://doi.org/10.3847/1538-3881/abb465>

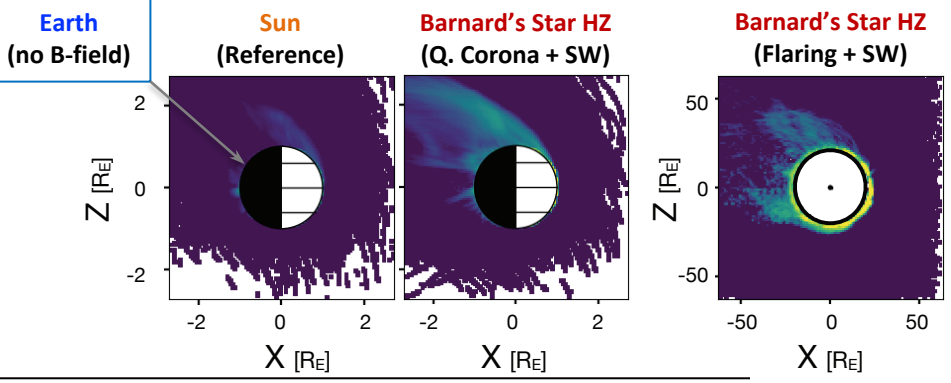
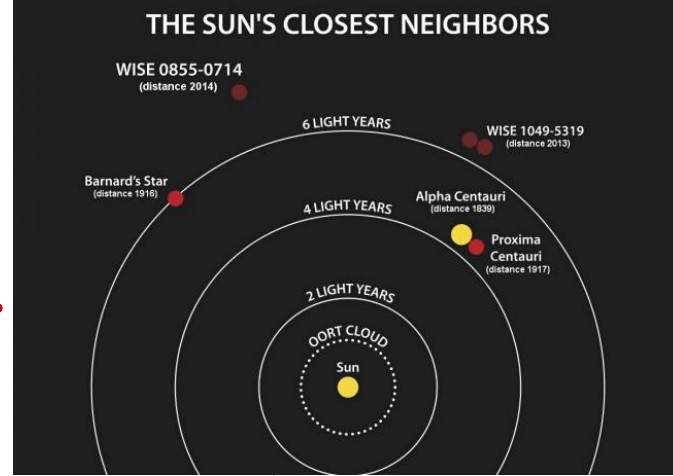


The High-energy Radiation Environment around a 10 Gyr M Dwarf: Habitable at Last?

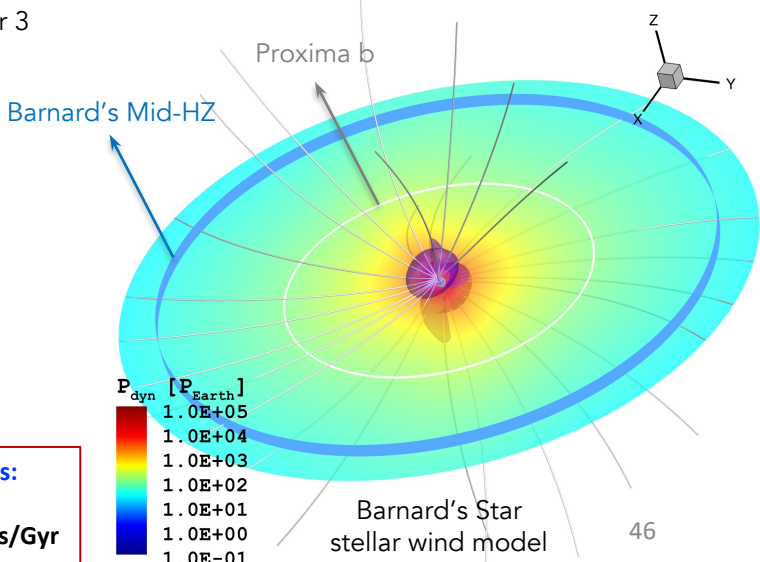
Kevin France^{1,2,3}, Girish Duvvuri², Hilary Egan¹, Tommi Koskinen⁴, David J. Wilson⁵, Allison Youngblood¹, Cynthia S. Froning⁵, Alexander Brown³, Julián D. Alvarado-Gómez^{6,7}, Zachory K. Berta-Thompson^{2,3}, Jeremy J. Drake⁷, Cecilia Garraffo^{7,8}, Lisa Kaltenegger⁹, Adam F. Kowalski¹, Jeffrey L. Linsky¹⁰, R. O. Parke Loyd¹¹, Pablo J. D. Mauas¹², Yamila Miguel^{13,14}, J. Sebastian Pineda¹, Sarah Rugheimer¹⁵, P. Christian Schneider¹⁶, Feng Tian¹⁷, and Mariela Vieytes¹⁸



Flare duty cycle: 25%
XUV flares: Barnard's: 6 flares/d
Sun: 4 flares/d (averaged over 3 solar cycles)



Ion losses: 3 Earth Atmospheres/Gyr



Numerical quantification of the wind properties of cool main sequence stars

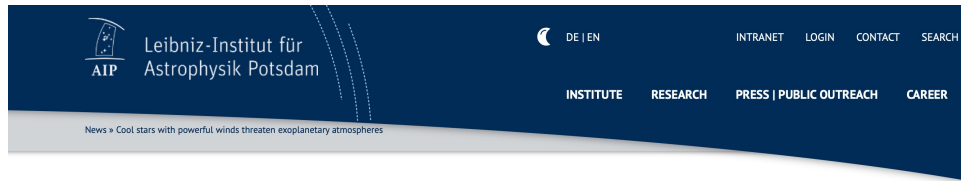
Judy J. Chebly ^{ID},^{1,2}★ Julián D. Alvarado-Gómez ^{ID},¹★ Katja Poppenhäger ^{ID},^{1,2} and Cecilia Garraffo³

¹Leibniz Institute for Astrophysics, An der Sternwarte 16, D-14482, Potsdam, Germany

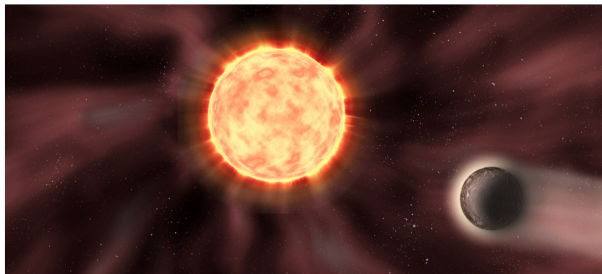
²Institute of Physics and Astronomy, University of Potsdam, Potsdam-Golm, D-14476, Germany

³Harvard-Smithsonian Center for Astrophysics, 60 Garden Street, Cambridge, MA 02138, USA

Accepted 2023 July 7. Received 2023 July 7; in original form 2023 April 21



Cool stars with powerful winds threaten exoplanetary atmospheres



ARTIST'S illustration of a star-planet system. The stellar wind around the star and the effect on the planet's atmosphere is visible.
Credit: AIP/K. Riebel / Fohlmeister

None

Dr. Julián Alvarado-Gómez

Science contact

Phone: +49 331 7499 533
julian.alvarado-gomez@aip.de

Prof. Dr.

Katja Poppenhäger

Science contact

Phone: +49 331 7499 521
kpoppenhaeger@aip.de

None

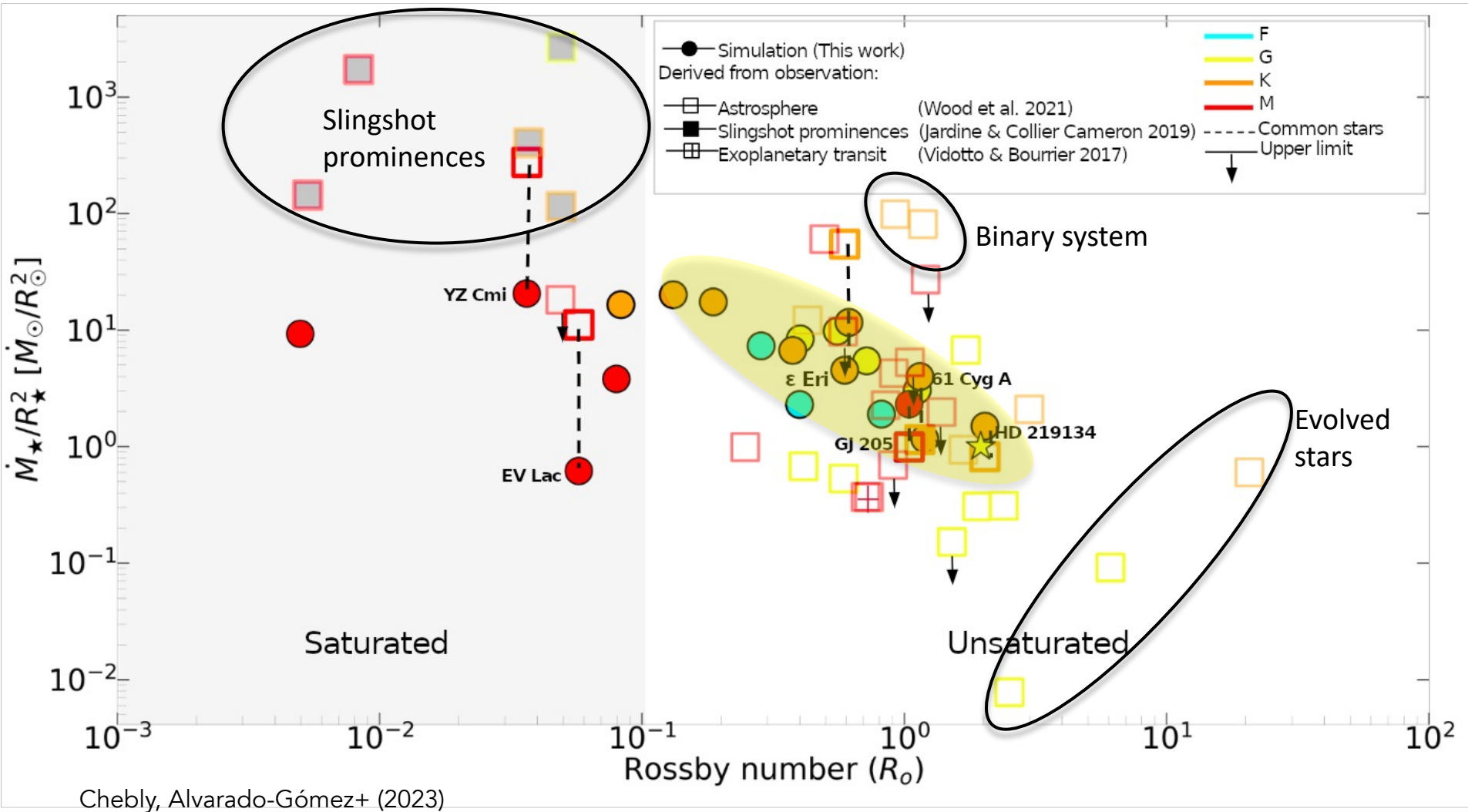
Sarah Hönig

Media contact

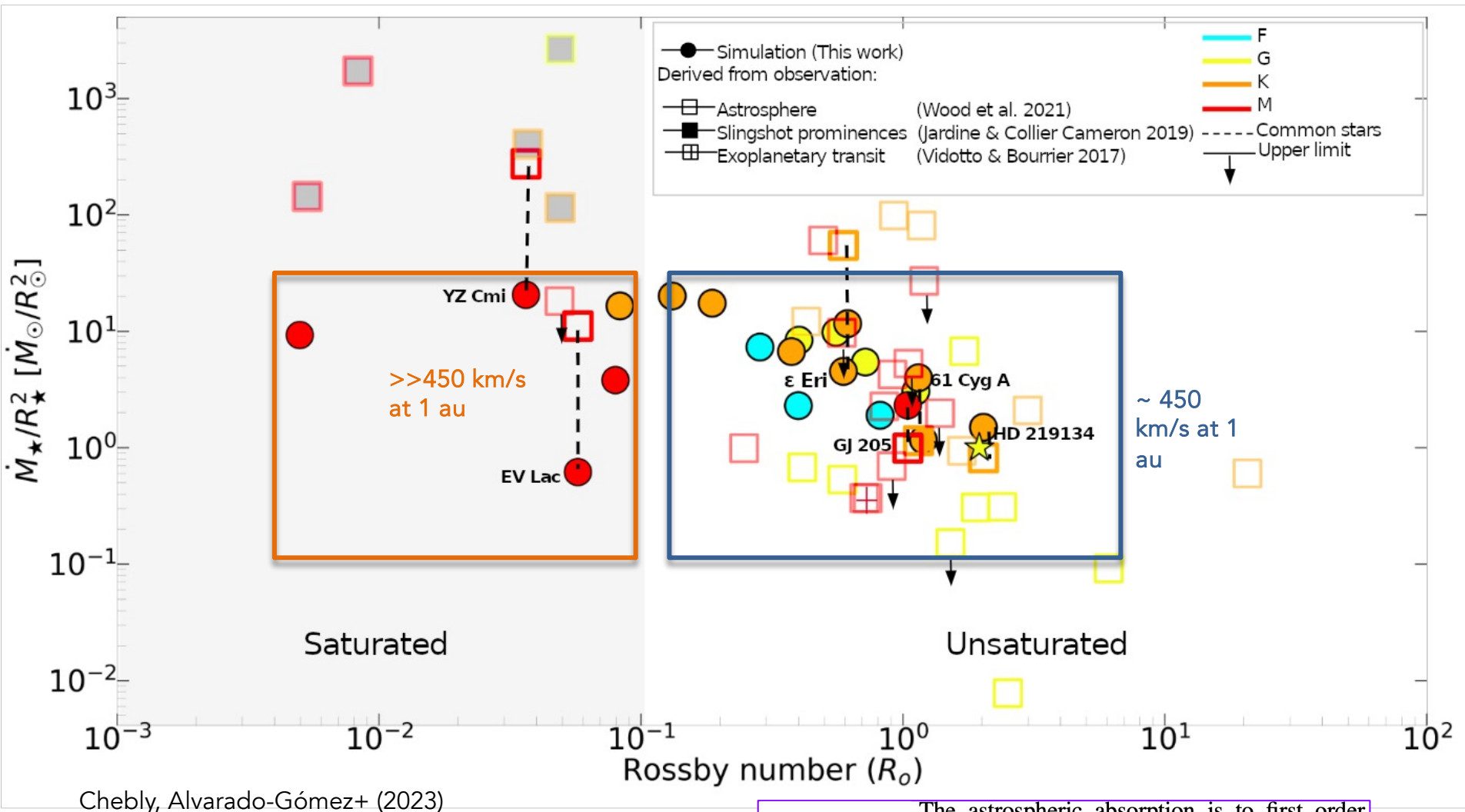
Phone: +49 331 7499 803
presse@aip.de

DOI: [10.1093/mnras/stad2100](https://doi.org/10.1093/mnras/stad2100)
arXiv.: [2307.04615](https://arxiv.org/abs/2307.04615)

Stellar Wind Mass Loss Rates

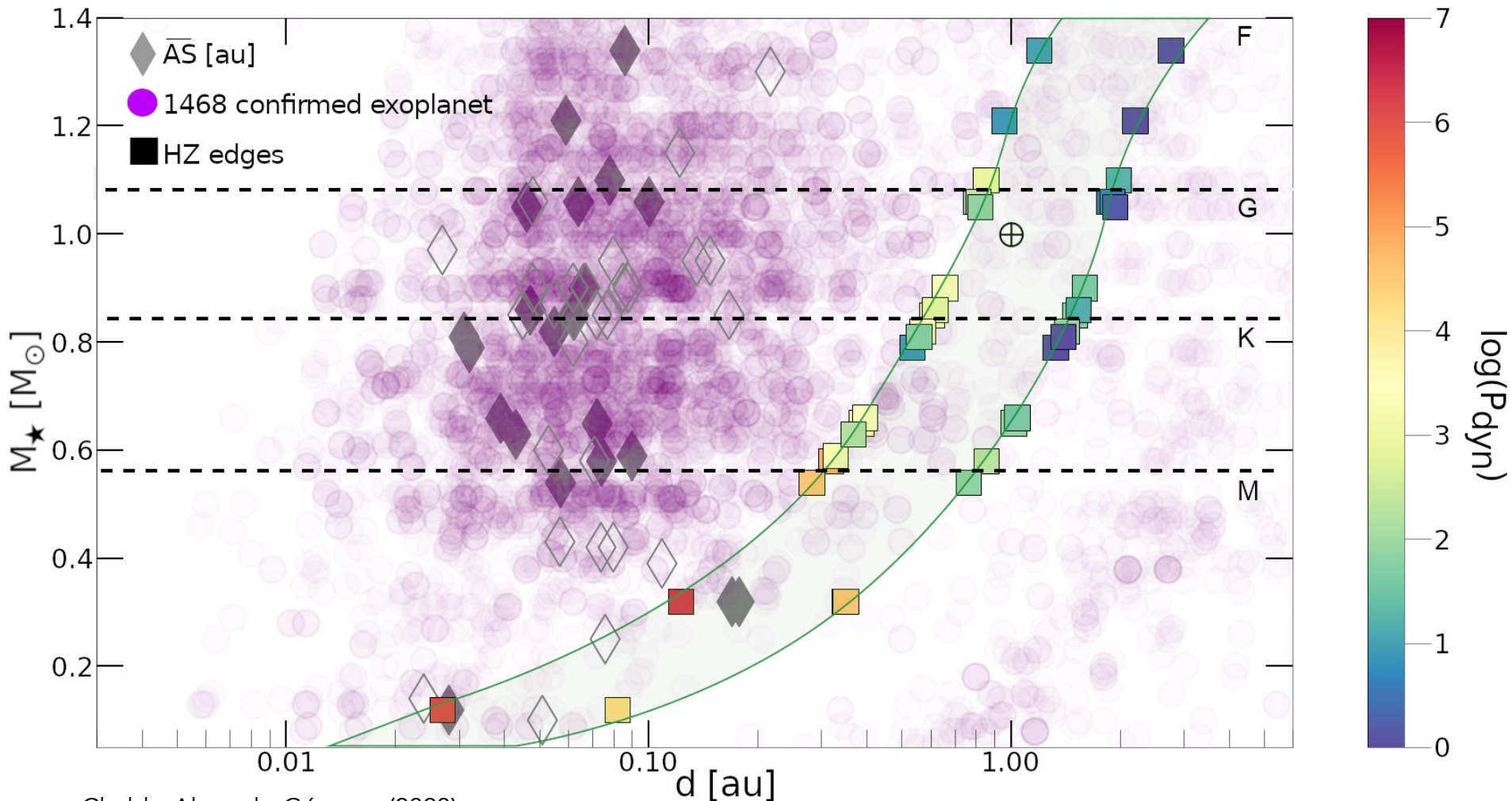


Stellar wind speeds and spectral types



The astrospheric absorption is to first order determined by the size scale of the astrosphere, which depends on the stellar wind ram pressure, P_w . Because $P_w \propto \dot{M}V_w$, mass-loss rate estimates will vary inversely with the assumed V_w (Wood et al. 2002).

Alfvén Surface (Average) Size and Stellar Winds at the HZ



Chebly, Alvarado-Gómez+ (2023)

$$\log \overline{AS}_R = (0.42 \pm 0.06) \log B_R^{\text{avg}} + (0.71 \pm 0.07)$$

$$\log \dot{M}_{\star} / R_{\star}^2 = (0.48 \pm 0.09) \log B_R^{\text{avg}} + (0.11 \pm 0.10)$$

Studying the Space Weather in Cool Main-Sequence Stars (Part II: Transients)

Energetic transient events:

Explosive phenomenon in the corona where a large amount of energy is suddenly released (heating, radiation, particle acceleration, plasma motions...)

Flares | Coronal Mass Ejections (CMEs) | Energetic Particles (EPs)

Examination of the possible energy sources shows that the magnetic field is the only plausible driver of these events.

X9.3

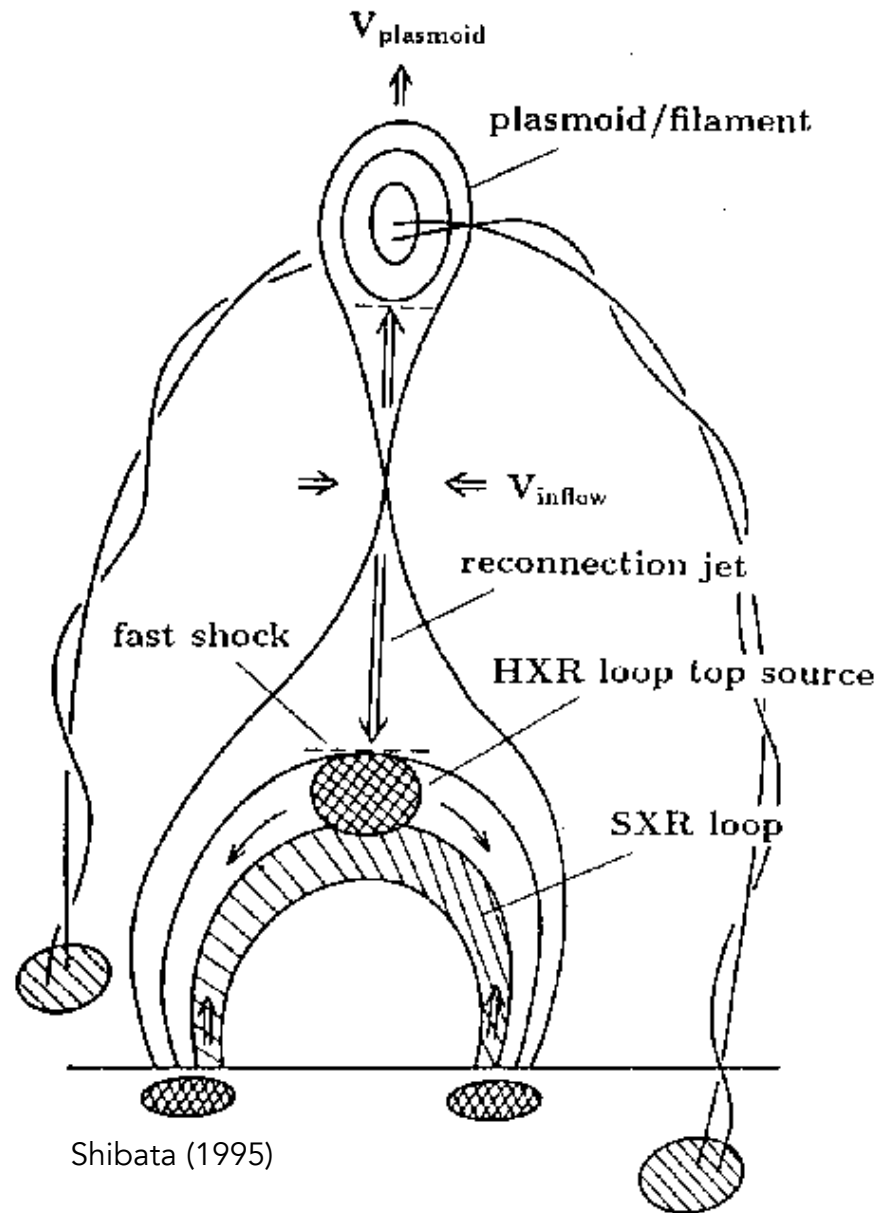
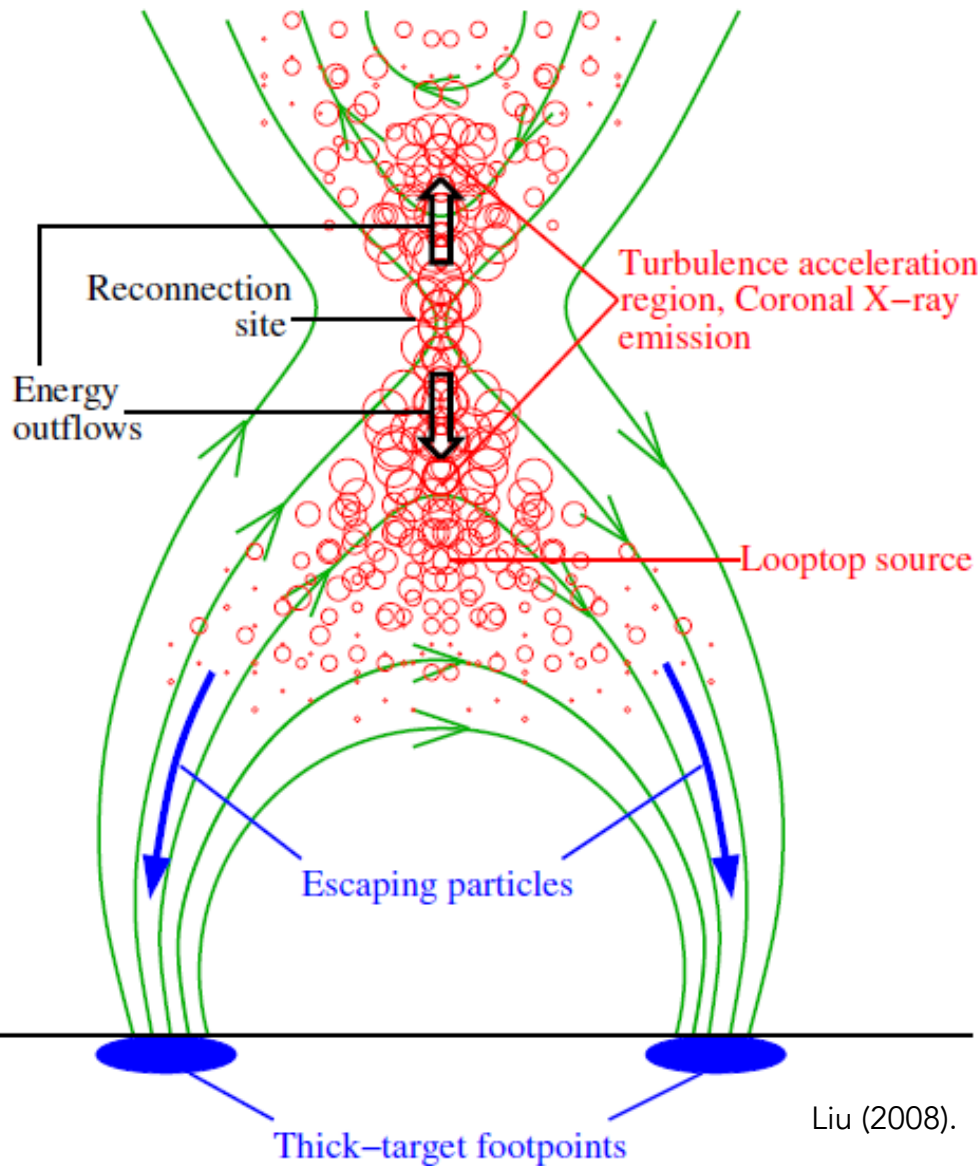
Energy sources (solar flare)

Typical values:
$$\left. \begin{array}{l} E \sim 10^{32} \text{erg} \\ V \sim d^3 \sim 10^{30} \text{cm}^3 \end{array} \right\} 100 \text{ erg cm}^{-3}$$

Energy source	Average observed values	Energy density [erg cm ⁻³]
Kinetic ($\sim m_p n v^2 / 2$)	$n \sim 10^9 \text{ cm}^{-3}$ $v \sim 10 \text{ km/s}$	$\sim 10^{-3}$
Thermal ($\sim n k_b T$)	$T \sim 10^6 - 10^7 \text{ K}$	$\sim 0.1 - 1.0$
Gravitational ($\sim m_p g H$)	$H \sim 10^5 \text{ km}$	~ 0.4
Magnetic ($\sim B^2 / 8\pi$)	$ B \sim 100 \text{ G}$	~ 400

Solar flares and CMEs are the most energetic phenomena in the solar system.

“Standard” model of a solar flare / CME

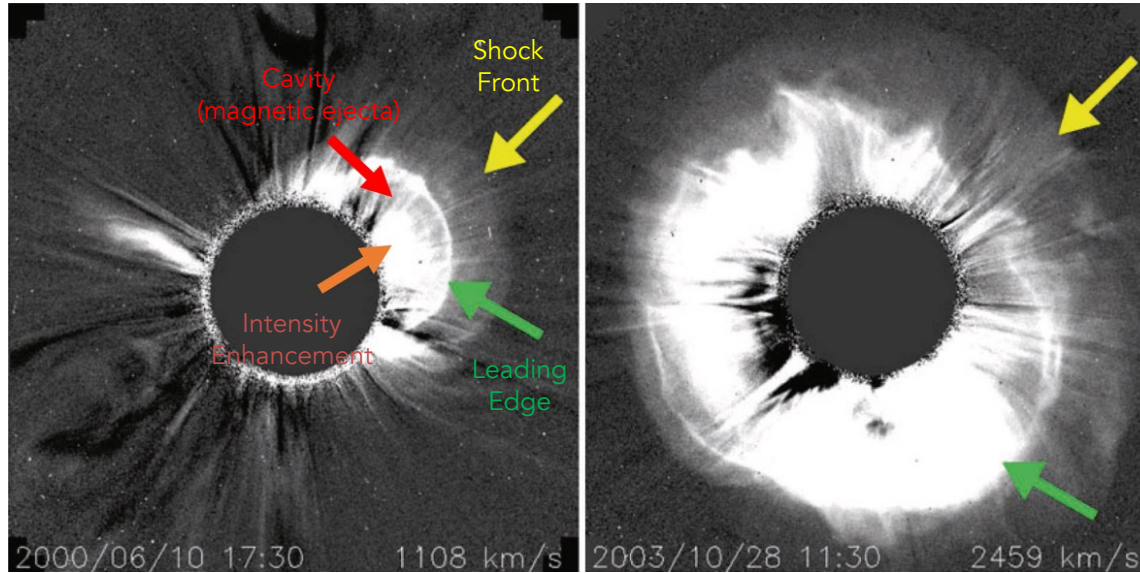


Grand archive of flare & CME cartoons:

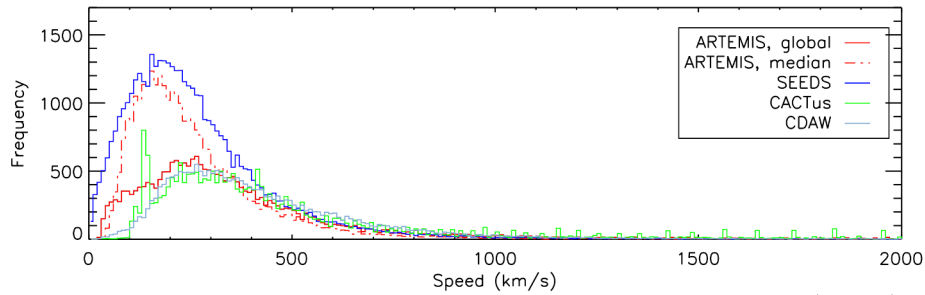
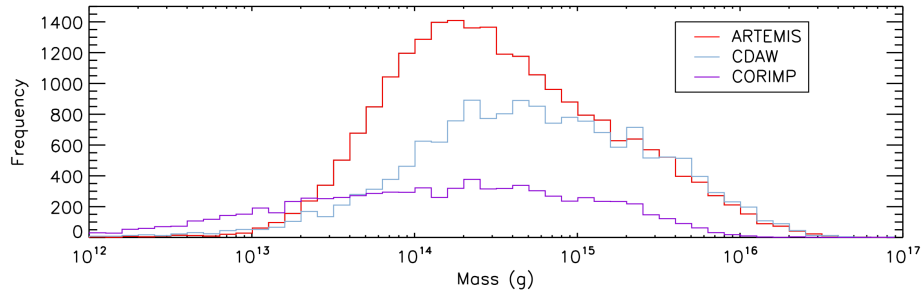
<https://www.astro.gla.ac.uk/cartoons/index.html>

CME: General Properties

Vourlidas+ (2013).

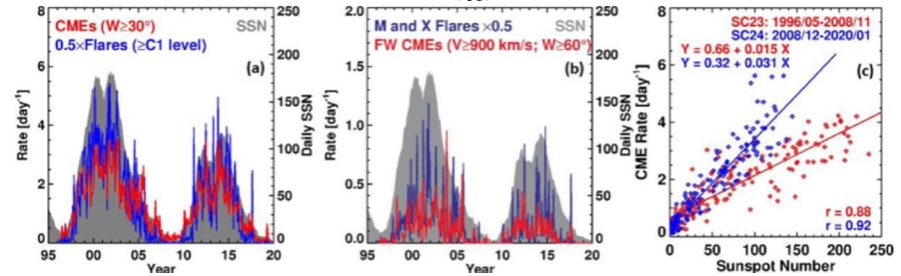
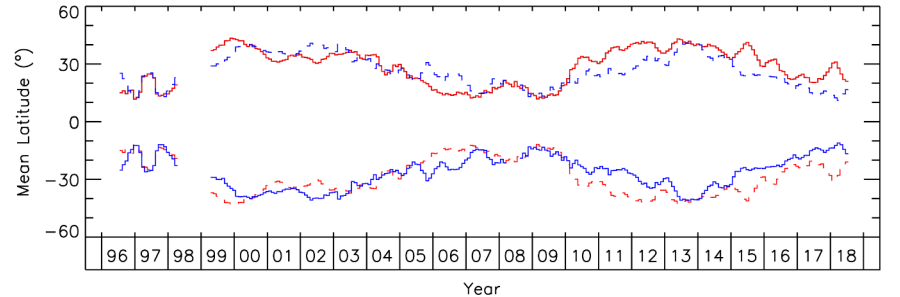


Mass and Velocity



Lamy+ (2019).

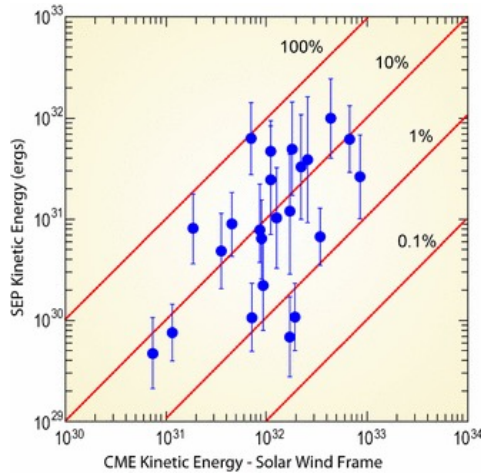
Connection with the (magnetic) activity cycle



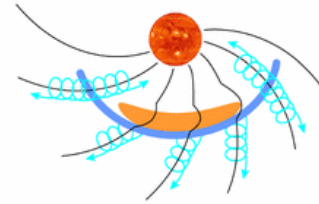
Zhang+ (2021).

Solar Energetic Particles (SEPs)

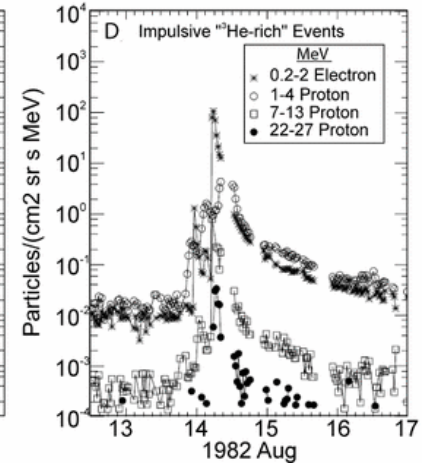
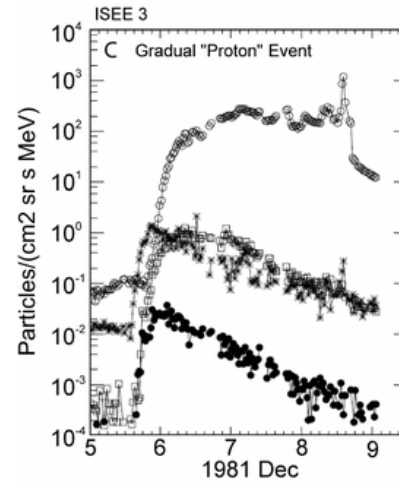
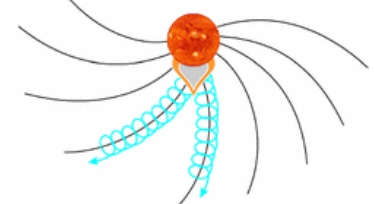
Property	Impulsive	Gradual
Electron/proton	$\sim 10^2 - 10^4$	$\sim 50 - 100$
$^3\text{He}/^4\text{He}$	~ 1	$\sim 4 \times 10^{-4}$
Fe/O	~ 1	~ 0.1
H/He	~ 10	~ 100
Q _{Fe}	~ 20	~ 14
SEP duration	$< 1 - 20$ h	$< 1 - 3$ days
Longitude cone	$< 30^\circ$	$< 100^\circ - 200^\circ$
Seed particles	Heated Corona	Ambient Corona or SW
Radio type	III	II
X-ray duration	~ 10 min - 1 h	$\gtrsim 1$ h
Coronagraph	N/A	CME
Solar eind	N/A	IP shock
Events/year	~ 1000	~ 10



(a) Gradual SEP events (CME shocks in corona and IP space)

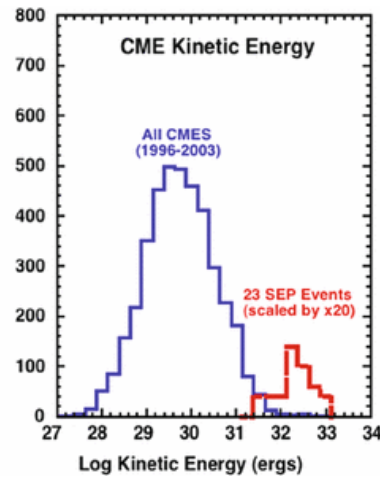
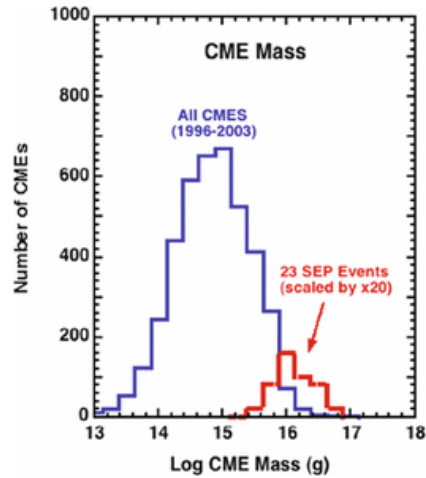


(b) Impulsive SEP events (acceleration in lower atmosphere)

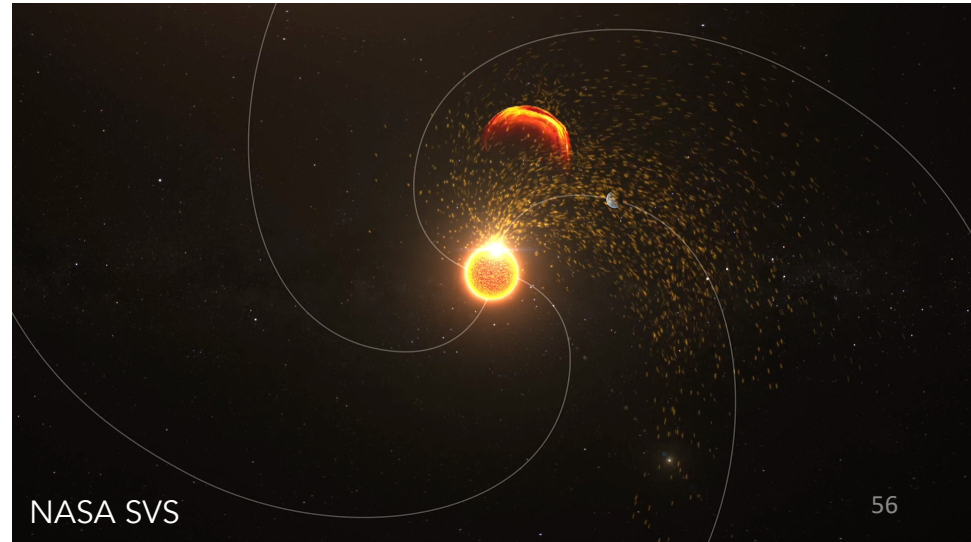


Reames (1999).

Desai & Giacalone (2016).

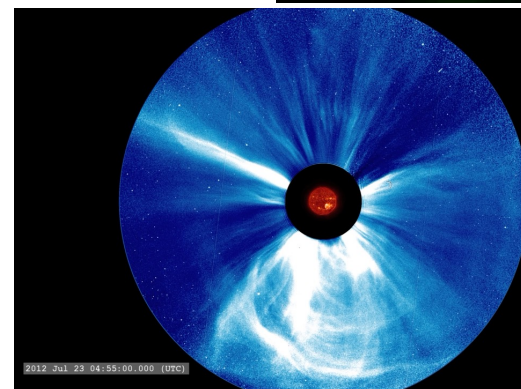
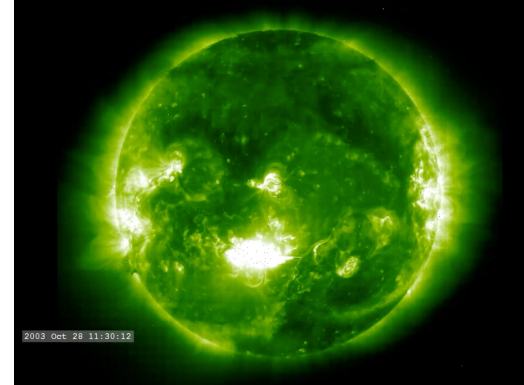


Mewald (2008).



Solar Flares – CMEs: Generalities and association

- **Flares:** Sudden energy release in the corona involving particle acceleration, radiation, and plasma heating.
- **CMEs:** "Localized" release of plasma and magnetic field into the solar/stellar wind (plasmoids/filament eruptions).
- Solar statistics: Large flares are nearly always accompanied by a CME (Yashiro & Gopalswamy 2009).



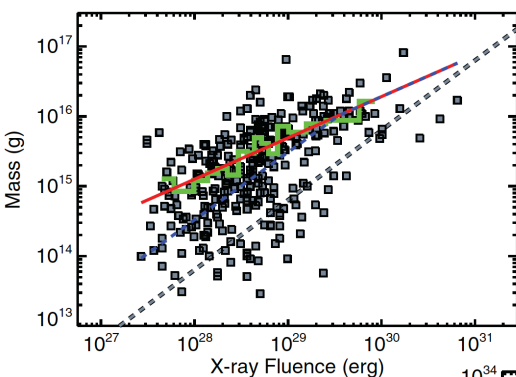
In the Sun:

$$E_K^{CME} \gg E_X^{FL}$$

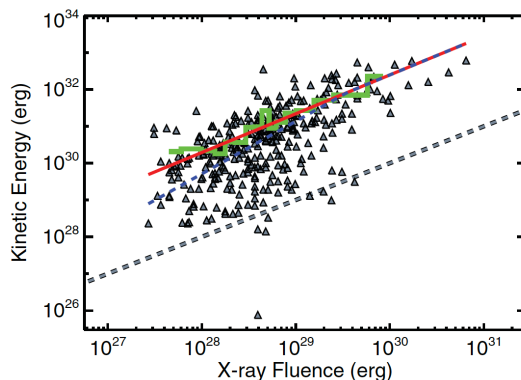
$$(E_K^{CME} \approx 2 - 3 E_X^{FL})$$

(Emslie+ 2012)

Extension to more active stars?



Studied by
Aarnio+ (2011)
Drake+ (2013)
Osten & Wolk (2015)
Odert+ (2017, 2020)



Consequences of extrapolating the observed mass and kinetic energy of CMEs associated with solar flares to more active stars.

A saturated Sun-like star ($L_x \sim 10^{30}$ erg/s) would have:

CME-Mass loss rate: $\dot{M} \sim 5 \times 10^{-10} M_\odot \text{ yr}^{-1}$

CME-Kinetic energy requirement: $\dot{E}_{ke} \sim 0.1 L_\odot$

Conclusion: The flare-CME relations (mass/energy) must flatten out for large energies ($\geq 10^{31}$ ergs)

Mass-loss rate considerations:

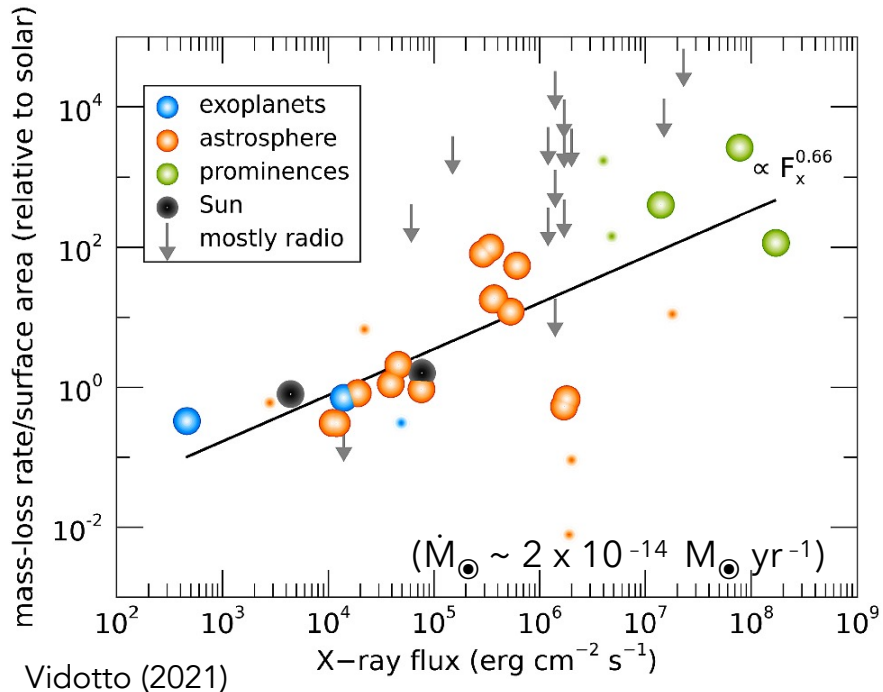
Aarnio+ (2012) finds similar values for T Tauri stars
($\dot{M} \sim 10^{-9} - 10^{-11} M_{\odot} \text{ yr}^{-1}$)

CME- \dot{M} values are inconsistent with the required radio transparency of the wind (Lim & White 1996)

Observational evidence supports weaker mass loss rates for very active stars (Wood+ 2018)

High scatter for M-dwarfs (Wood+ 2021)

X-ray charge exchange wind diagnostics: Relatively weak winds (Kislyakova+ 2024)



Energy and frequency considerations:

Largest GOES solar flare: $\sim 10^{31}$ ergs (SXR)

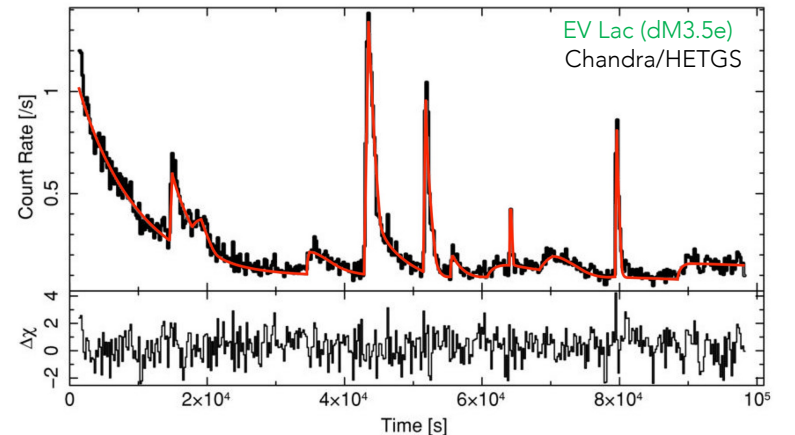
Active M-dwarfs: $\sim 10^{34}$ ergs / T-Tauri stars: $\sim 10^{36}$ ergs
(e.g. Güdel+ 2004, Osten+ 2007, Kowalski+ 2010)

Largest stellar flares (RS CVn/Algol-type): $\sim 10^{37}$ ergs
(e.g. Moschou+ 2017, Inoue+2023)

Flares on M-dwarfs occur approximately 1000 more often than on the Sun for a given energy (Loyd+ 2018).

Active/Inactive M-dwarfs show 10x difference in flare energies but the same flare frequency (Loyd+ 2018)

The corona of very active stars appears to be continuously flaring (e.g. Huenemoerder+ 2010)



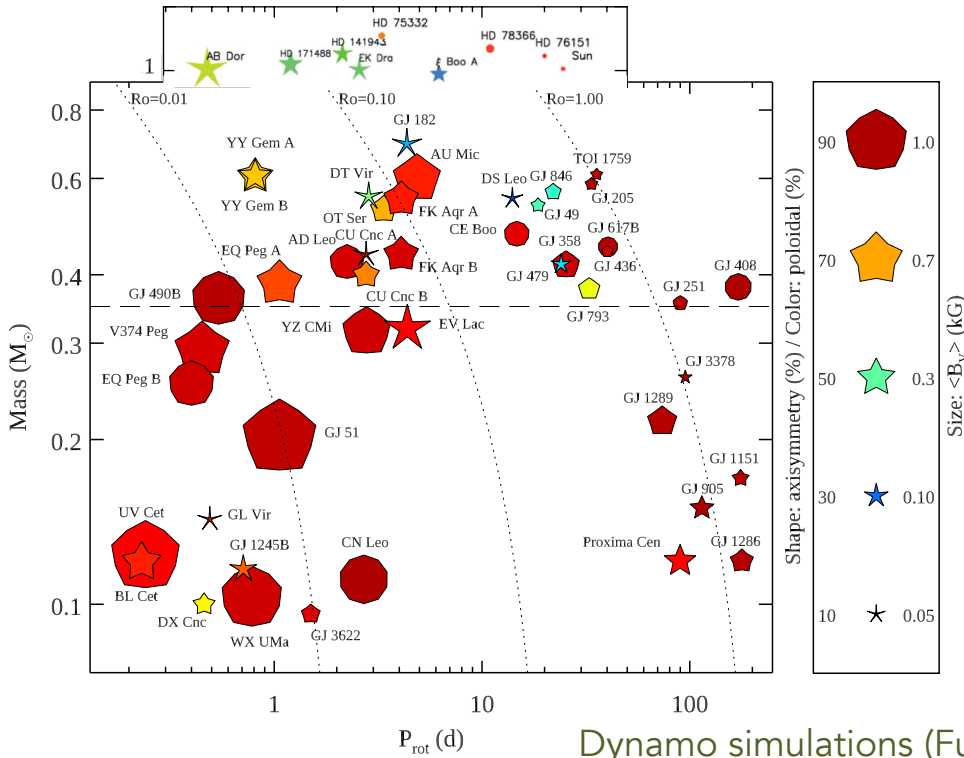
(Huenemoerder+ 2010)

Possible solution: Suppression of CMEs by an overlying magnetic field

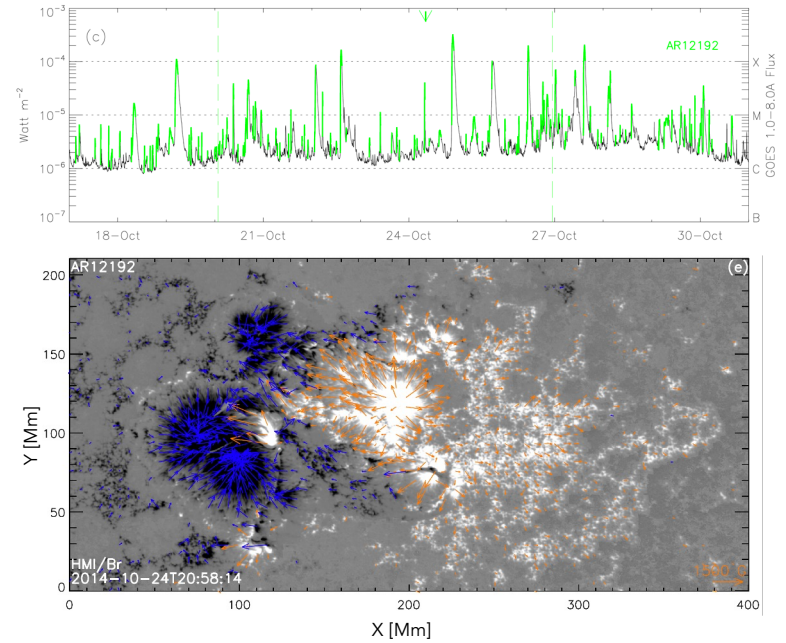
Stellar observations

Solar observations

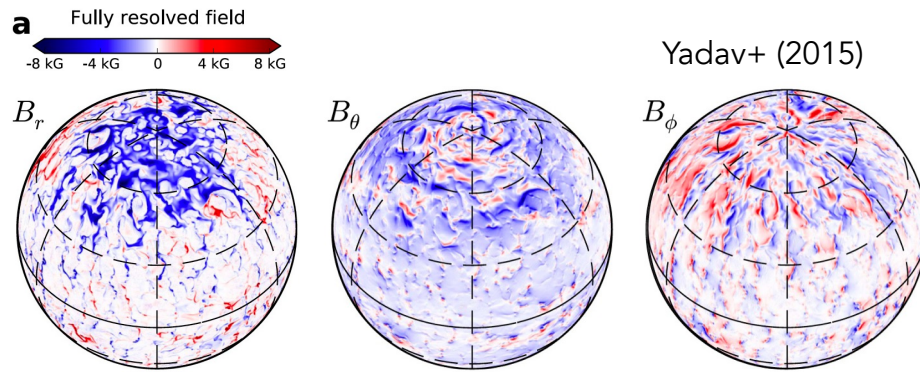
Donati & Landstreet (2009), Donati (2011); Kochukhov (2021)



Lin+ (2016)

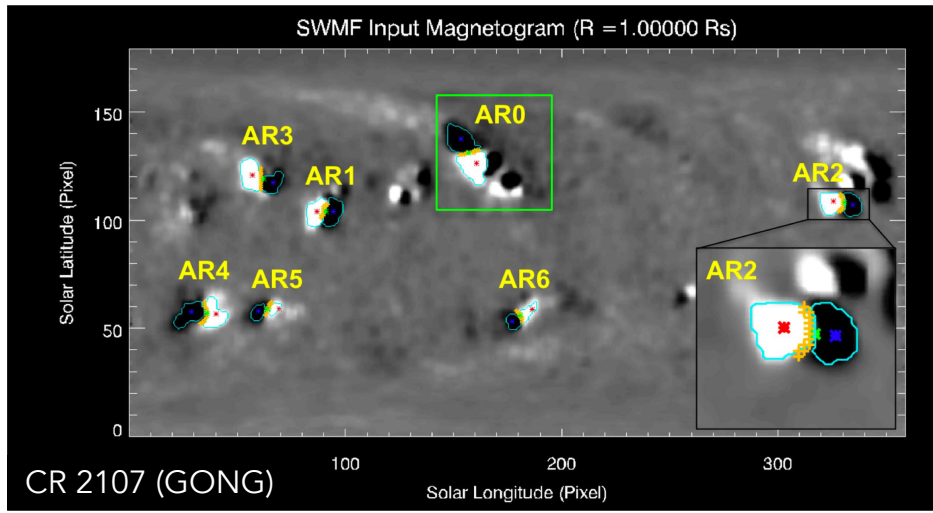


Dynamo simulations (Fully-convective stars)



3D CME simulations: Flux rope eruption models

Eruption of a twisted flux rope starting from the steady-state corona/wind solution (AWSoM; van der Holst+ 2014)
 Validated against Solar CME observations (Jin+ 2017)



Jin+ (2017)

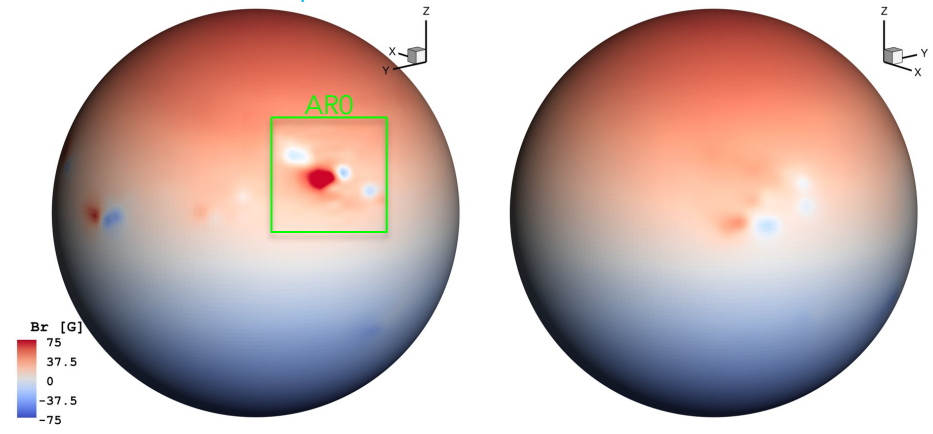
Parameters from the calibration study of the CME model applied on a "younger Sun".

Simulation domain: 1 – 50 R_{\odot}

Grid: Spherical + High-res spherical wedge (25 R_{\odot}).

1 hour wall-clock time for each CME simulation.

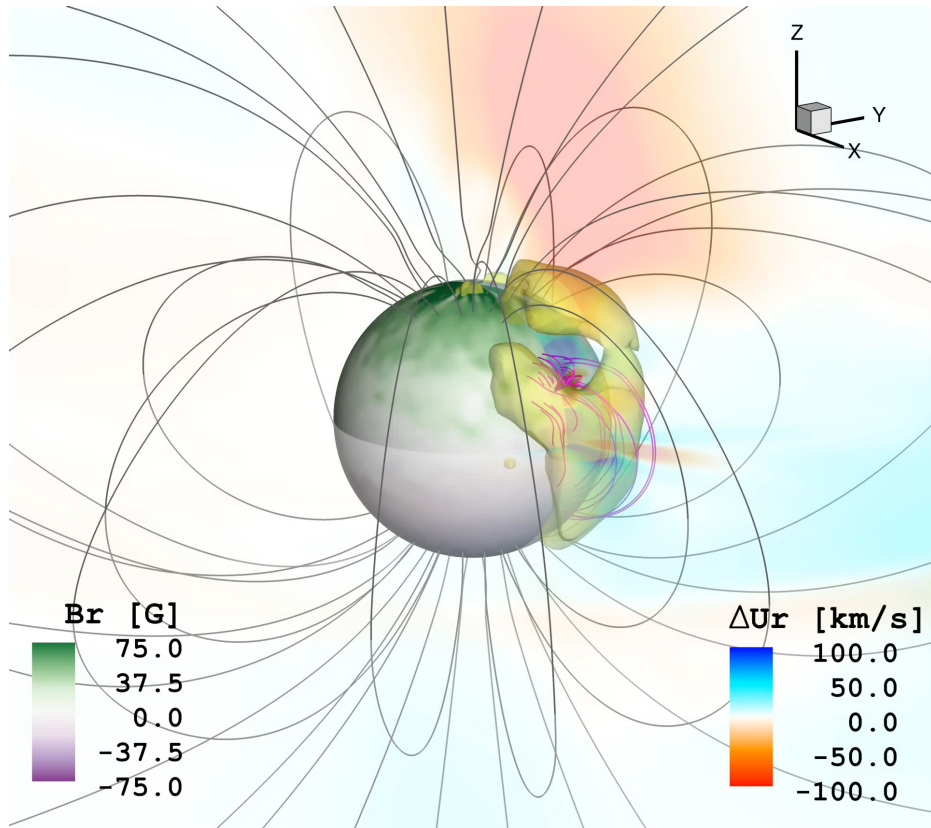
CR 2107 + 75 G Dipole



Alvarado-Gómez+ (2018)

Results:

Confined CMEs

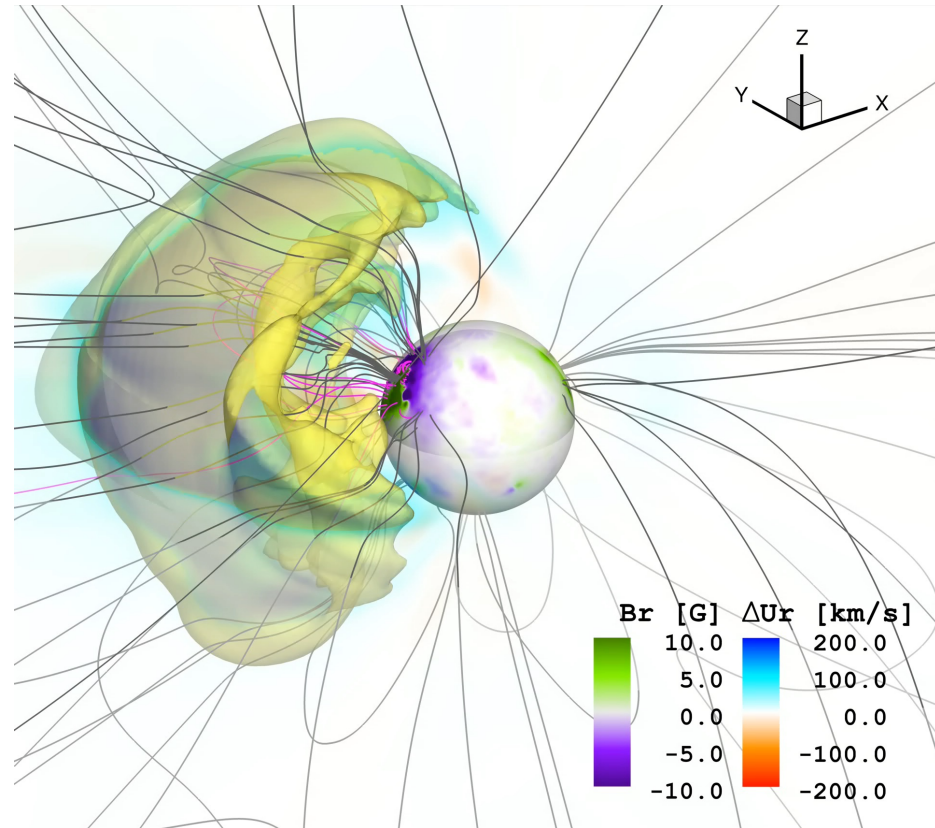


$\Phi_p = 1.94 \times 10^{22} \text{ Mx}$
(Equivalent GOES Class Flare: X5.0)

The coronal material rises following the overlying field lines.

The perturbed plasma remains confined within the region of the lower corona.

Alvarado-Gómez+ (2018, 2022)



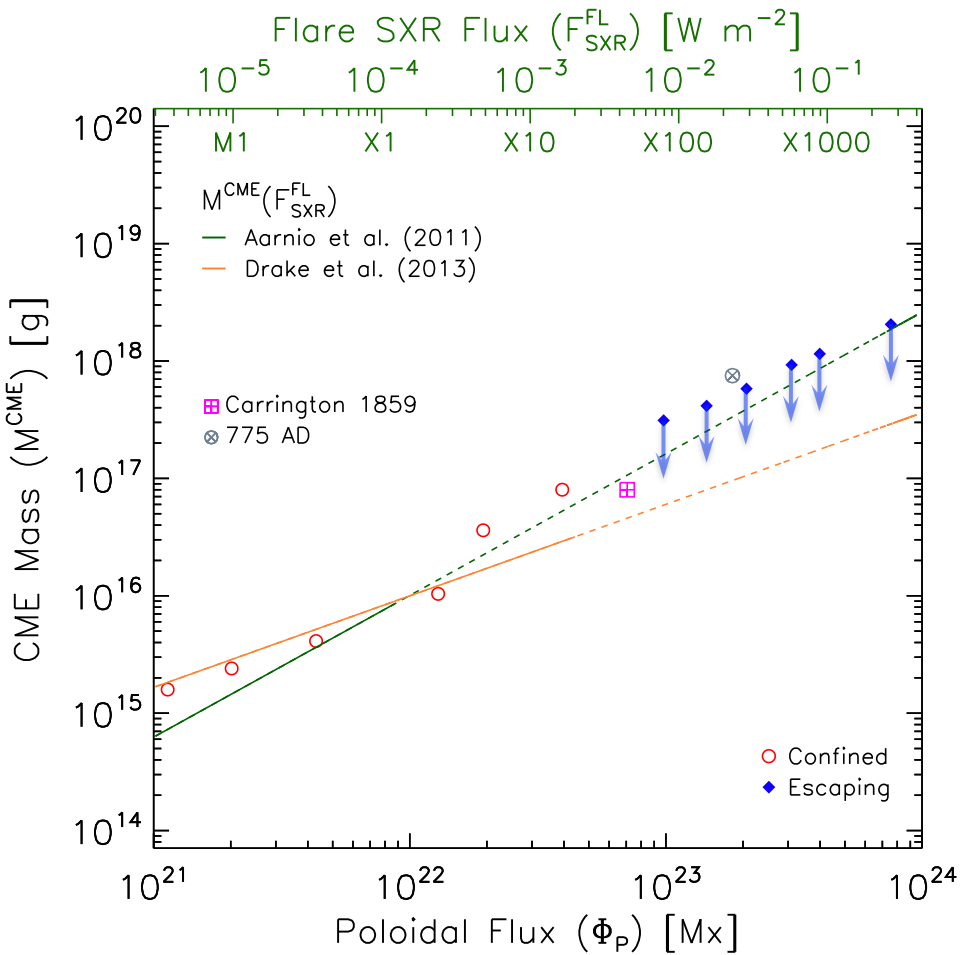
Solar CME simulation

Solar simulations: ~2500 – 3000 km/s
(CME-Speed – Φ_p Relation; Jin+ 2017)

See also: Sun, Torök & DeRosa (2021)

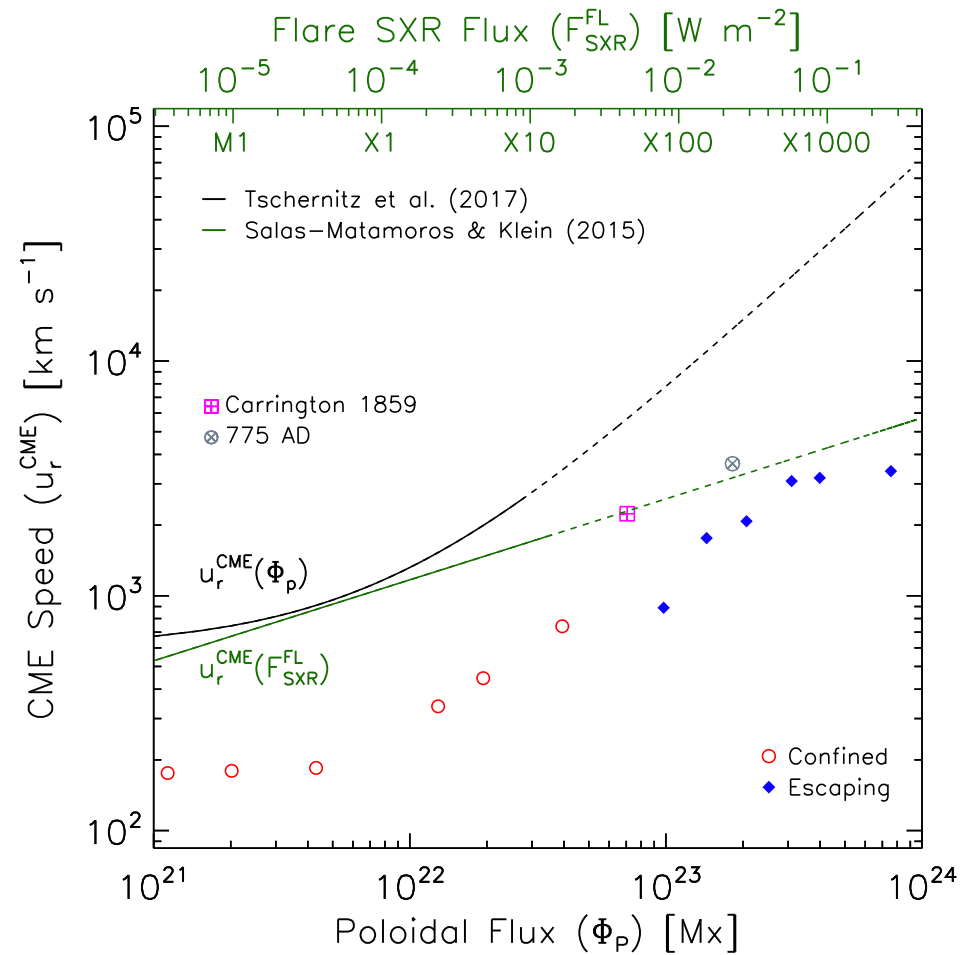
Results: CME radial speed and mass

Alvarado-Gómez+ (2018)



Simulated CME masses roughly align with extrapolations from solar data.

The large-scale field slows down all the CMEs.



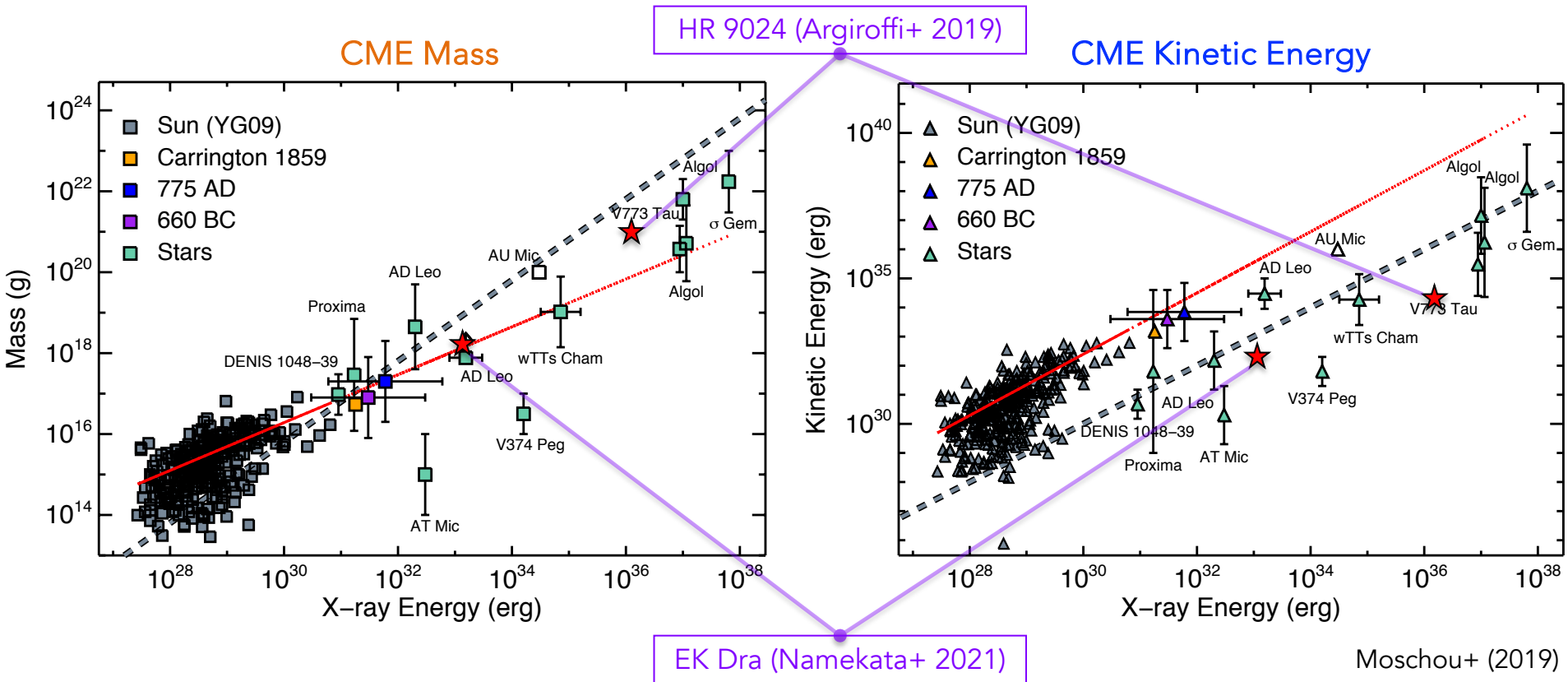
Escaping CMEs are less energetic than expected.

Predictions consistent with historical candidates and the recent direct detections of stellar CMEs!

Until very recently, there were **no definitive detections** of stellar CMEs

(e.g., Leitzinger+ 2014, 2020, Crosley+ 2016, Villadsen 2017, Crosley & Osten 2018, Muheki+ 2020a,b)

Moschou+ (2019): A comprehensive compilation of historical stellar **CME candidates**.
(see also Vida+ 2019)



Moschou+ (2019)

Red line: Fit to the solar data (and extrapolation)

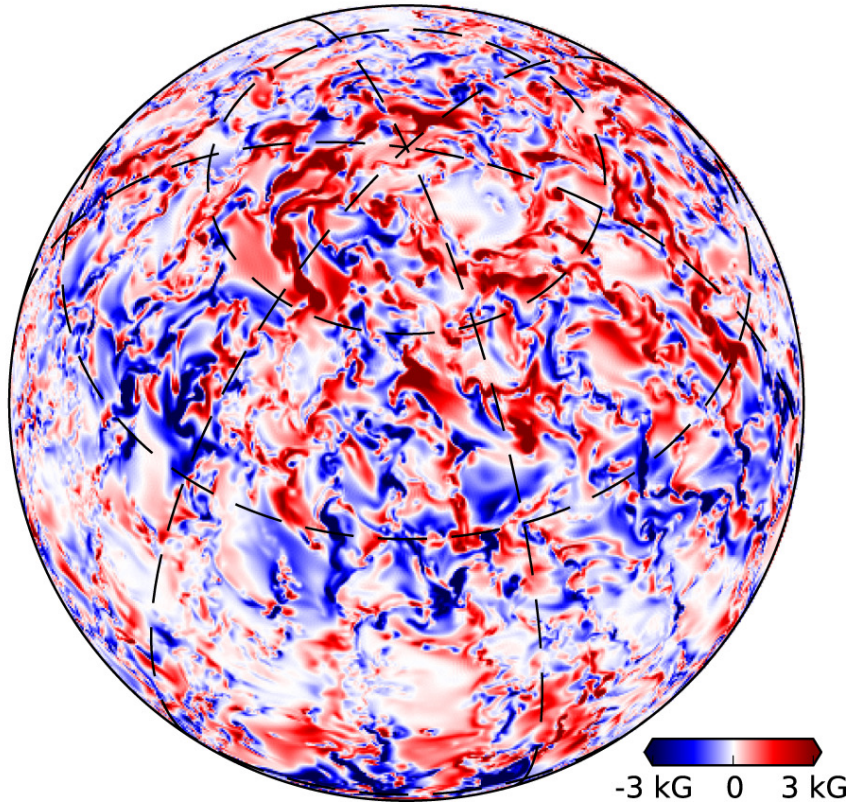
Dashed line: Constant ratio of CME mass loss to flare X-ray energy loss.

Parity between flare X-ray and CME Kinetic energies.

Moving into the Strong Field / High-Complexity Regime: M-Dwarf Stars

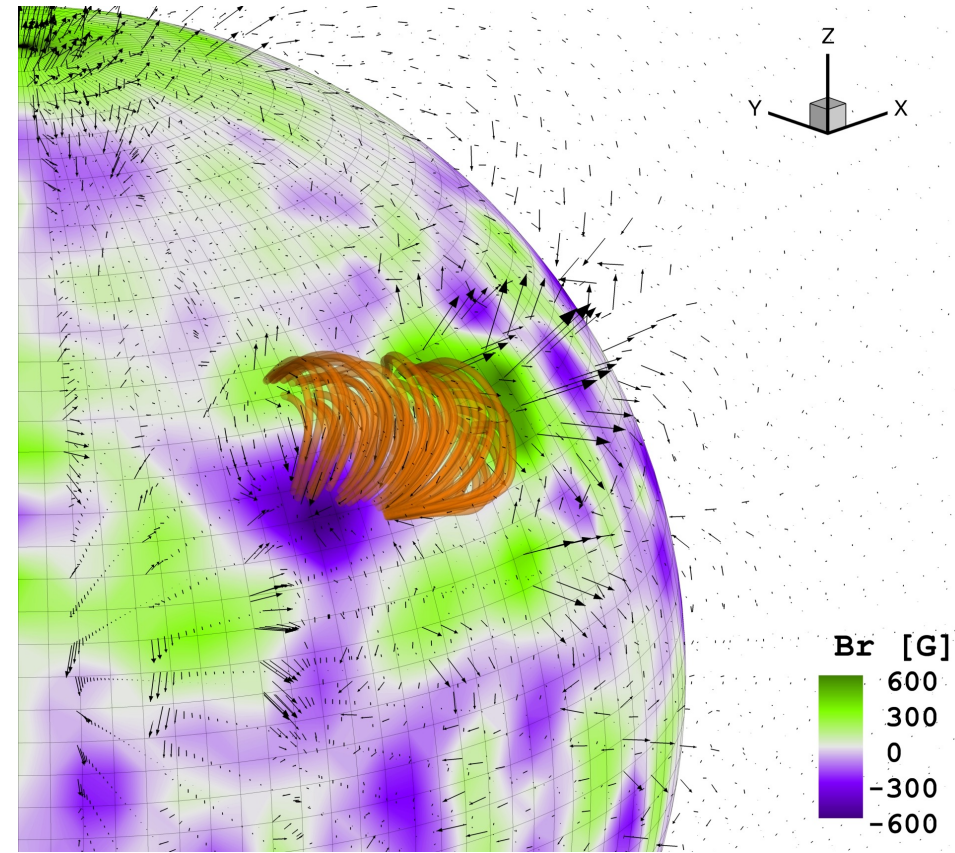
Surface magnetic field predictions from
fully-convective dynamo models

Radial magnetic field



Yadav+ (2016)

Consider different CME Eruption Models
(Gibson-Low / Titov-Démoulin)



Alvarado-Gómez+ (2019b)

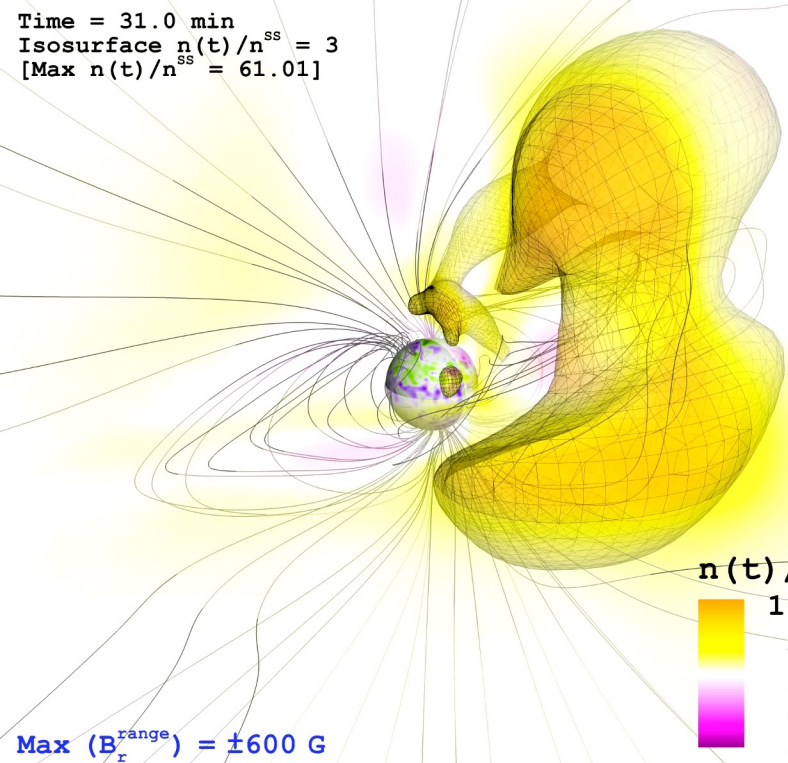
Coronal response after a flux-rope eruption event for different background magnetic fields
(consistent with low- to moderately-active M-dwarfs; see Reiners 2022).

Exploring the CME magnetic confinement spectrum

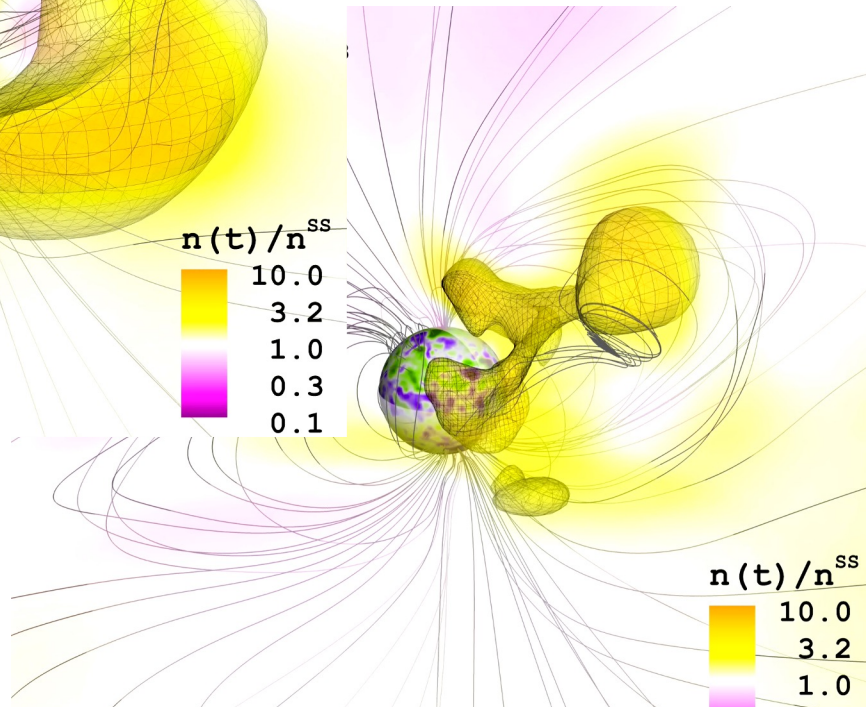
$$M_{\text{CME}} \sim 4 \times 10^{14} \text{ g}$$

$$E_{\text{B-Free}} \sim 6.5 \times 10^{34} \text{ erg}$$

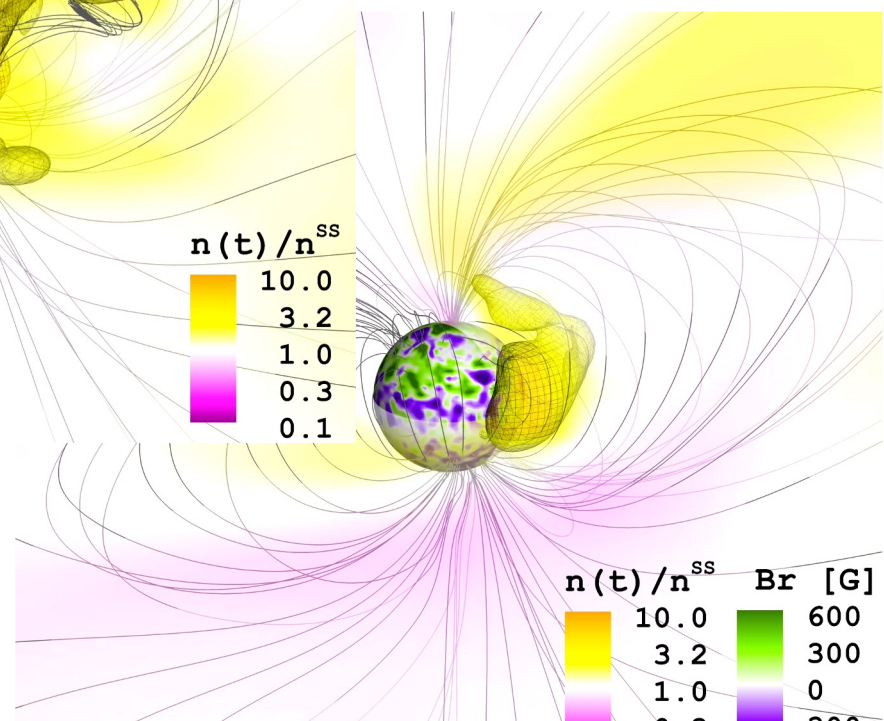
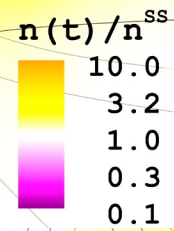
Alvarado-Gómez+ (2019b)



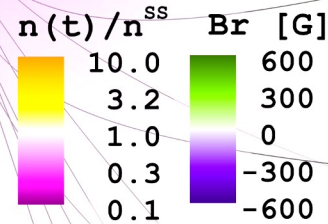
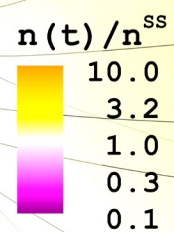
Max (B_r^{range}) = ± 600 G
Weak



Max (B_r^{range}) = ± 1000 G
Partial



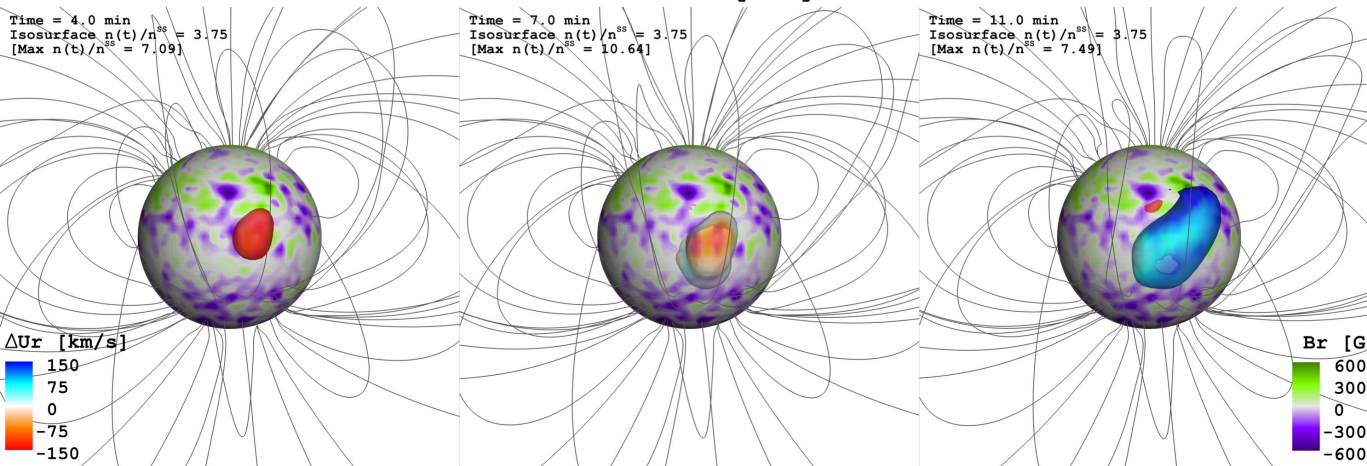
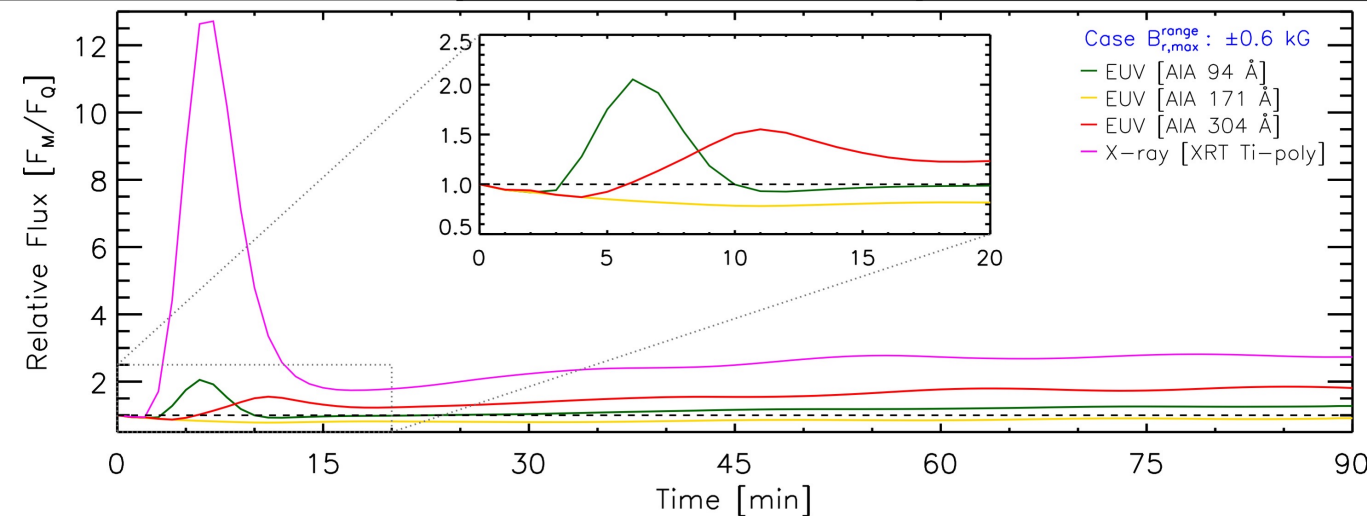
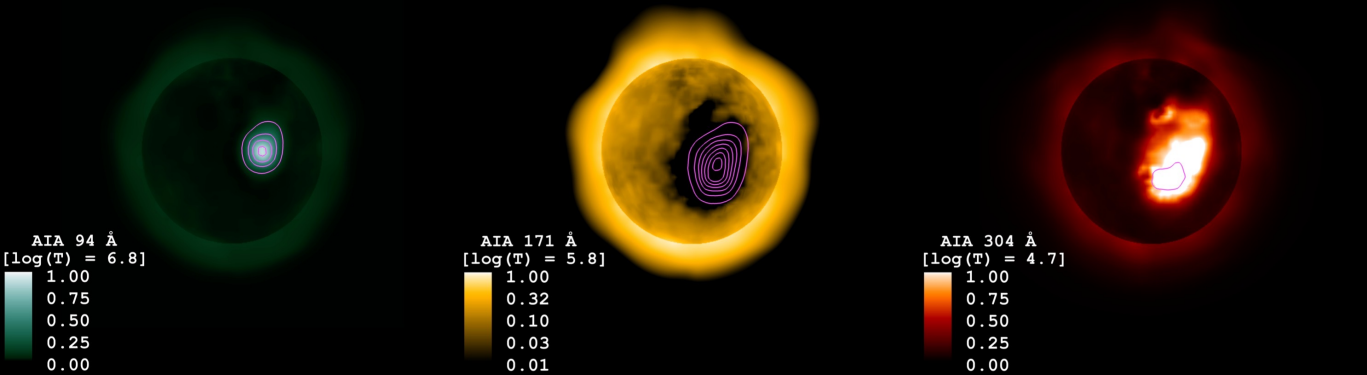
Max (B_r^{range}) = ± 1400 G



Time = 4.0 min

Time = 7.0 min

Time = 11.0 min



Weak CME confinement:

Collapse of the flux-rope towards the surface + 'bounce' against the underlying canopy.

Induced flare-like profile (X-rays and EUV).

Transient dimming feature at mid coronal temperatures.

Distinctive progression of high-energy emission and Doppler shifts (~ 150 km/s).

Hints of similar processes occurring on small-scales in the Sun (Sterling+ 2015).

Partial CME confinement:

The flux-rope collapse and escape is significantly slowed down.

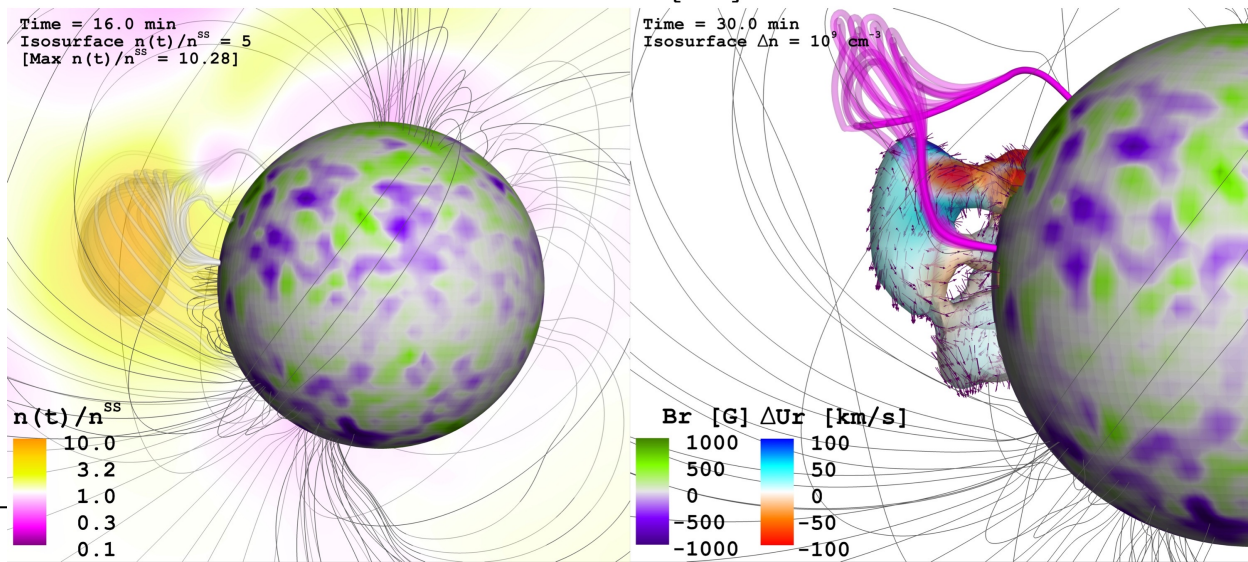
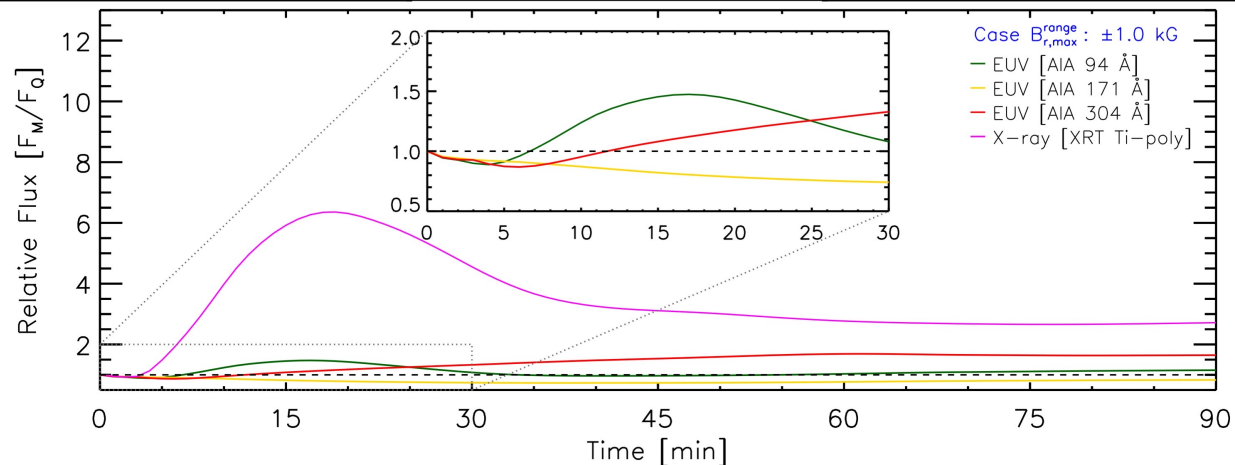
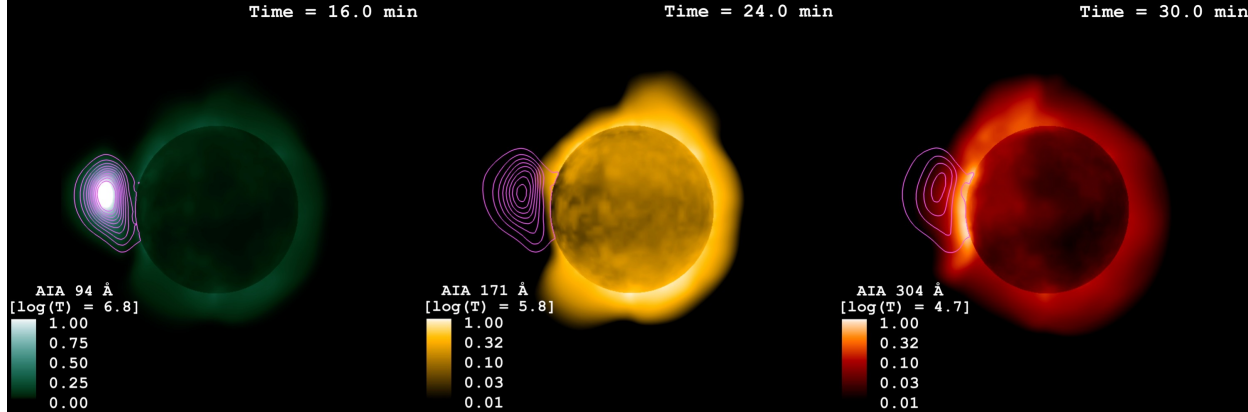
Longer and weaker flare-like coronal response (strong B-compression).

Longer duration coronal dimming event (mid-T).

The eruption gets disrupted. Only a small fraction escapes.

A short-lived dense prominence-like structure is formed (± 100 km/s).

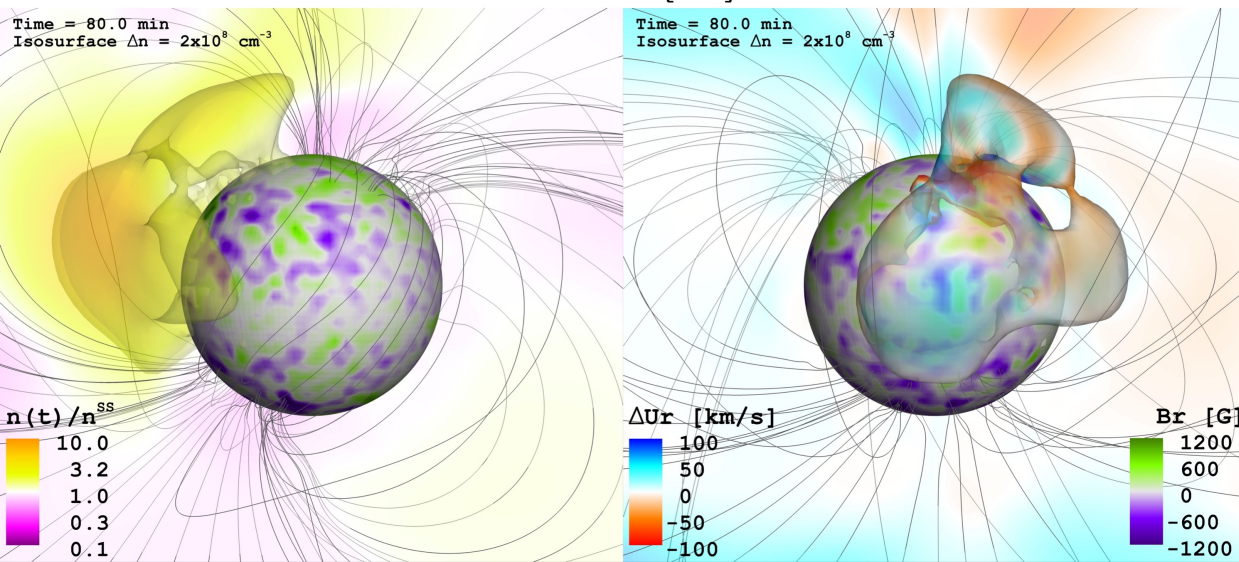
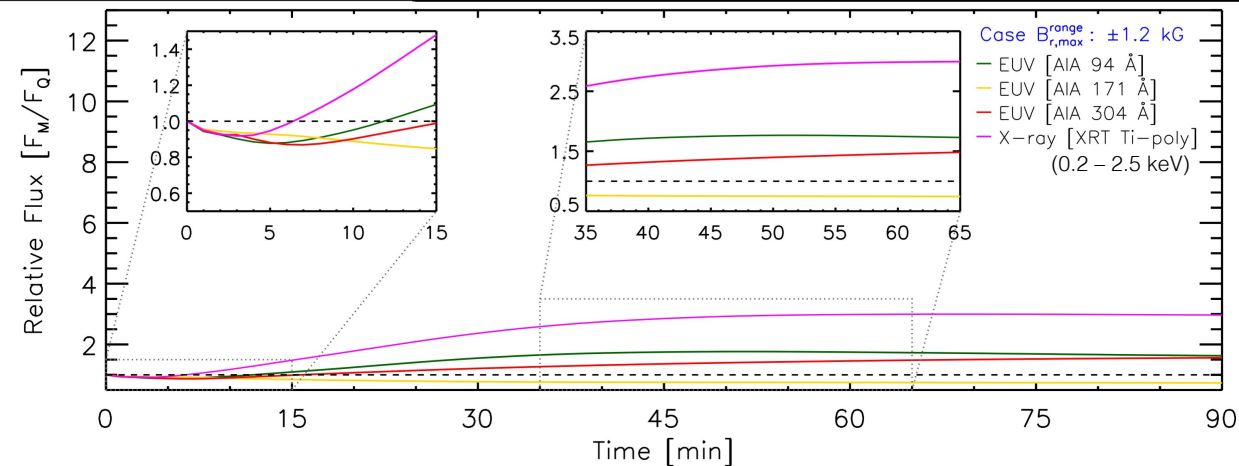
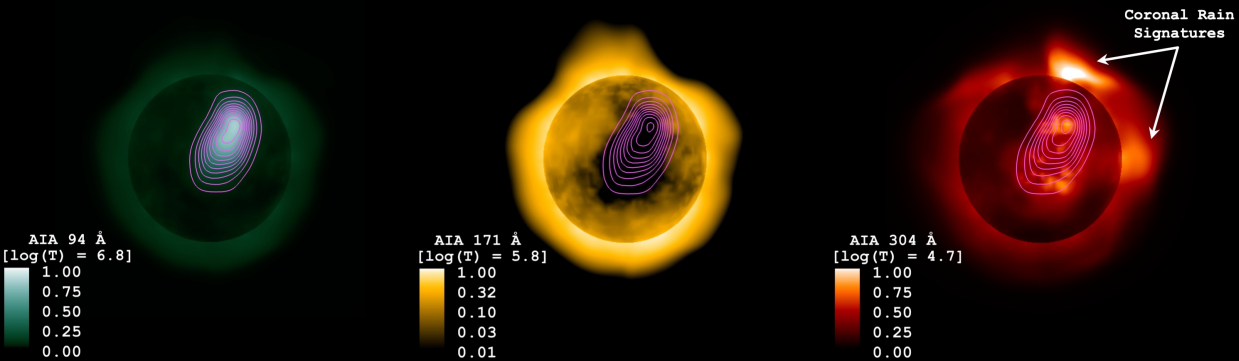
Signatures of coronal rain/condensations in low-T corona (± 50 km/s). Similar to solar counterparts (Antolin+ 2012).



Time = 50.0 min

Time = 65.0 min

Time = 80.0 min



Strong CME confinement:

The eruption is strongly restricted. Velocities of collapse are greatly reduced.

Gradual and weak increase in the high-energy emission (factors ~ 2 -3).

Long-lasting dimming feature at mid coronal temperatures.

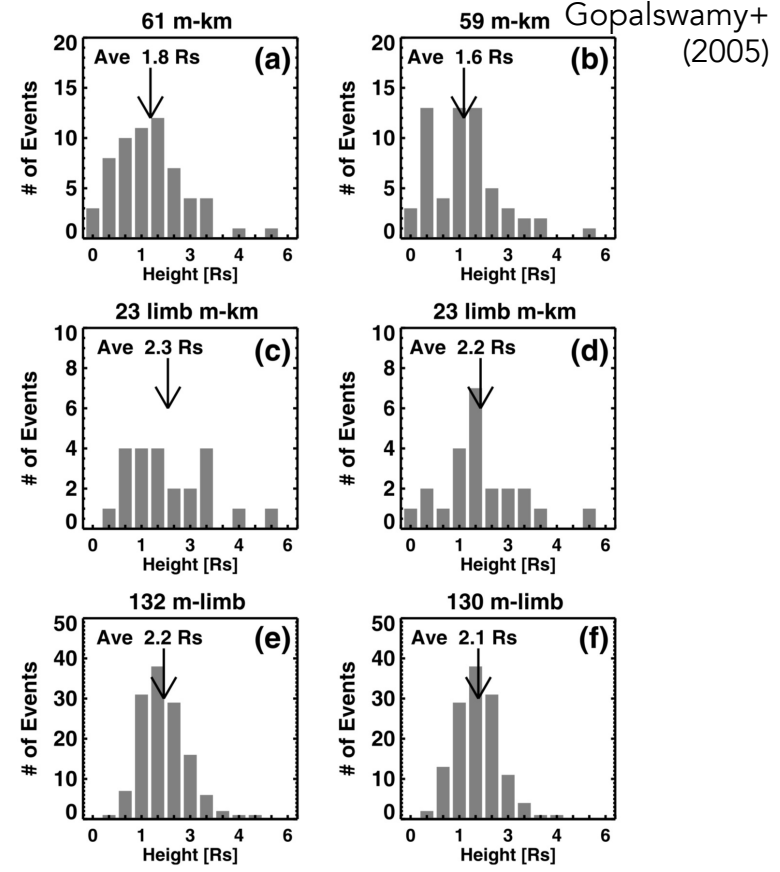
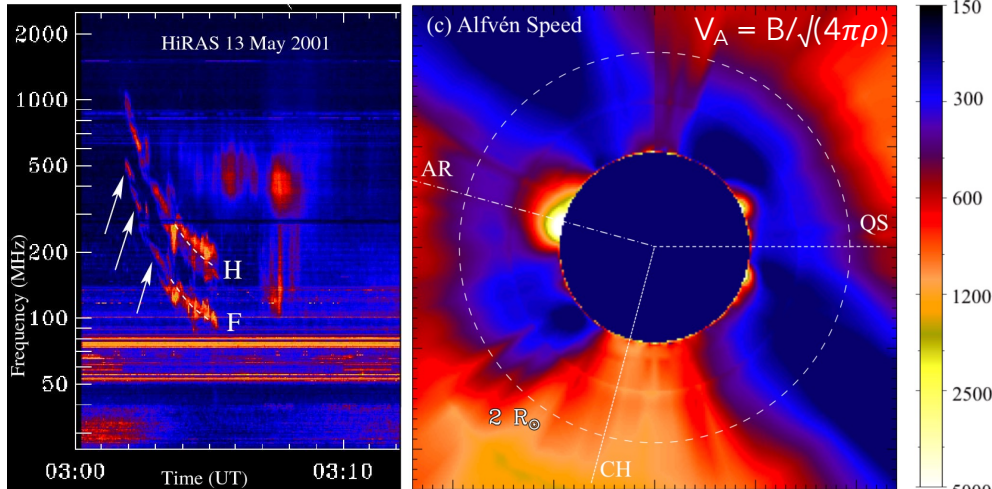
The perturbation remains confined to the low corona. A very small fraction of mass escapes in the form of a polar streamer.

A “coronal rain cloud” is formed. The material falls back to the star (net redshift $\sim 2.5 \text{ km/s}$).

Similar behavior has been reported for EK Draconis (Ayres 2015).

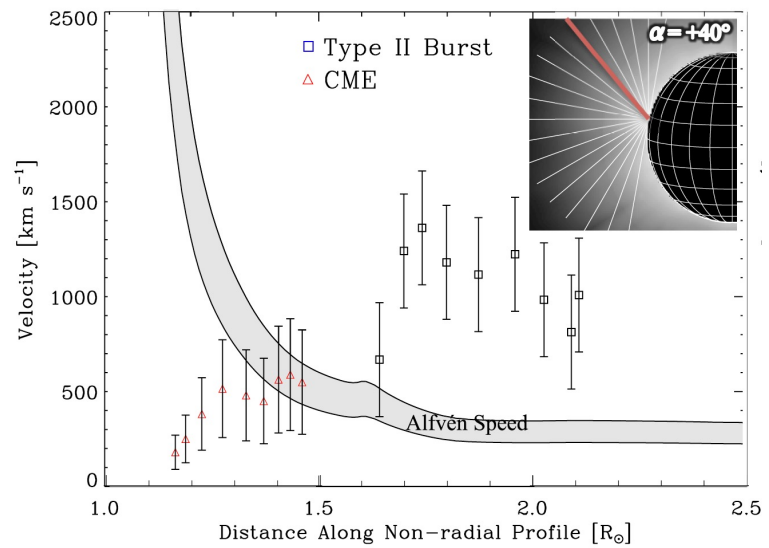
Stellar CME detectability based on Type-II radio bursts:

Solar radio bursts of Type II are indicative of an MHD shock in the corona/inner heliosphere, accompanied by electron acceleration. Strong connection with Solar Energetic Particle events (SEPs).



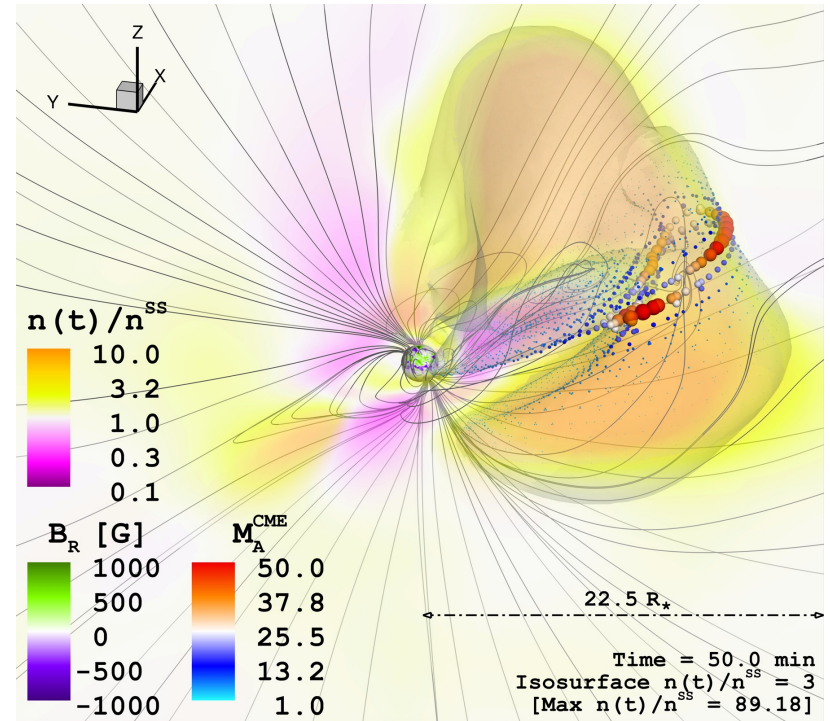
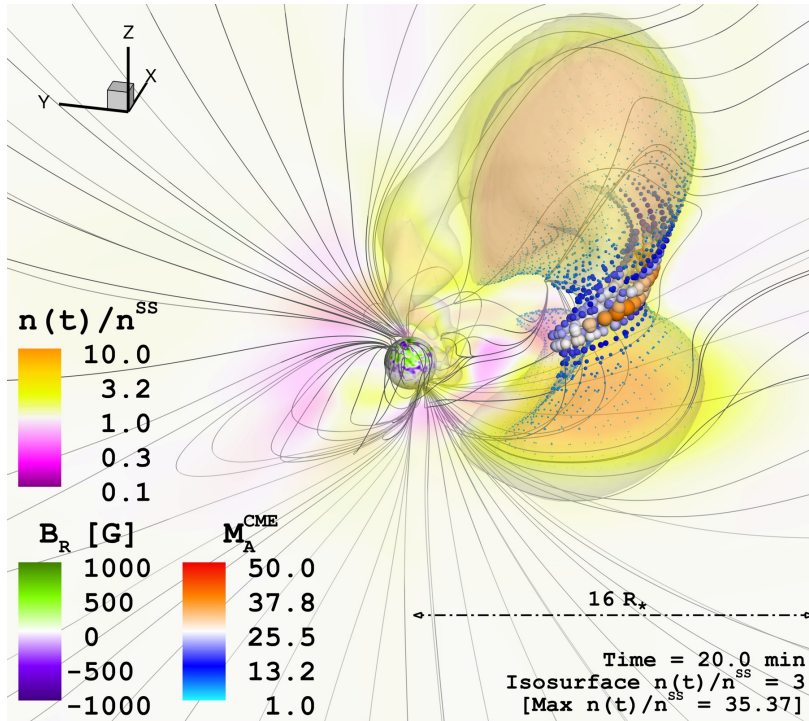
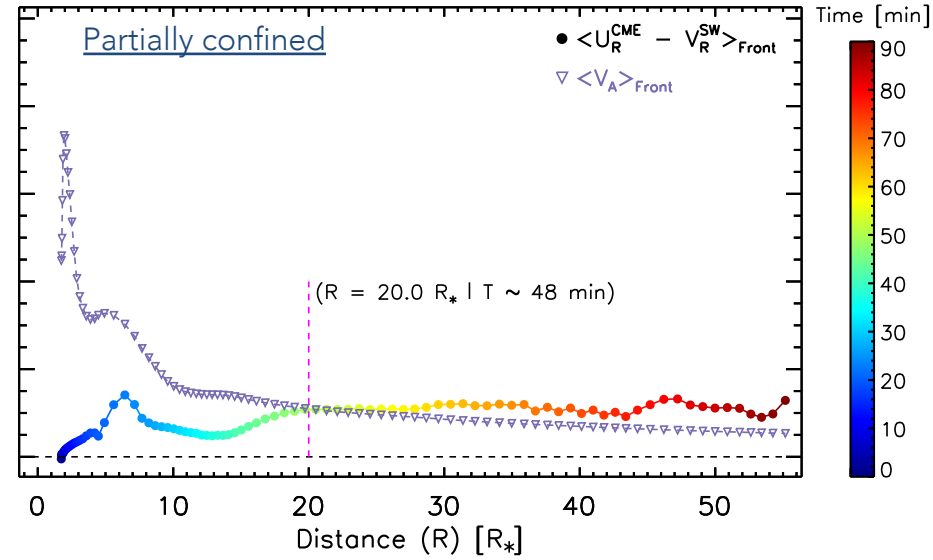
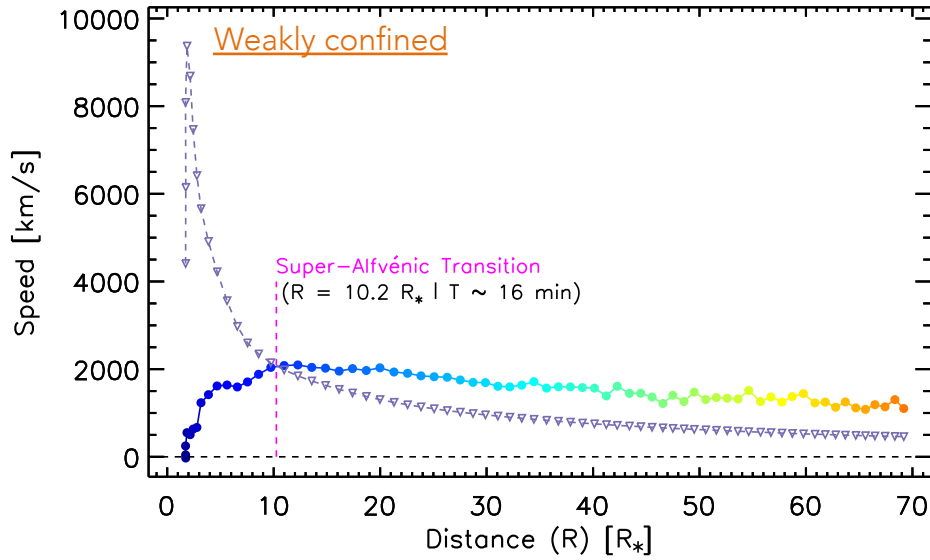
Shocks in solar Type II Radio bursts take place close to the surface.

The frequency (and intensity) of a type II radio burst depends on the value of the ambient density (\sqrt{n}).



Zucca+ (2014)

Due to **magnetic suppression**, stellar CMEs become super-Alfvénic (inducing shocks) **further away from the star**.



Therefore, the associated Type II radio bursts are **shifted to lower frequencies** (compared to the standard solar case).

$$\nu_p = (2\pi)^{-1} \sqrt{(4\pi e^2/m_e)} \sqrt{n} \approx 8980 \sqrt{n} \text{ [Hz]}$$

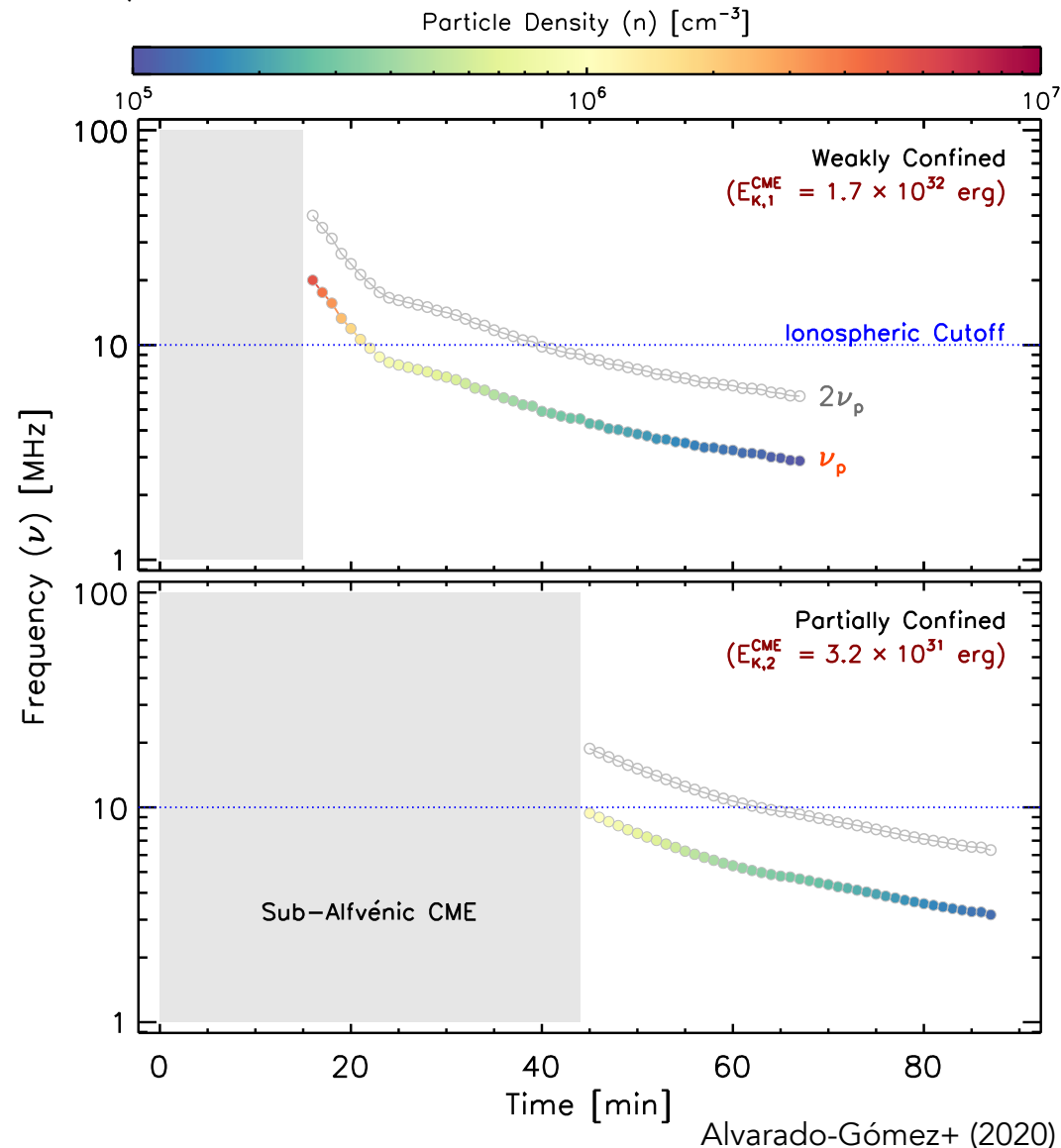
Both fundamental and harmonic lanes appear very close to the ionospheric cutoff (~ 10 MHz)

Not entirely "Radio Quiet" but:

- The **strongest solar type II radio bursts** reach spectral fluxes up to 10^8 Jy (Schmidt & Cairns 2016).
- If occurring in Proxima: **1.4 mJy** (1.3 pc) LOFAR sensitivity: **~ 5 mJy*** SKA might reach the sensitivity but will only start at **50 MHz**.

Our numerical description of Proxima Centauri provides a "best case scenario":

- A lower bound on the mean surface field strength (~ 450 G, Reiners & Basri 2008).
- Highest stellar wind density allowed by observations ($\dot{M} \approx 0.3 \dot{M}_\odot$, Wood+ 2001).
- A CME shock trajectory following the current sheet (global minimum of V_A).



The B-suppression of stellar CMEs greatly hampers their detectability through type II radio bursts from the ground.

Space Weather in the AU Mic System

AU Microscopii (M1V)

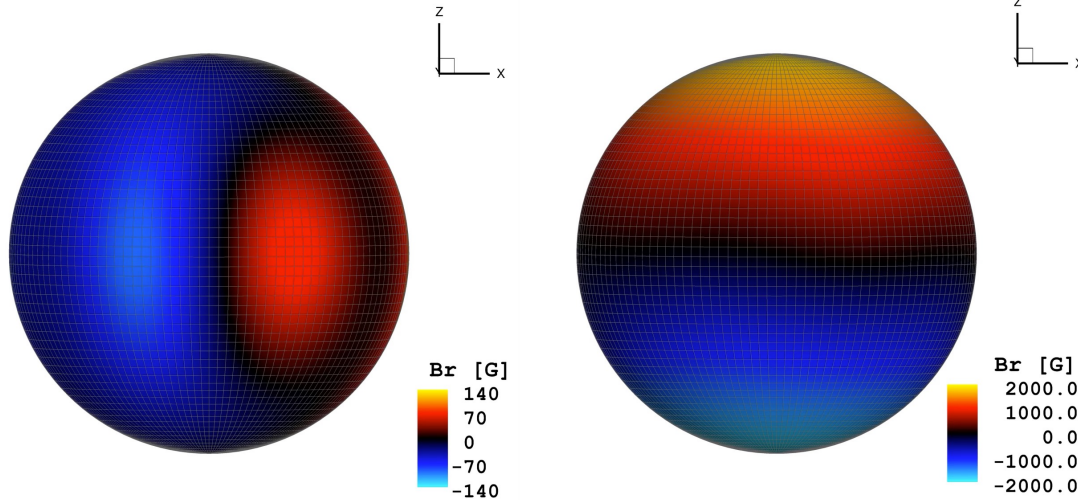
$M_{\star} \approx 0.50 M_{\odot}$

$R_{\star} \approx 0.75 R_{\odot}$

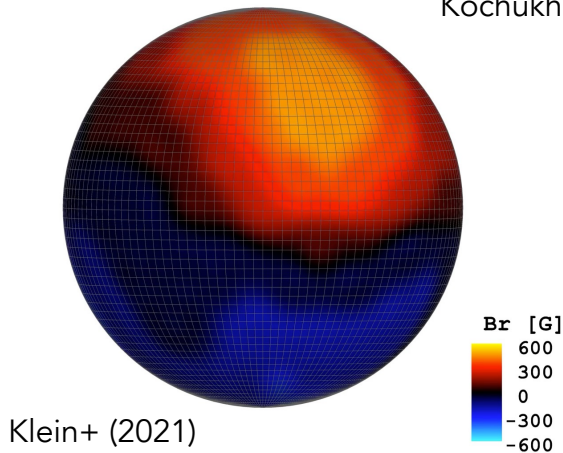
$P_{\text{ROT}} \approx 4.85$ days

Two transiting Neptune-sized planets.
(Plavchan+ 2020, Martioli+2021)

Constraints on its surface magnetism (polarimetry + ZDI)



Kochukhov & Reiners (2020)



Klein+ (2021)

Extremely active flare star (Age: 22 Mys)



Complete characterization of the space weather environment:
Stellar wind, CMEs, Atmospheric loss, Energetic particles...



Simulating the Space Weather in the AU Mic System: Stellar Winds and Extreme Coronal Mass Ejections

Julián D. Alvarado-Gómez^{1,8}, Ofer Cohen², Jeremy J. Drake³, Federico Fraschetti^{3,4}, Katja Poppenhaeger^{1,5}, Cecilia Garraffo³, Judy Chebly^{1,5}, Ekaterina Ilin^{1,5}, Laura Harbach⁶, and Oleg Kochukhov⁷

¹ Leibniz Institute for Astrophysics Potsdam, An der Sternwarte 16, D-14482 Potsdam, Germany; julian.alvarado-gomez@aip.de

² University of Massachusetts at Lowell, Department of Physics & Applied Physics, 600 Suffolk Street, Lowell, MA 01854, USA

³ Center for Astrophysics | Harvard & Smithsonian, 60 Garden Street, Cambridge, MA 02138, USA

⁴ Department of Planetary Sciences-Lunar and Planetary Laboratory, University of Arizona, Tucson, AZ 85721, USA

⁵ University of Potsdam, Institute for Physics and Astronomy, Karl-Liebknecht-Str. 24/25, D-14476 Potsdam, Germany

⁶ Imperial College London, Astrophysics Group, Department of Physics, Prince Consort Road, London, SW7 2AZ, UK

⁷ Department of Physics and Astronomy, Uppsala University, Box 516, SE-75120 Uppsala, Sweden

⁸ Received 2021 November 23; revised 2022 January 26; accepted 2022 February 14; published 2022 April 4



Space-weather-driven Variations in Ly α Absorption Signatures of Exoplanet Atmospheric Escape: MHD Simulations and the Case of AU Mic b

Ofer Cohen¹, Julián D. Alvarado-Gómez², Jeremy J. Drake³, Laura M. Harbach⁴, Cecilia Garraffo³, and Federico Fraschetti^{3,5}

¹ Lowell Center for Space Science and Technology, University of Massachusetts Lowell, 600 Suffolk Street, Lowell, MA 01854, USA; ofer_cohen@uml.edu

² Leibniz Institute for Astrophysics Potsdam, An der Sternwarte 16, D-14482 Potsdam, Germany

³ Center for Astrophysics | Harvard & Smithsonian, 60 Garden Street, Cambridge, MA 02138, USA

⁴ Astrophysics Group, Department of Physics, Imperial College London, Prince Consort Rd, London, SW7 2AZ, UK

⁵ Dept. of Planetary Sciences-Lunar and Planetary Laboratory, University of Arizona, Tucson, AZ 85721, USA

Received 2022 March 25; revised 2022 May 26; accepted 2022 June 13; published 2022 August 5



Stellar Energetic Particle Transport in the Turbulent and CME-disrupted Stellar Wind of AU Microscopii

Federico Fraschetti^{1,2}, Julián D. Alvarado-Gómez³, Jeremy J. Drake¹, Ofer Cohen⁴, and Cecilia Garraffo¹

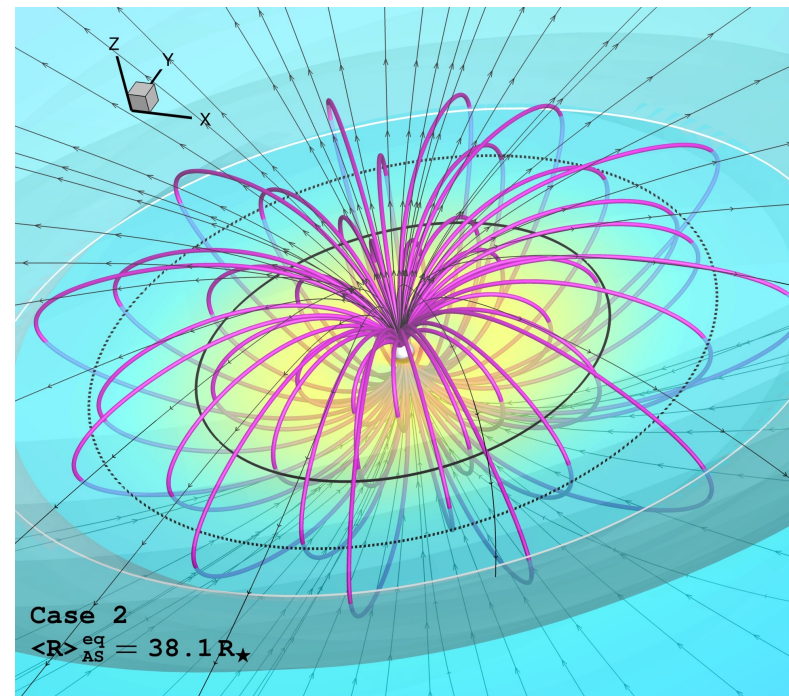
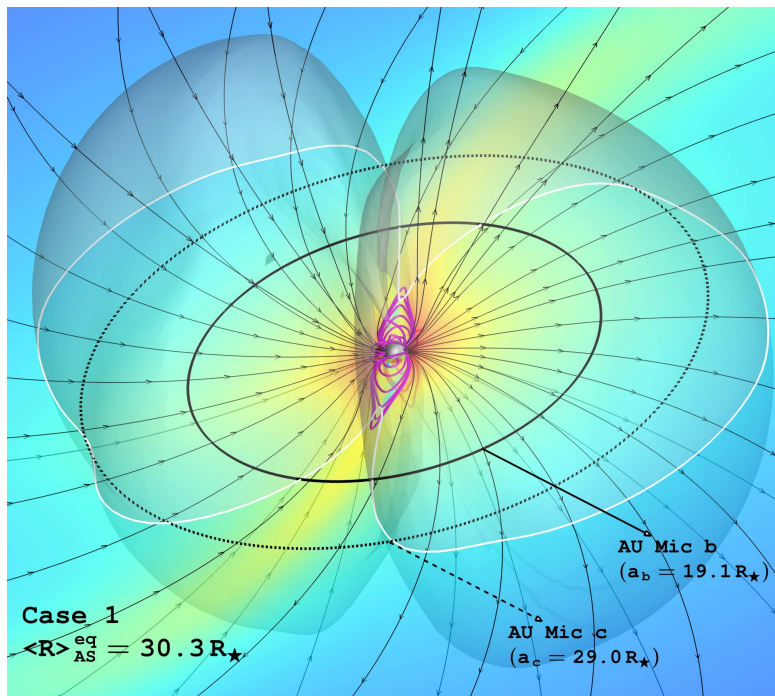
¹ Center for Astrophysics | Harvard & Smithsonian, 60 Garden Street, Cambridge, MA, 02138, USA; federico.fraschetti@cfa.harvard.edu

² Dept. of Planetary Sciences-Lunar and Planetary Laboratory, University of Arizona, Tucson, AZ, 85721, USA

³ Leibniz Institute for Astrophysics Potsdam, An der Sternwarte 16, D-14482 Potsdam, Germany

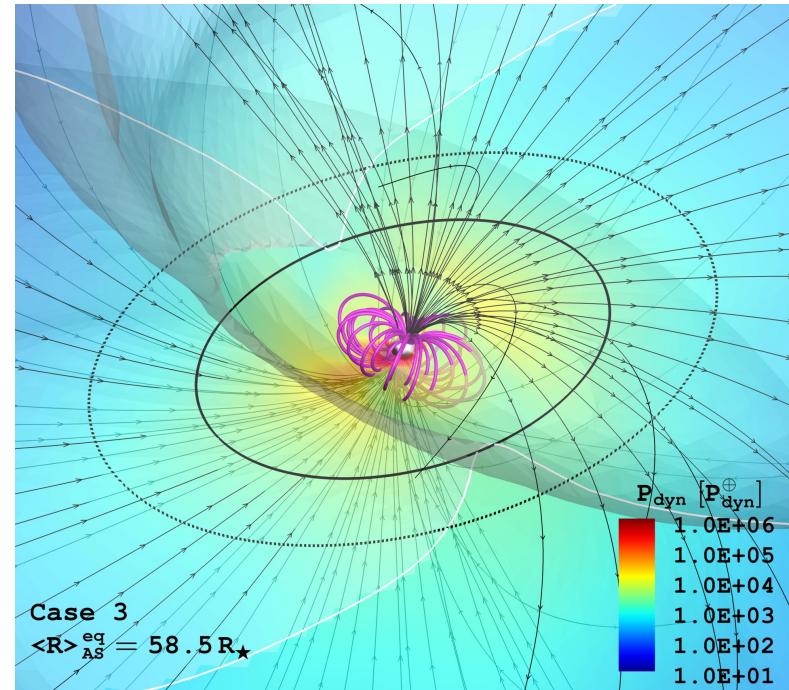
⁴ University of Massachusetts at Lowell, Department of Physics & Applied Physics, 600 Suffolk Street, Lowell, MA, 01854, USA

Received 2022 June 6; revised 2022 July 27; accepted 2022 July 28; published 2022 October 5



Resulting stellar wind conditions around AU Mic:

- Wind speeds: $\sim 1200 - 2200$ km/s
- Stellar wind mass loss rate: $5 - 10 \dot{M}_{\odot}$
- Average Alfvén surface sizes: $\sim 28 - 106 R_{\star}$
Sub-Alfvénic conditions for planets b & c
(see Kavanagh+ 2021)
- Stellar wind dynamic pressures:
AU Mic b: $10^3 - 10^4 P_{dyn}^{\oplus}$ | AU Mic c: $10^2 - 10^3 P_{dyn}^{\oplus}$
Comparable to other M-dwarf planets
(e.g., Vidotto+ 2015, Garraffo+ 2016)
- Magnetically-dominated environment ($P_{mag} > P_{dyn}$)



A super CME event in AU Mic

Simulated eruption with sufficient magnetic energy to power the best CME candidate on this star so far:

$$M_{\text{CME}} \sim 10^{20} \text{ g}$$

$$K_{\text{CME}} \sim 10^{36} \text{ erg}$$

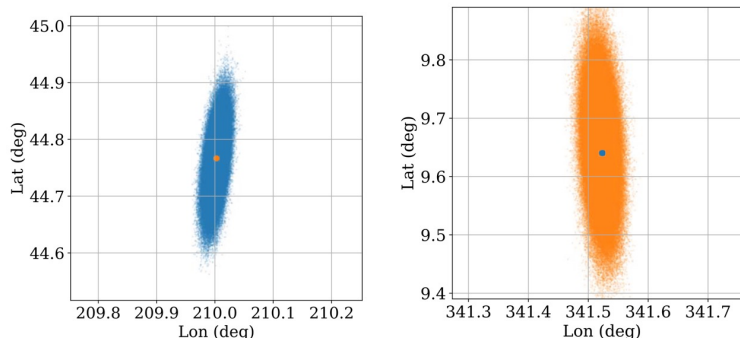
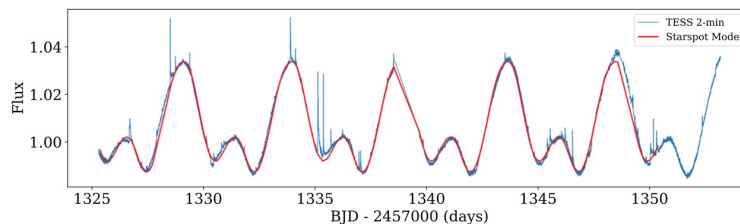
(Cully+ 1994, Katsova+ 1999)

We employ a TD flux-rope eruption model with:

$$M_{\text{FR}} \sim 10^{19} \text{ g}$$

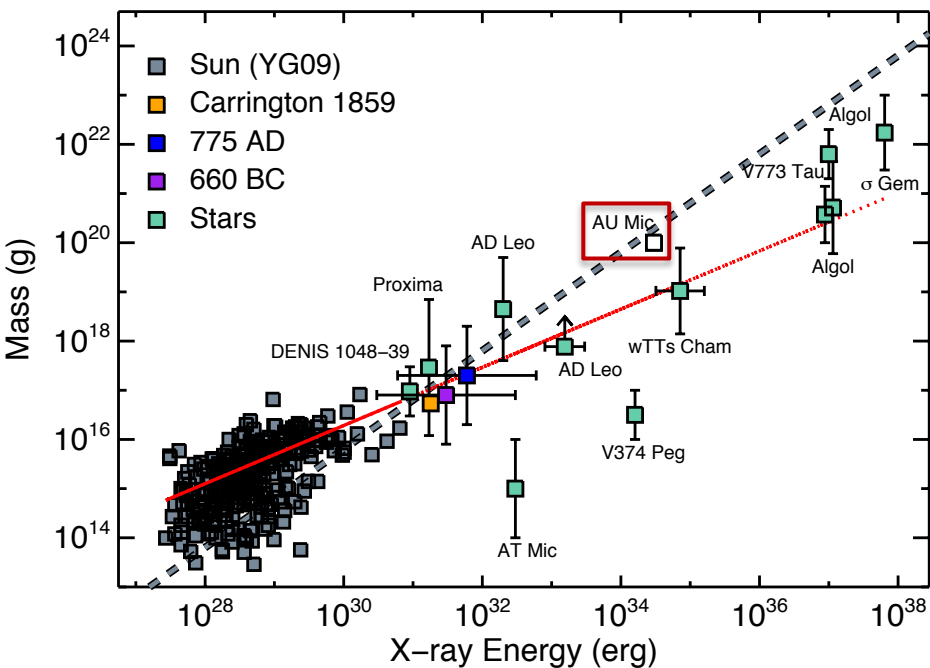
$$E_{\text{FR}}^{\text{B}} \sim 3 \times 10^{37} \text{ erg}$$

Launching latitude: 9.65 deg

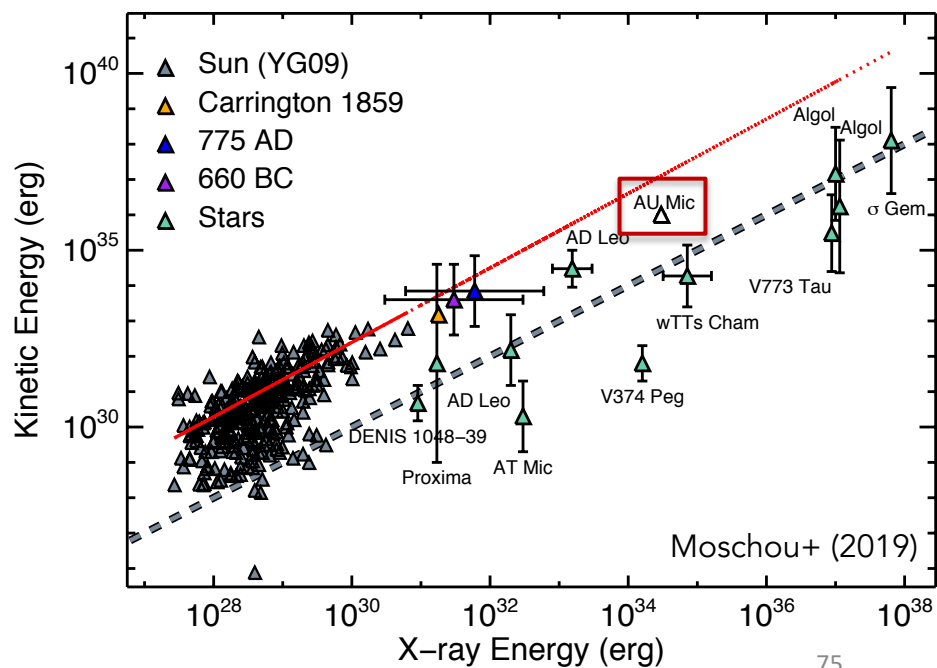


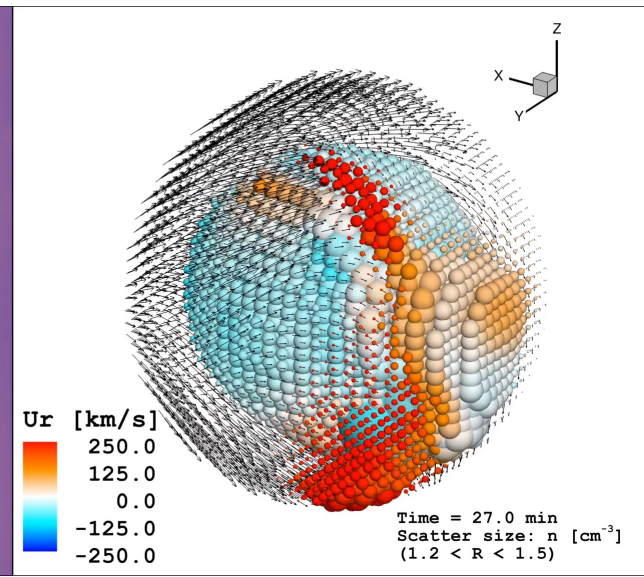
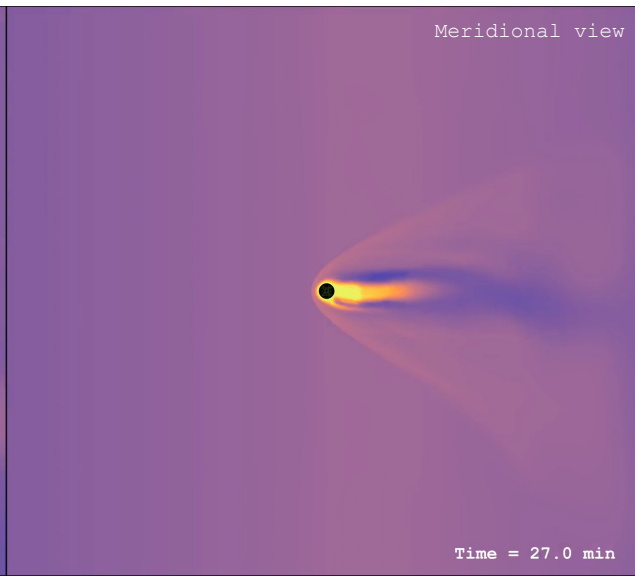
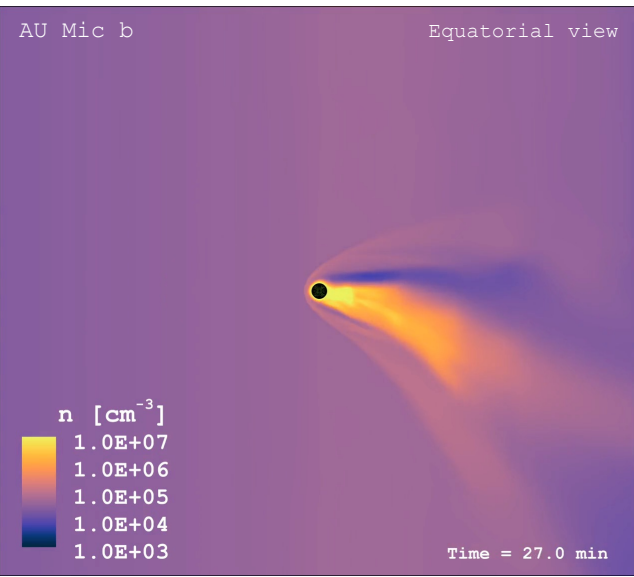
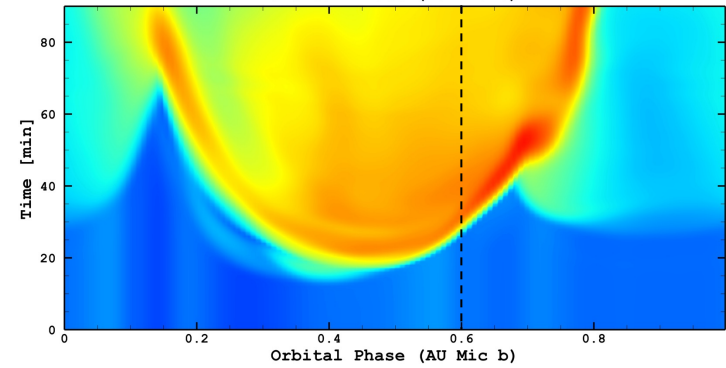
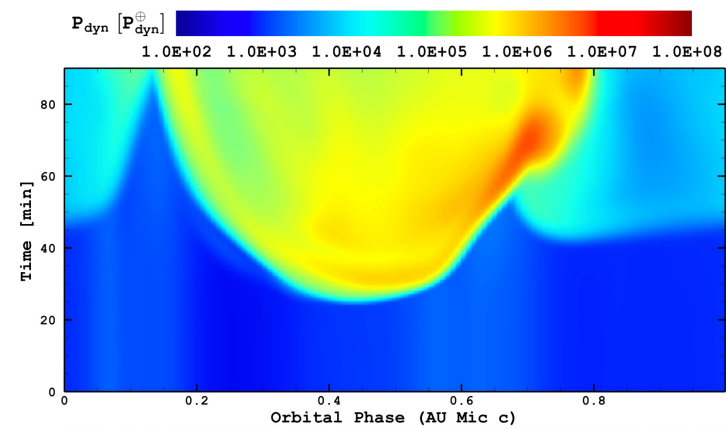
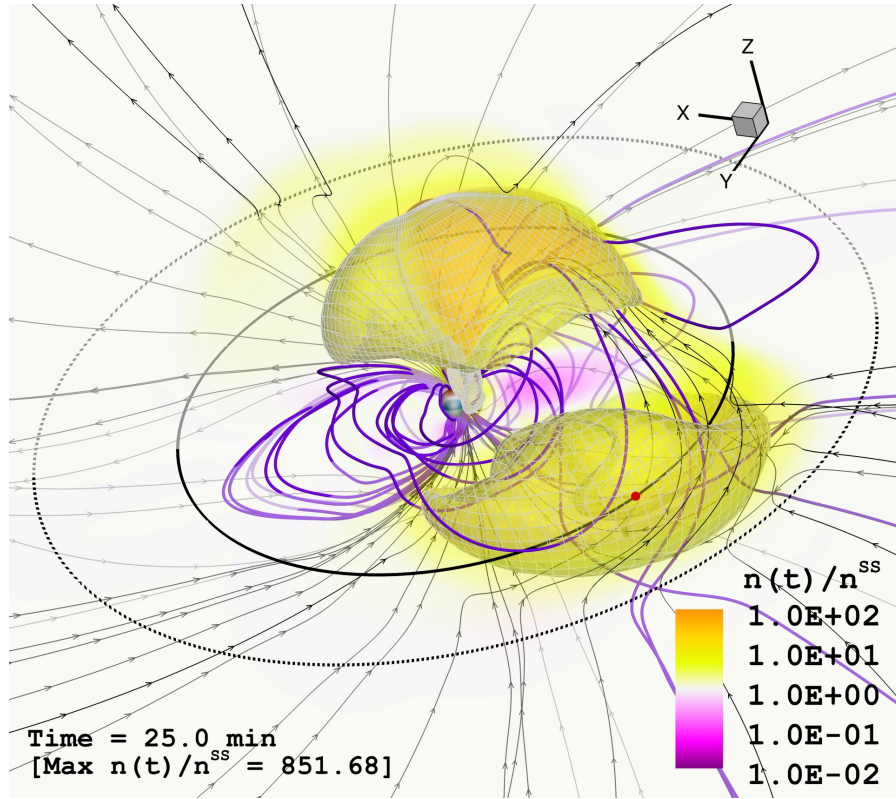
Wisniewski+ (2019)

CME Mass

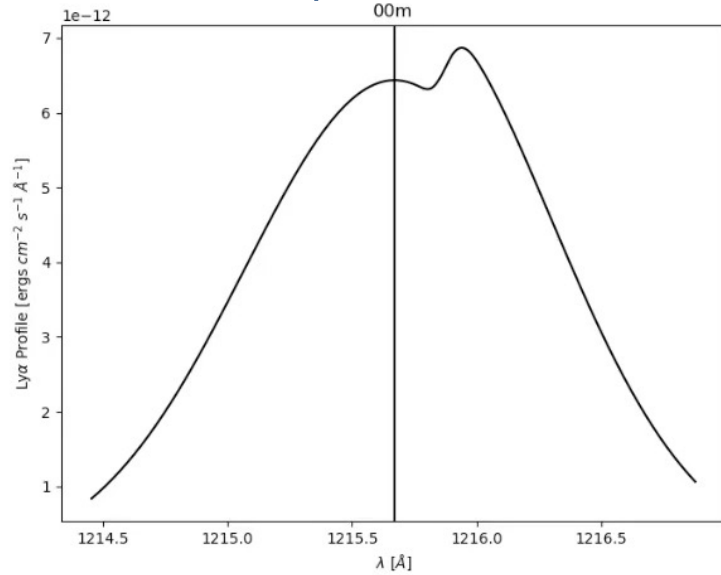


CME Kinetic Energy

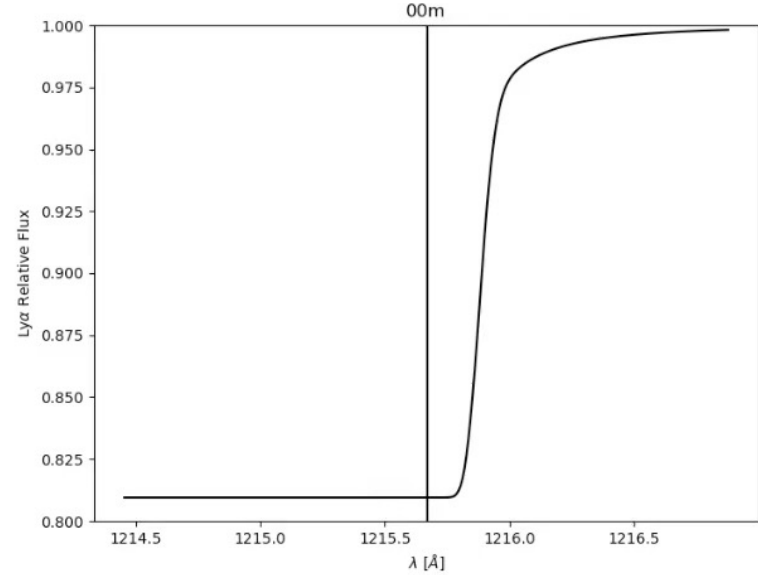




Synthetic planetary outflow diagnostics during the CME event (AU Mic b)

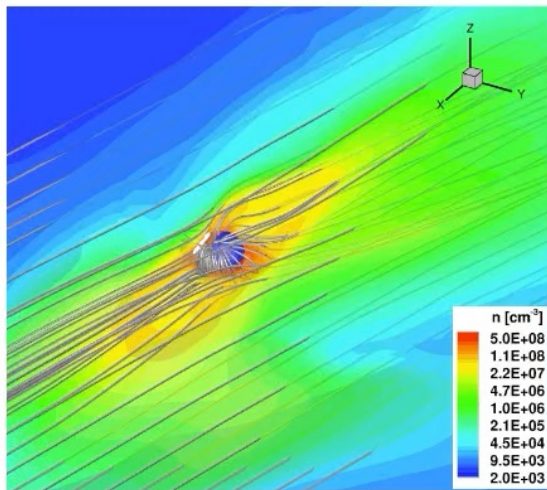


Ly- α line profile (star + planetary outflow absorption)

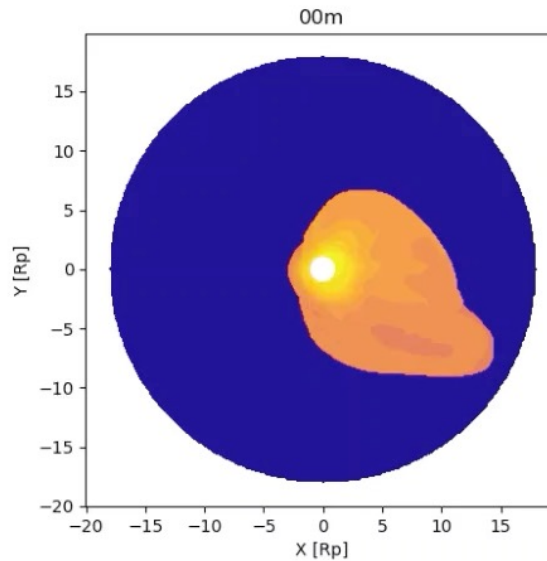


Relative Ly- α flux (Absorbed/Un-absorbed)

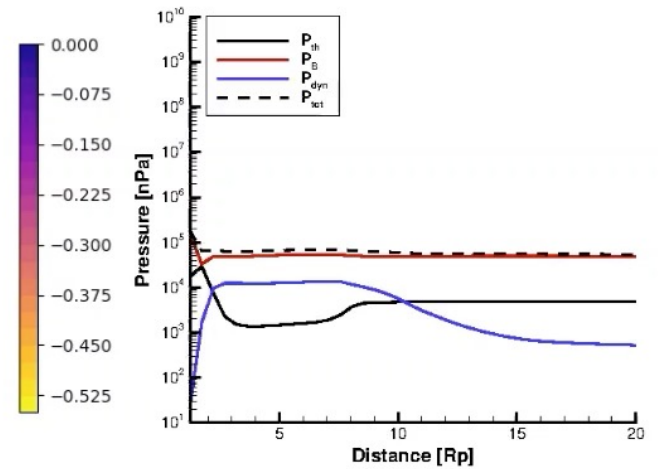
3D density structure

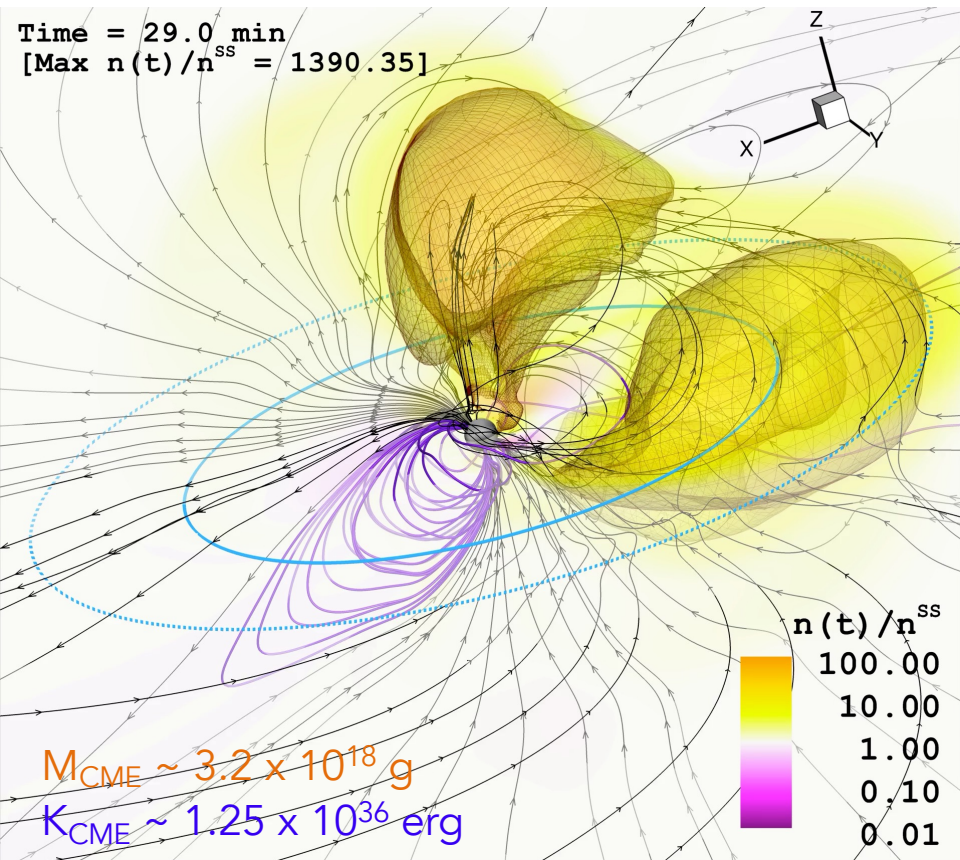


Absorption column (2D projection)

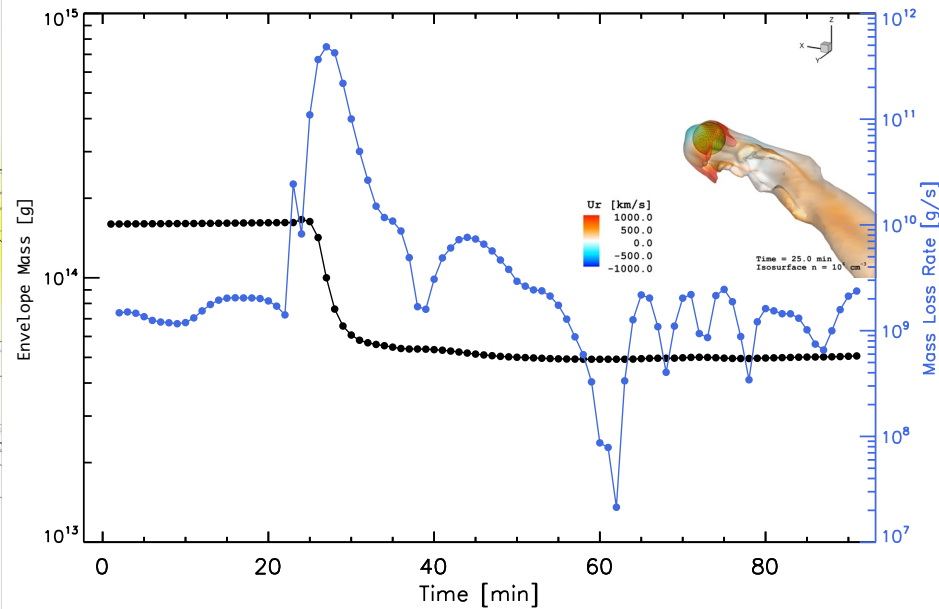


Pressure profiles





CME-impact on a planetary outflow



Alvarado-Gómez+ (2022); Cohen, Alvarado-Gómez+ (2022)

The CME depletes a large fraction of the planetary envelope mass ($\sim 70\%$)

The planetary mass loss rate increases by more than 2 orders of magnitude in a time scale of tens of minutes (CME crossing time).

In the CME aftermath the planetary outflow is suppressed. Additionally, the environmental conditions are changed to the super-alfvenic regime.

Strong CME fragmentation is obtained

(e.g., Alvarado-Gómez+ 2018)

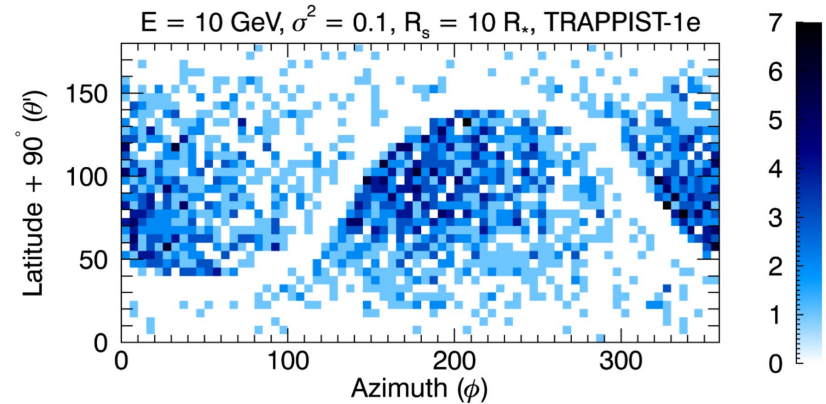
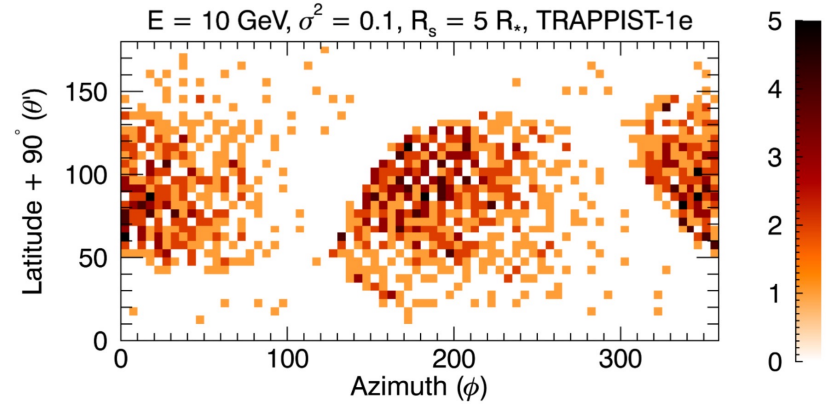
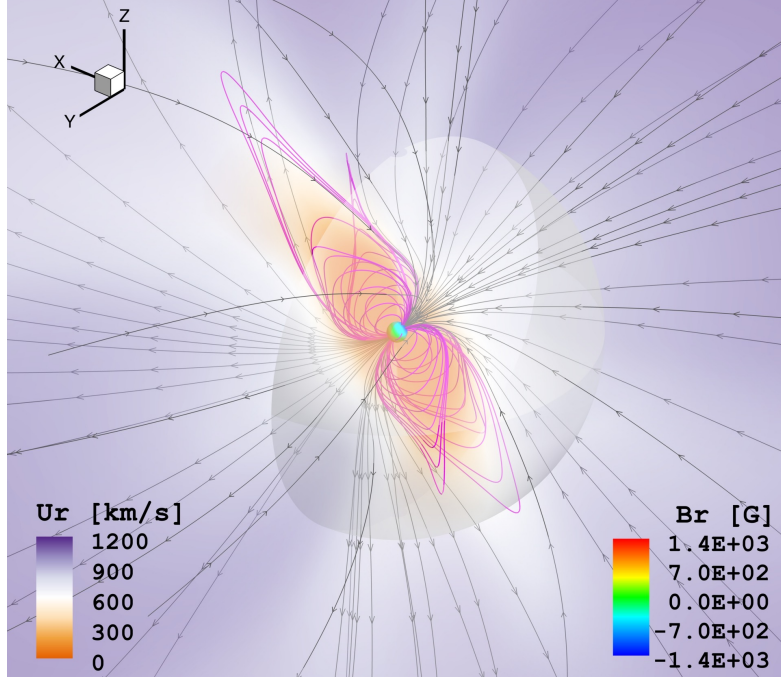
Only a small part of the escaping CME is exoplanetary-effective

$$(M_{CME})_{\text{equatorial}} \sim (0.07) M_{CME}$$

$$(K_{CME})_{\text{equatorial}} \sim (0.08) K_{CME}$$

Energetic particles in the TRAPPIST-1 System

(Fraschetti+ 2019)



Only a **few percent** of particles injected within half a stellar radius from the stellar surface escape.

The escaping fraction increases strongly with **increasing injection radius**.

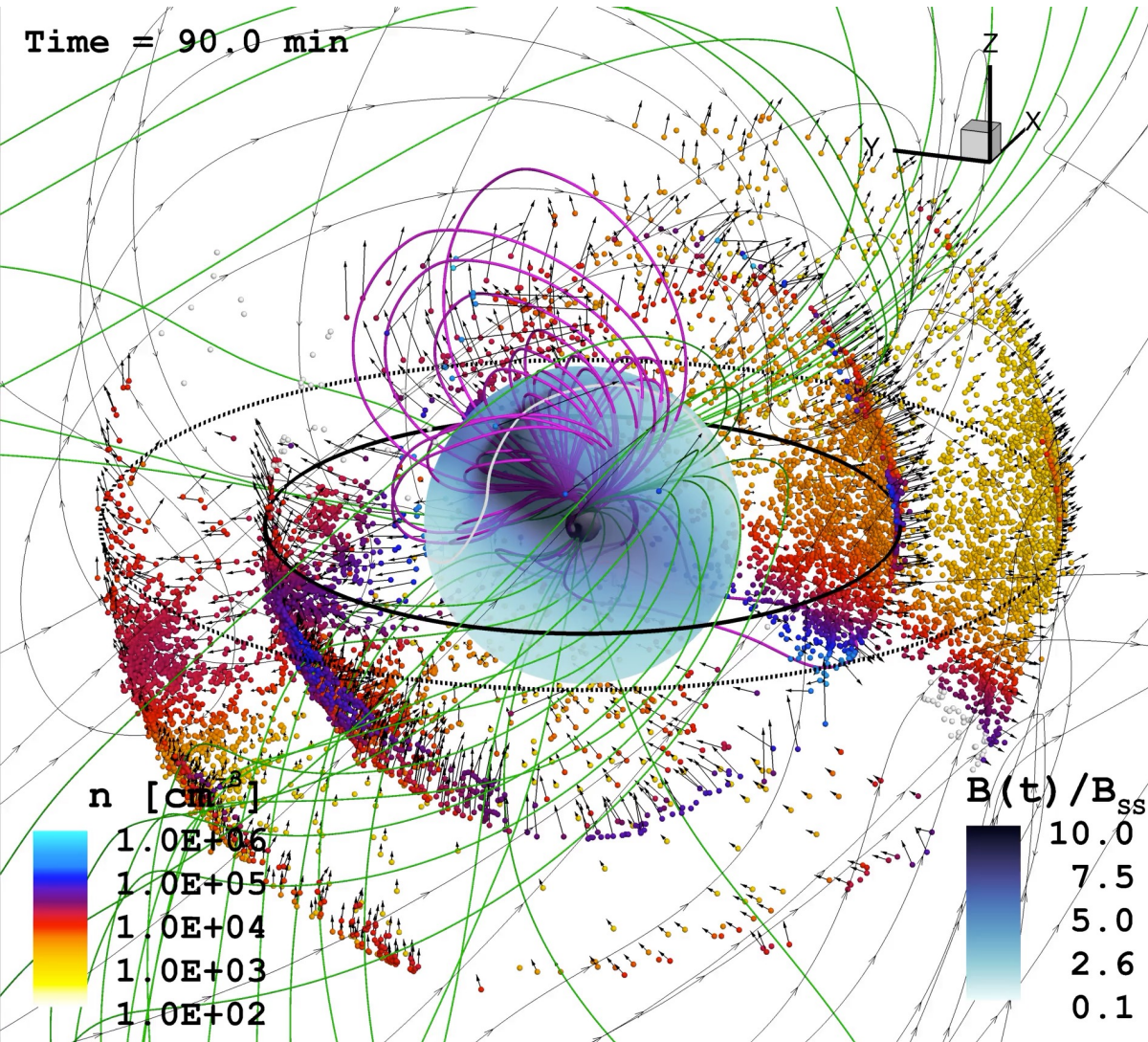
Escaping particles are increasingly deflected and focused by the ambient spiraling magnetic field (two caps in the fast wind region).

Energetic particles in the AU Mic System

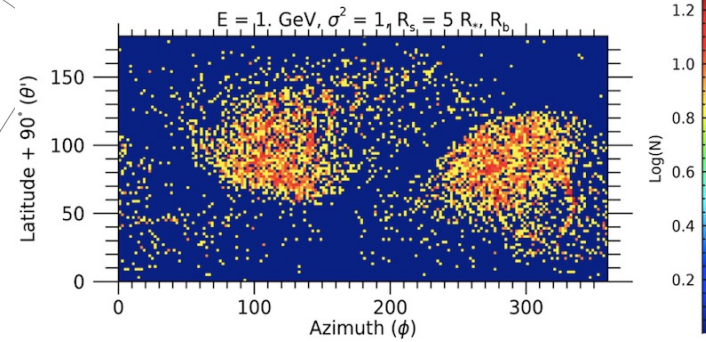
(Fraschetti, Alvarado-Gómez+ 2022)

Test-particle simulations of \sim GeV protons propagating in the steady- and CME-disrupted magnetized wind of AU Mic

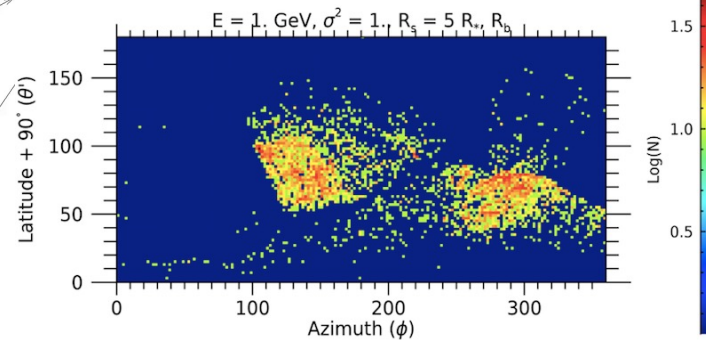
Ensemble of EPs reaching the orbital distance of AU Mic b



Steady-State Stellar Wind:



CME-disrupted Stellar Wind:



Report from a Keck Institute for Space Studies Workshop on Exo-Space Weather

The screenshot displays the Keck Institute for Space Studies website. At the top, the navigation bar includes 'Earth', 'Planetary', 'Keck' (with logo), 'Astrophysics', and 'Engineering'. A left sidebar menu lists 'SUPPORT US', 'Home', 'About', 'Connect and Visit', 'Programs', 'Events', 'Workshops', 'Lectures', 'Short Courses', 'Symposia', 'Special Events', 'Impact', and 'People'. The main content area features a large group photo of workshop participants. Below the photo, the text reads: 'Workshop: Blazing Paths to Observing Stellar and Exoplanet Particle Environments', 'November 6 - 10, 2023', and 'California Institute of Technology - Pasadena, CA 91125'. A 'Team Leads' section follows, with four entries: R. O. Parke Loyd (Eureka Scientific, Inc.), Gregg Hallinan (California Institute of Technology), Joseph Lazio (Jet Propulsion Laboratory, California Institute of Technology), and Evgenya Shkolnik (Arizona State University). A 'Description' section is partially visible at the bottom. On the right, a search bar and a list of links (SHORT COURSE, SCHEDULE (PDF), WORKSHOP #2, LECTURE, STUDY PAGE) are present, along with contact information: 'Contact Us: 8:30 A.M. - 4:30 P.M. (626) 395-6630' and an 'Email Us' button.

Concluding remarks:

- It is now possible to study in detail the properties of magnetic fields of stars other than the Sun. The wide parameter space on the stellar domain is fundamental for our understanding of how magnetism is generated on the Sun and stars.
- The study and characterization of stellar activity in any context (e.g., exoplanets) can only be complete with knowledge of its relationship with the magnetic field.
- Current exoplanet characterization efforts must include the influence due to the space weather generated by the star (e.g., corona, stellar wind, flares/CMEs/EPs).
- Magnetic suppression is a viable mechanism for reducing the flare-CME association rate in active stars. The large-scale field tends to decrease the speed and energy of the CMEs. Consequences for their expected signatures and detection (e.g., "Radio quiet CMEs").
- The CME confinement mechanism can be extended to a stronger / high-complexity field regime (M-dwarfs). Critical effects on the habitability around low-mass stars. This process would induce additional coronal activity (e.g., flaring, up flows/down flows), possibly detectable by next-generation high-energy astrophysics instrumentation.
- While the Sun and its planets serve as the best possible guide, in the realm of stars and exoplanets our minds must always remain open to possibilities (specially for those rarely or never observed in the solar system).

Thanks for your attention.